Politecnico di Torino

MASTER OF SCIENCE IN CIVIL ENGINEERING

Master's Thesis

FATIGUE CHARACTERIZATION OF BITUMINOUS MIXTURES USING THE FOUR-POINT BENDING TEST

Candidate:
Ahmed Salah Ismail Abdallah

Supervisors:
Prof. Ezio Santagata
Prof. Davide Dalmazzo
Prof. Lucia Tsantilis

Academic Year 2021-2022

Acknowledgment

I would first like to thank my supervisors, Professor Ezio Santagata, Professor Davide Dalmazzo, and Professor Lucia Tsantilis whose expertise was invaluable in formulating the research questions and methodology. Your insightful feedback pushed me to sharpen my thinking and brought my work to a higher level.

I am deeply grateful to the laboratory engineers, Eng. Riccardo Rabezzana, and Eng. Leonardo Urbano for their technical support, and their guidance in the laboratory.

Dedication

To my mother, thank you for being my guiding light, for inspiring me, and for always putting me first. I truly appreciate and treasure everything you did. May Allah's love, blessing, and mercy be with you every day.

To the soul of my father, the only role model I look up for, thank you for always being my inspiration, for teaching me the right values, and for always being a giver. May Allah bless your soul and grant you the highest state in heaven.

To my brother and sister, thank you so much for supporting me along my journey in life. To you, I will forever owe my achievements. I would not be the person I am today without your help.

To her, my comfort zone, thank you for always being there for me, for believing in me, and for loving me the way that you do.

Abstract

This thesis aims to define a proper reliable procedure to characterize the fatigue resistance of bituminous mixtures according to European standards. This is achieved by using the four-point bending beam test device under strain-controlled sinusoidal loading configuration at different strain levels, with a reference frequency of 10 Hz, and a constant temperature of 20 °C. By analysing the vast literature on the subject, five failure criteria were selected and compared to come up with the best path to follow for fatigue resistance characterization.

The first two failure criteria are based on the modulus reduction: 50 % reduction in the initial modulus taken at the 100^{th} cycle, and 50 % reduction in the modulus extrapolated from the phase of linear reduction of the modulus (Intermediate phase). The third failure criterion is the peak in the phase angle. The last two criteria are based on energy concepts, the first one is the energy ratio, and the second one is the dissipated energy approach.

In consequence, five dissimilar fatigue curves have been produced, using three strain amplitude levels (140 μm/m, 200 μm/m, 300 μm/m) and a minimum of six replicates at each strain level.

Some additional relationships have been introduced like the relationship between the visco-elastic-related modulus versus the void ratio of the beams, and fatigue-related modulus versus the void ratio. Also, the positions of the beams derived from the wheel compacted slab were drawn against the corresponding air voids.

Statistical analysis is carried out, dealing with the expected non-homogeneity of the results. Consequently, a sensitive pavement design was carried out using KENLAYER non-linear analysis software. The design is based on a fixed pavement configuration, adopting the mechanistic-empirical pavement design fatigue model (Transfer function). The purpose was to see how pavement design is affected by variability in fatigue resistance characterization.

List of contents.

List of figures.

List of tables.

Chapter 1: Introduction

1.1 Background

The past decade has witnessed the build-up of in-depth laboratory knowledge coping with the interrelationships of materials properties, testing techniques, and environmental factors as these relate to the fatigue lifetime of compacted asphalt mixtures. The need for designing and constructing sturdy versatile pavements is overriding. The requirement for considering and evaluating flexural fatigue characteristics of asphaltic concrete was given by Hveem in 1955. Examination of pavements showed that surface cracking was occurring while not the loss of cross or longitudinal slopes, and so, the pattern of cracking was related to repetition instead of excessive magnitudes of loads. Throughout this era (1950-60) several pavement engineers were learning factors poignant stress distribution during a pavement layered system. These investigations indicated the requirement for deciding values for stiffness of asphaltic concrete once subjected to perennial and quick rates of loading. Investigations on flexural fatigue and dynamic stiffness were being conducted at that point by researchers like bird genus and Hennes, Nijboer and van der Poel, Monismith, Papazian and Baker, and others.[1]

Since that time up to present, the scientific research was growing. Many tests were developed, and various techniques were introduced to characterize the fatigue of bituminous mixture. As a consequence, many characterization paths were presented, leaving a question of what is the best path to be followed?

This thesis is considered as a contribution to the international community, by defining the procedure of characterizing the fatigue of bituminous mixtures using the four-point bending test, which is one of the most common testing devices used nowadays.

1.2 Research objectives

The purpose of this project is to define the procedure to characterize the fatigue phenomenon of bituminous mixtures, using the four point bending testing device, highlighting the differences between the standards. Then, different failure criterion will be investigated, and the corresponding results will be compared. After that a statistical analysis is carried out, dealing with the expected non-homogeneity of the results. Finally, the outcome of this study will be used for a sensitivity pavement design.

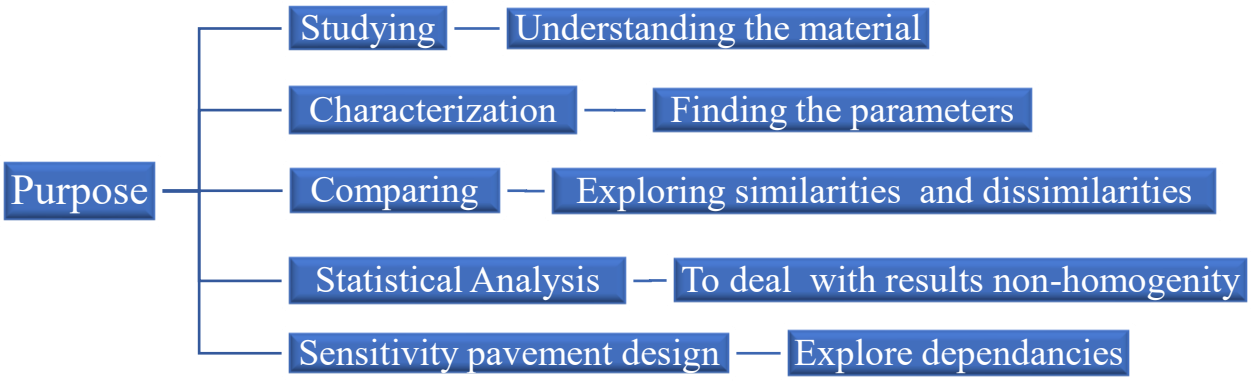

Figure 1 Research objectives

- In the first phase, a clear understanding of the material properties was required, so, many tests were carried out in order to characterize the used mixture which was imported to the laboratory.
- In the second phase the characterized material is tested, finding the fatigue parameters, which will be used later for the characterization.
- In the third stage, the results are compared in order to see the similarities and dissimilarities.
- The fourth phase includes a statistical analysis of the results because we are expecting a degree of uncertainty among our data, so a reliability analysis must be carried out.
- The final stage is a form of exercise to see how pavement design is affected by changing the first two regression parameters of the fatigue transfer function f_1, f_2 while keeping the third regression parameter f_3 fixed.
- This workflow will not only allow us to define the best characterization path to be followed, but also it will highlight the differences between the different approaches.

1.3 Thesis outline

The thesis is organized in five chapters including the following contents:

- ❖ Chapter 1: Introduction

This chapter includes a background on the fatigue of bituminous mixtures, followed by the research objectives and the thesis outline.

- ❖ Chapter 2: Literature review

This chapter is divided into five sub-sections. The first sub-section is dedicated to explore general aspects related to the fatigue of bituminous mixtures. The next part will be focused on addressing the fatigue characterization methods across the standards (European and American). In the third sub-section some fatigue models were introduced and briefly discussed. The most common fatigue failure criteria were presented in the fourth sub-section. The last sub-section was devoted to the pavement design.

- ❖ Chapter 3: Materials and methods:

This chapter reports a detailed description of the experimental campaign. Starting from the description of the material in the first part. Then, the detailed material's characterization tests are explained. After that specimens' sampling steps are illustrated in order to obtain the final beams which will be tested in the four point bending device.

- ❖ Chapter 4: Analysis of the results

This part in the core of the thesis, where a detailed analysis of the results is presented. This analysis includes the estimation of the fatigue life using five different fatigue failure criteria. After that a reliability analysis is carried out on the obtained results, to find a representative value for the fatigue life for each failure criteria. Next, the fatigue curve is constructed for each failure criteria and the results are compared. Finally, a sensitivity pavement design is carried out to see the how the pavement design is affected by changing the regression parameters of the fatigue transfer function.

- ❖ Chapter 5: Conclusion and recommendations

Conclusions are gathered from the most relevant testing results and consequently some recommendations were offered in this section. A suggested route for future work is also provided.

Chapter 2: Literature review

In this chapter five sub-sections are presented to cover the topic of fatigue of bituminous mixtures. The first part is dedicated to the definition of the problem and the related parameters. The second part focuses on comparing the different characterization tests across the standards. In the third sub-section we introduced the fatigue modelling, highlighting some of the most common fatigue models. The fourth sub-section discussed the chosen fatigue failure criteria. Finally, the last sub-section was devoted to pavement design.

2.1 Fatigue of bituminous mixtures

2.1.1 Bituminous materials

Bituminous materials are in proverbial use since 3000 B.C., when bitumen mastics were utilized in geographic region as waterproofing for reservoirs. the fabric used then was a present asphalt (such as Trinidad Lake Asphalt, TLA) that is a combination of bitumen, that nowadays could be a specially created by-product of crude refinement, and fine natural mineral materials, and it was in this natural form that sole use was created till the eighteenth century. it absolutely was throughout this era that Telford and McAdam began to construct roads victimisation techniques and materials acquainted to users nowadays. However, they created intensive use of tar, a dark brown or black viscous liquid obtained from distillation of wood, coal and similar substances that was out there in fittingly massive quantities at that point, instead of bitumen as the binder within the mixture. The use of tars has step by step reduced over the years because of so much less production, health considerations over the carcinogenic nature of the fabric and since of the superior properties exhibited by bituminous binders. Rolled asphalt began to be created within the middle of the 19th century as a manmade imitation of present asphalts. [2]

The first specifications for asphalts appeared in 1933 and continued to evolve as B.S. 594 from 1935 to this format of these days. Widespread use of bituminous macadam for construction began within the early 1900's. The mixtures used were coated single-sized macadams set cold by hand. the requirement for a more hierarchical mixture was step by step did not though the fines content failed to rise higher than 15% for several years. the primary specification for macadams was issued within the early 1940's and by the 1960's dense coated macadams had been introduced for the most load bearing layers of the road

This development of bituminous materials has led to the two generic mixture varieties:

- Asphalts
- Macadams

The distinction between the 2 is apparently the amount and particle size distribution of the coarse aggregate. Asphalts principally comprises a fine aggregate and bitumen matrix with differing amounts of coarse aggregate, usually single sized, distributed throughout the mixture. this kind of mixture is then remarked as gap-graded. McAdams, however, are cited as continuously graded and are created from roughly equal amounts of each individual aggregate size (based on McAdams's early work).

This leads to an aggregate skeleton wherever there's stone on stone contact throughout the mixture. Figure (2) shows samples of the 2 generic forms of grading. Rolled asphalts use the dense mortar of sand, bitumen, and filler (fine material that encompasses a particle size less than 75µm) to produce the structural performance of the layer (resistance to permanent deformation and load spreading ability), as against macadams that apply their interlocked aggregate skeleton to produce these properties. all sorts of bituminous material use the bitumen to resist fatigue cracking as this is often caused by tensile strains generated within the pavement and also the solely constituent of a bituminous mixture that has a tensile capability is the bitumen. Macadams usually give higher resistance to permanent deformation than asphalts and might be stiffer, if a thought of the grade and type of bitumen employed in the mixture is taken into account.

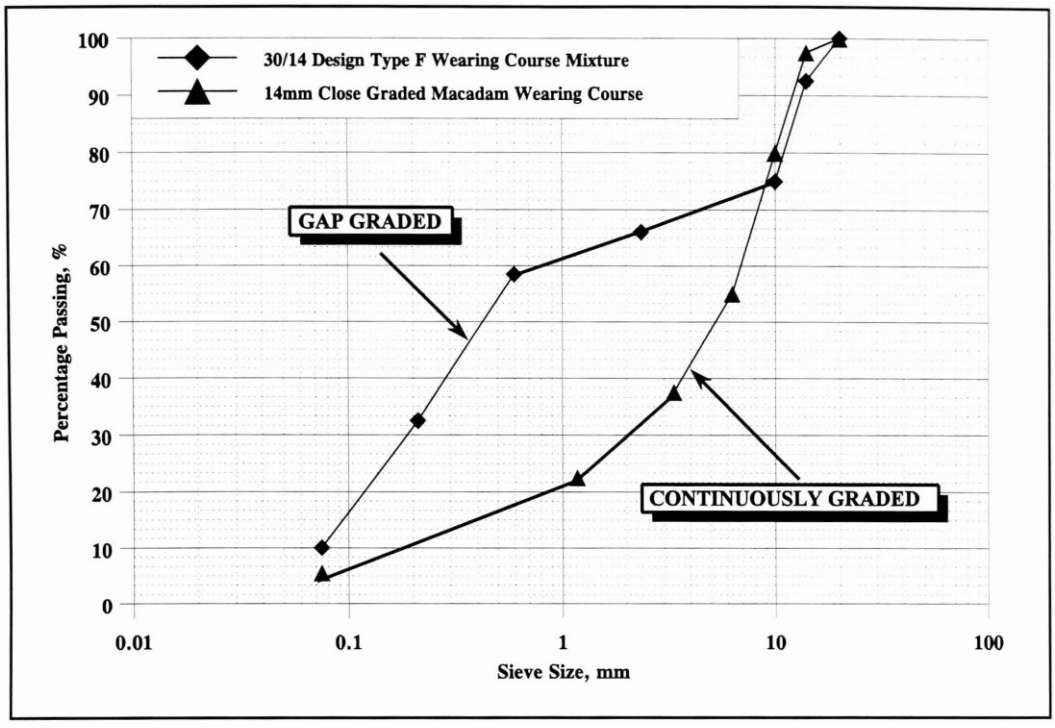

Figure 2 Comparison of Gap Graded and Continuously Graded Mixtures

Asphalts have a larger amount of fine material than macadams and, therefore, surface area of the mixture is higher resulting in an accrued demand for binder and, therefore as bitumen is the most expensively constituent; asphalts are costly to produce. However, the increased binder content and, hence, binder volume provide asphalts a far better resistance to fatigue cracking. This conjointly makes them less permeable to each air and water, and further increasing their durability over macadams.

Durability of a bituminous paving mixture has been defined as:

"The ability of the materials comprising the mixture to resist the effects of water, ageing and temperature variation, in the context of a given amount of traffic loading, without significant deterioration for an extended period"[3]

2.1.2 Types of asphalt mixtures:

According to (Information Series 128 HMA Pavement Mix Type Selection Guide HMA Pavement Mix Type Selection Guide HMA Pavement Mix Type Selection Guide) [4]. Hot mixed asphalt pavement mix types include Open-Graded Friction Courses (OGFC), Stone Matrix Asphalt (SMA), and fine- and coarse graded dense mixes.

- **Open-Graded Mixes**

Open-graded mixes are designed to be leaky to water, that differentiates them from dense hierarchic and SMA mixtures that are comparatively imperviable. Crushed stone is used in these types of mixtures, or alternatively, crushed gravel with a tiny low amount of factory-made sands. the employment of modified asphalts and probably fibres is extremely counselled for surface mixtures. This will increase the quantity of asphalt that may be used with these mixes, rising their sturdiness and performance.

- Purpose:

Under this category, three types of mixtures have been defined: open graded friction, porous European mixes, and asphalt treated permeable bases. The first two types are used for surface or wearing courses only. They cut back splash/spray from tires in wet weather and usually lead to a smoother surface than dense-graded HMA. each are costlier per ton than dense-graded HMA, however the unit weight of the combo in-place is lower, that part offsets this higher price. each mixtures ought to solely be used on high or medium-traffic volume roadways with denote high speeds solely. Higher speed traffic helps to keep the pores from hindering.

In low temperature climates, open graded friction and porous European mixtures require a particular approach for winter maintenance. The open pore structure causes these mixes to cool down quicker and then freeze before less permeable mixtures. Sand shouldn't be mixed with defrosting materials since the sand will seal the pores and cut back the effectiveness of these mixtures. These surfaces conjointly need further frequent application of de-frosting materials although at a reduced rate whenever.

Table (1) presents which mixes are appropriate for different layers and for what purpose you may use the mix:

	Mix Purpose		
Layer	9.5 mm	12.5 mm	19 mm
Surface	• Wearing surface • Friction • Noise reduction • Splash/spray reduction		N/A
Base	N/A	N/A	• Drainage

Table 1 Appropriate Layers and Purpose

- Materials:

Table (2) provides general guidelines for materials used in open-graded mixtures:

Layer	Traffic	Medium	High
Surface OGFC or PEB	Aggregate	• Crushed stone • Crushed gravel • Manufactured sands	
	Asphalt Binder	• Modified binder	
	Other	• Fibers • Antistrip as determined by testing	
Base ATPB	Aggregate	• Crushed stone • Crushed gravel • Manufactured sands	
	Asphalt Binder	• Unmodified	
	Other	• Antistrip as determined by testing	

Table 2 Materials for Open-graded Mixes

- Mix design:

Mix design for open-graded mixes is less structured than for dense-graded or SMA mixtures. The main components of open graded friction mixtures design are:

- Selection of materials.
- Gradation.
- Compaction and void determination.
- Binder drain-down evaluation.

The National Centre for Asphalt Technology (NCAT) Report 99-3, *Design of New-Generation Open Graded Friction Courses*, provides a recommended mix design procedure for OGFCs.

- **Stone Matrix Asphalt (SMA) Mixes**

Stone matrix asphalt is a gap-graded hot asphalt mixture that maximizes rutting resistance and sturdiness with a stable stone-on-stone skeleton command along by a rich mixture of asphalt concrete, filler, and stabilising agents like fibres and/or asphalt modifiers. Stone matrix asphalt was developed in Europe to resist rutting (permanent deformation) and studded tire wear.

Stone matrix asphalt is usually thought of a premium mix owing higher initial costs thanks to accrued asphalt contents and also the use of additional durable aggregates. Nevertheless, this rocketing cost is compensated by improved performance for medium to high traffic configuration Along with the improved sturdiness, fatigue resistance, permeant deformation, other reported advantages include better-quality wet weather friction are also presented, due to coarser surface texture, and minor tire noise. Reflective cracking in a stone matrix mixtures is usually not as severe as dense-graded mixtures since cracks have less tendency to fragment.

- Purpose:

As antecedental mentioned, the first purpose of this stone matrix mixes is the improved resistance to permanent deformation and sturdiness. Therefore, these mixes are exclusively used for surface courses on high volume interstates and highways. Heavy and slow-moving vehicles could warrant the employment of stone mixtures for intermediate and base layers.

Table (3) presents which mixes are appropriate for different layers and for what purpose you may use the mix:

	Mix Purpose		
Nominal Max. Agg.	9.5 mm	12.5 mm	19 mm
Layer			
Surface	• Wearing surface • Friction • Structure • Smoothness		
Intermediate	N/A	N/A	• Structure

Table 3 Appropriate Layers and Purpose of SMA

- Materials for SMA:

Stone matrix asphalt is a premium combine requiring top quality materials. Cubical, low abrasion, crushed stone and synthetic sands are suggested because the mixture gains most of its strength from the stone-on-stone aggregate skeleton. Aggregates ought to have 100% of the particles with one or additional broken faces. Natural sands shouldn't be used. Aggregates should also have high polish values to retain sensible skid resistance wherever this mix is the final surface.

The matrix of sand, asphalt, mineral filler, and additives is also important to performance. Manufactured sands, mineral fillers, and additives (fibres and/or polymers) make a stiff matrix that is important to the rutting resistance of these mixes. Mineral fillers and additives also reduce the amount of asphalt drain down in the mix during construction, increasing the amount of asphalt used in the mix, improving its durability.

Table (4) provides general guidelines for materials used in SMA mixtures:

Layer	Material	Medium Traffic	High Traffic
Surface and Intermediate/Binder	Aggregate	• Crushed stone • Crushed gravel • Manufactured sands • Mineral filler	
	Asphalt Binder	• Modified binder typically used • Unmodified may be used at lower traffic levels	• Modification likely • Unmodified asphalts based on local experience
	Other	• Fibers • Antistrip as determined by testing	

Table 4 Materials for SMA Mixtures

- Mix design:

Marshall and Superpave compaction procedures can be used to design stone matrix asphalt mixtures. For information on designing SMA mixtures, refer to the National Cooperative Highway Research Program (NCHRP) Report 425, Designing Stone Matrix Asphalt Mixtures for Rut-resistance pavements

- **Dense-Graded Mixes**

A dense-graded mix is a well-graded (even distribution of combination particles from coarse to fine), those mixes are consisting of aggregates and asphalt binder. Properly designed and created mixtures are comparatively imperviable.

- Nominal Maximum Size (NMS):

This is defined in the Superpave mix design system as, “one sieve size larger than the first sieve to retain more than 10 percent.”

- Fine- and Coarse-Graded Mixes:

Dense-graded mixes can further be categorized as either fine-graded or coarse-graded. Simply put, fine-graded mixes have more fine sand size particles than coarse-graded mixes. Table (5) can be used to define whether a mix is coarse or fine-graded. The relative advantages of the mixes are presented in Table (6).

Mixture NMS	Coarse-Graded	Fine-Graded
37.5 mm (1 1/2")	< 35% Passing 4.75 Sieve	> 35% Passing 4.75 Sieve
25.0 mm (1")	< 40% Passing 4.75 Sieve	> 40% Passing 4.75 Sieve
19.0 mm (3/4")	< 35% Passing 2.36 Sieve	> 35% Passing 2.36 Sieve
12.5 mm (1/2")	< 40% Passing 2.36 Sieve	> 40% Passing 2.36 Sieve
9.5 mm (3/8")	< 45% Passing 2.36 Sieve	> 45% Passing 2.36 Sieve
4.75 mm (No. 4 Sieve)	N/A (No standard Superpave gradation)	

Table 5 Definition of Fine- and Coarse Dense-graded Mixtures

Fine-Graded	Coarse-Graded
Lower permeability	Allows thicker lifts (< 25 mm (1") NMS)
Workability (< 25 mm (1") NMS)	Increased macro texture (< 25 mm (1") NMS)
Thinner lifts (< 25 mm (1") NMS)	
Greater durability for low volume roads(< 25 mm (1") NMS)	
Smooth texture (< 25 mm (1") NMS)	

Table 6 Advantages of Fine- and Coarse Dense-graded Mixtures

- Purpose:

Dense-graded mixes are deemed the pillar of hot mixed asphalt, since they'll be used effectively all over pavement layers, for all traffic configurations. A dense-graded mix is also accustomed to fulfilling any or all of the subsequent pavement designers' needs:

Structural: This is the primary purpose of dense-graded mixes and is primarily a function of the thickness of the layer. However, select materials may improve the structural value of mixes.

Friction: This is a vital thought for surface courses. Friction could be a perform of combination and blend properties.

Levelling: This blend is also employed in lean or thick layers to fill depressions in roadways.

Patching up: The mixture ought to meet an equivalent needs as if used for brand new construction.

Table (7) presents which mixes are appropriate for different layers and the purpose of each mix.

Nominal Max. Agg.	4.75 and 9.5 mm	12.5 mm	19 mm	25.0 and 37.5 mm
Layer				
Surface	• Wearing surface • Friction • Smoothness	• Wearing surface • Friction • Smoothness • Structure	• Friction • Structure	N/A
Intermediate	• Leveling • Smoothness	• Structure • Smoothness	• Structure	
Base	N/A			

Table 7 Appropriate Layers and Purpose of Dense-graded Mix

- Materials:

Table (8) provides general guidelines for materials used in dense-graded mixtures:

Layer	Material	Low Traffic	Medium Traffic	High Traffic
Surface	Aggregate	• Gravel (limited) • Crushed gravel and stone • Manufactured sands and natural sand	• Crushed gravel and stone • Manufactured sands and natural sand	
	Asphalt Binder	• Typically unmodified • Modification may be necessary for heavier traffic, intersections at higher traffic levels.	• Typically unmodified	• Modification likely • Unmodified asphalts based on local experience
	Other	• RAP (Reclaimed Asphalt Pavement) • Antistrip as determined by testing		
Intermediate/ Binder	Aggregate	• Gravel (limited) • Crushed gravel and stone • Manufactured sands and natural sand	• Crushed gravel and stone • Manufactured sands and natural sand	
	Asphalt Binder	• Typically unmodified		• Unmodified except for very heavy loading situations or when traffic will travel on layer for extended periods
	Other	• RAP (Reclaimed Asphalt Pavement) • Antistrip as determined by testing		
Base	Aggregate	N/A	• Crushed gravel and stone • Manufactured sands and natural sand	
	Asphalt Binder	N/A	• Typically unmodified	• Unmodified except for very heavy loading situations or when traffic will travel on layer for extended periods
	Other	N/A	• RAP (Reclaimed asphalt pavement)	• Antistrip as determined by testing

Table 8 Materials for Dense-graded Mixtures

- Mix design:

Dense-graded mixes may be designed using Marshall, Hveem, and Superpave procedures. For further information on Marshall and Hveem mix design procedures, refer to the AI's publication MS-2, Mix Design Methods for Asphalt Concrete and Other Hot-Mix Types. For information on designing mixes using the Superpave system, refer to the AI's publication SP-2, Superpave Mix Design. **The Superpave system is recommended for designing dense-graded HMA.**

2.1.3 Material properties:

There are several basic properties that are of concern to the design engineer, and directly affects the pavement performance, among that the foremost vital parameters are:

- Volumetric properties.
- Stiffness.
- Resistance to Permanent Deformation.
- Fatigue Cracking Characteristics.

2.1.3.1 Volumetric properties:

"Whether a mix design is developed through a Marshall, Hveem, or Superpave mix design process there are basic volumetric requirements of all. Volumetric properties are the properties of a defined material contained in a known volume. Asphalt mixture volumetric properties can include bulk specific gravity, theoretical maximum specific gravity, air voids, and voids in mineral aggregate. Many agencies specify values of the volumetric properties to ensure optimum performance of the pavement. The asphalt mixture must be designed to meet these criteria. In production the asphalt mixture is evaluated to determine if the mix still meets the specifications and is consistent with the original mix design (JMF). The production asphalt mixture may vary from the mix design and may need to be modified to meet the specified volumetric criteria" [5]

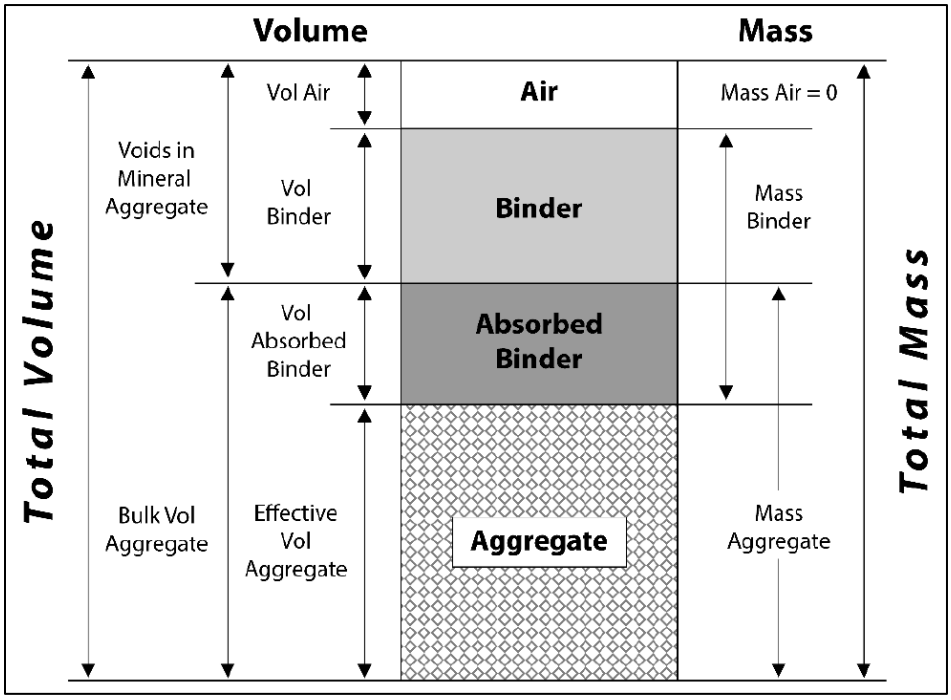

Figure 3 Asphalt mixture phase diagram

Each of the properties in the previously mentioned diagram can be quantified, along with their corresponding volumes. Those properties of a compacted asphalt mixture like the: air voids, voids in mineral aggregate, voids filled with asphalt binder, and effective asphalt binder content; offer some indication of the mixture's probable performance. To quantify those amounts we have to know the specific gravities and the masses of each component.

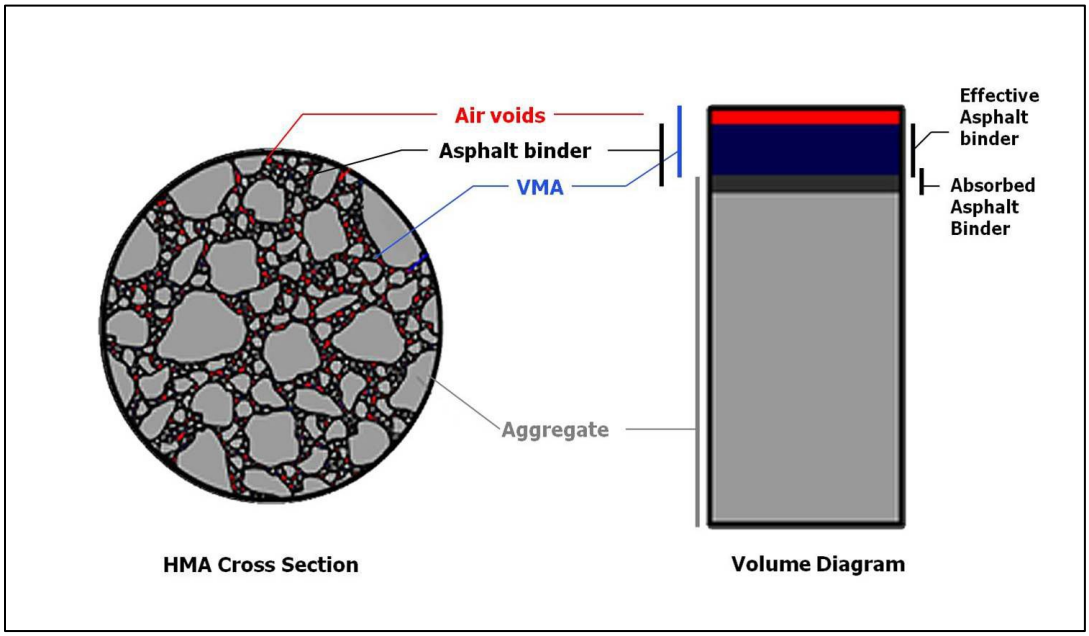

Figure 4 Volumetric Relationship of Asphalt Mixture Constituents

- Air Voids (Va)

Air voids are the overall volume of the little pockets of air between the coated aggregate particles throughout a compacted paving mixture. Proper air voids impact the stability of the asphalt mixture and facilitate the pavement stand up to the combined action of atmosphere and traffic loads. The chosen air voids ratio allows thermal enlargement of the asphalt binder and contributes a support for future compaction. Air voids are expressed as a portion of the total volume of the condensed mixture, compared to the maximum specific gravity.

$$V_a = 100\left[\frac{G_{mm} - G_{mb}}{G_{mm}}\right]$$

Where:

V_a = air voids in compacted mixture, percent of total volume.
G_{mm}= maximum specific gravity of paving mixture.
G_{mb} = bulk specific gravity of compacted mixture.

❖ Percent Aggregate (Stone) (Ps)

Ps is the portion of aggregate included in our mix, expressed as a fraction of the overall mass of the sample.

$$P_s = 100 - P_b$$

Where:

P_s = percent aggregate (stone) percent by total weight.
P_b = asphalt binder content.

❖ Voids in the Mineral Aggregate (VMA)

This component represents the volume of intergranular void space between the aggregate particles of the compacted paving mixture that comprises the air voids and the effective binder content, communicated as a fraction of the entire volume of the specimen.

$$VMA = 100\left[\frac{G_{mb} * P_s}{G_{sb}}\right]$$

Where:

VMA = voids in mineral aggregate, percent of bulk volume.
G_{sb} = bulk specific gravity of combined aggregate.
G_{mb} = bulk specific gravity of compacted mixture.
P_s = aggregate content, percent by total weight = 100 – P_b
P_b = asphalt binder content percent by total weight.

- Voids Filled with Asphalt (binder) (VFA)

This is the volume of void among the aggregate particles of the compacted paving mixture covered with asphalt binder, represented as a proportion of the overall volume of the sample. The quantity rises as the asphalt binder content increases as it is the percent of voids that are packed with asphalt which doesn't include the absorbed asphalt.

$$VFA = 100\left[\frac{VMA - V_a}{VMA}\right]$$

Where:

VFA = voids filled with asphalt, percent of VMA.
VMA = voids in mineral aggregate, percent of bulk volume.
V_a = air voids in compacted mixture, percent of total volume.

- Effective Specific Gravity of the Aggregate (Stone) (G_{se})

This quantity is used to measure the asphalt binder absorbed into the aggregate particle. This is a determined quantity based on the specific gravity of the mixture, maximum specific gravity, and the specific gravity of the asphalt binder. This magnitude includes the volume of the aggregate particle added to the void volume that becomes filled with water during the test soaking phase without the volume of the voids that absorb asphalt binder. Effective specific gravity is between apparent and bulk specific gravity.

The effective specific gravity of the aggregate is officially identified as the ratio of the mass in air of a unit volume of a pervious material (excluding voids permeable to asphalt binder) at a specified temperature to the mass in air (of equal density) of an equal volume of purified water at a specified temperature.

$$G_{se} = \frac{P_s}{\left[\frac{100}{G_{mm}} - \frac{P_b}{G_b}\right]}$$

Where:

G_{se} = effective specific gravity of combined aggregate.
P_s = aggregate content, percent by total weight = 100 – P_b
G_{mm} = maximum specific gravity of mix.
P_b = asphalt binder content percent by total weight.
G_b = specific gravity of asphalt binder.

- **Percent of Absorbed (asphalt) Binder (P_{ba})**

It is the total fraction of the asphalt binder that is absorbed into the aggregate, stated as a percentage of the mass of aggregate instead of the total mass percentage of the mixture. This part of the asphalt binder content does not promote the performance of the mix.

$$P_{ba} = 100\left[\frac{G_{se} - G_{sb}}{G_{sb} * G_{se}}\right] * G_b$$

Where:

P_{ba} = absorbed asphalt binder percent of aggregate.
G_{se} = effective specific gravity of combined aggregate.
G_{sb} = bulk specific gravity of combined aggregate.
G_b= specific gravity of asphalt binder.

- Percent of Effective (asphalt) Binder (P_{be})

This quantity represents the overall binder content of the mixture excluding the binder that is gone by assimilation into the aggregate fragments, conveyed as a percentage of the mass of aggregate. It is the portion of the asphalt binder content that stays as a glaze on the surface of the aggregate particles. This is the asphalt content that monitors the performance of the mix.

$$P_{be} = P_b - \left[\frac{P_{ba}}{100} * P_s\right]$$

Where:

P_{be} = effective asphalt binder content percent by total weight.
P_s = aggregate content, percent by total weight = 100 – P_b
P_b = asphalt binder content percent by total weight.
P_{ba} = absorbed asphalt binder.

- Dust Proportion – DP (Dust to Effective (asphalt) Binder Ratio)

The dust proportion is the percent passing on sieve #200 of the scale divided by the percent of effective asphalt binder. Too much dust will diminish the thickness of the binder film, and consequently decreasing the durability. On the other hand, deficient dust may induce excessive binder film thickness, subsequently creating a tender, unstable mix.

$$DP = \frac{P\_\#200}{P_{be}}$$

Where:

DP = Dust Proportion, (dust-to-binder ratio).
$P\_\#200$ = aggregate passing the #200 (75 μm) sieve, percent by mass of aggregate.
P_{be} = effective asphalt binder content, percent by total weight.

2.1.3.2 Stiffness:

The elastic stiffness in a pavement is a measure of a material ability to distribute the traffic loading over an area, The higher the elastic stiffness of the pavement and, hence, the individual layers the wider the area which reduces the level of strain experienced lower down in the pavement structure, dependent upon both the temperature and speed of loading.[2]

According to BS EN 12697-26:2018 [6]. The stiffness modulus is defined as the relationship between maximum applied stress and maximum measured strain response and expressed as:

$$E = \frac{\sigma}{\varepsilon}$$

where:

E = the elastic stiffness (modulus), in megapascals (MPa).
σ = the applied stress, in megapascals (MPa).
ε = the applied strain, in micrometre per meter or in microstrain (μm/m).

Another parameter is the complex modulus, which describes the relationship between stress and strain for a linear visco-elastic material submitted to a sinusoidal load wave form at time, *t*, where applying a stress $\sigma \times \sin(\omega \times t)$ results in a strain $\varepsilon \times \sin(\omega \times t - \Phi)$ that has a phase angle, Φ, with respect to the stress.

The amplitude of strain and the phase angle are functions of the frequency, *f*, and the test temperature, *Θ*.

The stress strain ratio defines the complex modulus E^* as:

$$E^* = E^*.(\cos(\Phi) + i.\sin(\Phi))$$

The complex modulus depends on the frequency f and the temperature θ. The complex modulus is characterised in two ways:

1- By the real component *E*1 and the imaginary components *E*2:

$$E_1 = |E^*|.\cos(\Phi)$$

$$E_1 = |E^*|.\cos(\Phi)$$

2- By the absolute value of the complex modulus |*E**| and the phase angle, Φ:

$$|E^*| = \sqrt{E_1^2 + E_2^2}$$

$$\Phi = \arctan\left(\frac{E_2}{E_1}\right)$$

Where:

E* = the visco-elastic complex modulus, in megapascals (MPa).

|E*| absolute modulus of the complex modulus, in megapascals (MPa).

*E*1 the real component of the complex modulus, in megapascals (MPa).

*E*2 the imaginary component of the complex modulus, in megapascals (MPa).

Φ the modulus phase angle of the material (argument), in degrees (°).

The later description is usually used in practice. In linear elastic multi-layer calculations for instance the E^* modulus is commonly used as input value for young's modulus.

To describe the correlation between stress and strain at the loading time, t, for a material exposed to controlled loading (force or displacement), the secant modulus is used:

$$E(t) = \frac{\sigma(t)}{\varepsilon(t)}$$

with stress, $\sigma(t)$, and strain, $\varepsilon(t)$, at time t.

- **Tests methods:**

The stiffness could be assessed using several practices:

- **Sinusoidal bending tests:**

The bending test options are:

2PB-TR: Two point bending application to trapezoidal specimens.
2PB-PR: Two point bending application to prismatic specimens.
3PB-PR: Three point bending application to prismatic specimens.
4PB-PR: Four point bending application to prismatic specimens.

- **Indirect tensile test (pulse or cyclic):**

The indirect tensile test options are:

IT-CY: Indirect tension pulse application to cylindrical specimens.
CIT-CY: Indirect tension cyclic application to cylindrical specimens.

- **Cyclic or monotonous uniaxial tests:**

The direct uniaxial test options are:

DTC-CY: cyclic tension-compression to cylindrical specimens.
DT-CY: monotonous direct tension to cylindrical specimens.
DT-PR: monotonous direct tension to prismatic specimens.

The method of stiffness testing employed throughout this work is the four point bending test (4PB-PR) test as given in the British Standard [BS EN 12697-26:2018]. A detailed description of the test and factors which affect it are given in next sections.

2.1.3.3 Permanent deformation:

Permanent deformation or rutting is the accumulation of little irretrievable strains in a material underneath perennial loading that ultimately cause a measurable rut to be developed. These tiny strains are because of the Visco-elastic response of bituminous materials to dynamic loading (Figure 5), and they accumulate over numerous applications of wheel passages to create an oversized deformation. A schematic of this is shown in Figure (6).

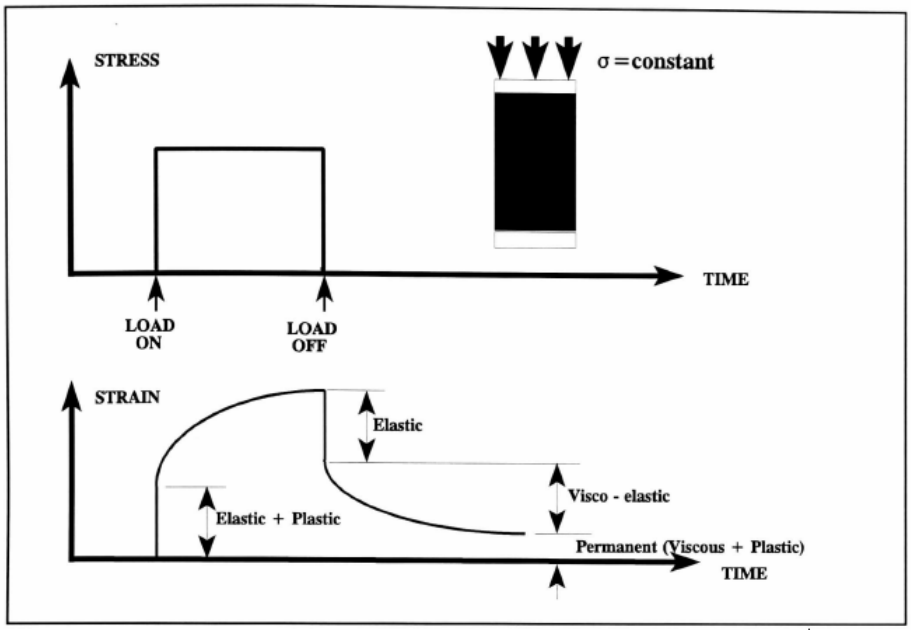

Figure 5 Generalized Strain Response to an Applied Stress Pulse

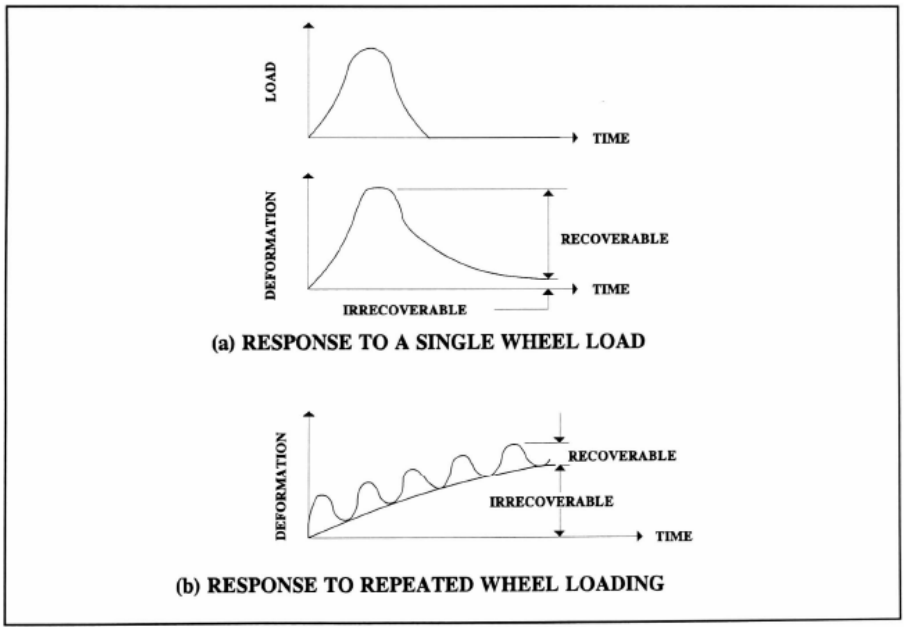

Figure 6 Visco-elastic Response to Millions of Wheel Loadings

2.1.3.4 Fatigue cracking:

Traditionally fatigue has been defined as:

"The phenomenon of fracture under repeated or fluctuating stress having a maximum value generally less than the tensile strength of the material."[7]

The previously mentioned definition has been employed to pavements by presuming that the appliance of wheel loads is the solely mechanism which may produce these continual stresses, and so strains. The magnitude of the tensile strain relies on the stiffness modulus and also the nature of the pavement. Speculative analysis and field studies have indicated that tensile strains are of the order 30 to 200 microstrain beneath a typical axle load at the bottom of the primary structural layer in a typical pavement construction. Consequently, under these conditions and applying the above definition, the likelihood of fatigue cracking exists. [2].

Fatigue cracking represents one of the most distresses liable for the decline within the service lifetime of pavements. Examining the fatigue is thus a field of investigation that has grown to be fundamentally crucial for improving the sturdiness of those structures.

Typically, the fatigue cracking comprises two key phases: crack initiation and crack propagation. Crack initiation is generally delineated because the coalition of micro-cracks to create a macro crack below the continual application of tensile strains. Crack propagation is the development of the macro crack across the fabric under further application of tensile strains.[2].

During a fatigue test, modulus value declines according to Figure (7), where three phases can be recognized:

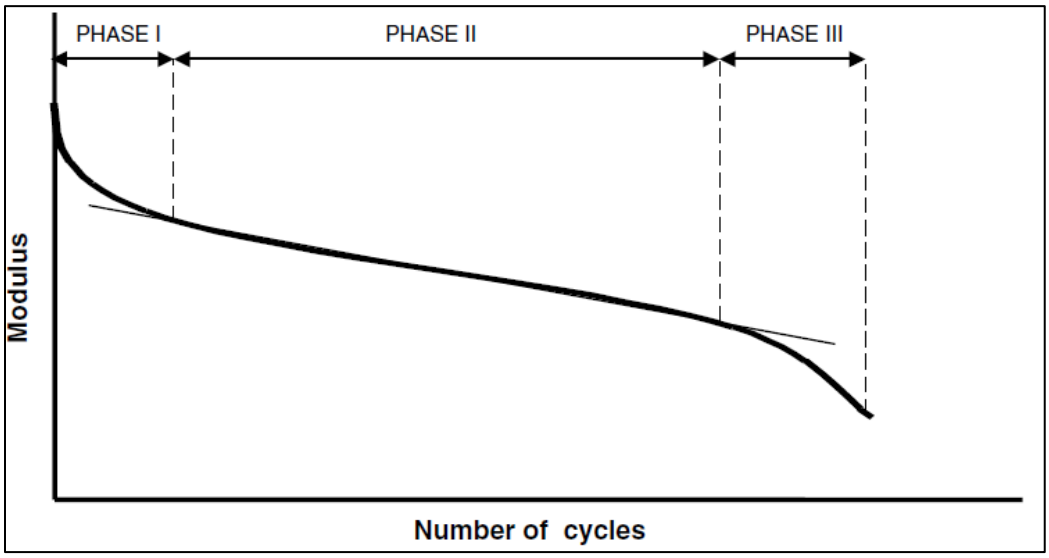

Figure 7 Modulus variation during a fatigue test

- Phase I: at the beginning of the test there is a rapid reduction of the modulus value.
- Phase II: modulus variation is approximately linear.
- Phase III: rapid decrease of the modulus value.

Widespread fatigue testing has been carried out since the first fifties and through this time a number of various test configurations have emerged. Nowadays, there are several tests to estimate the resistance to fatigue.

According to [BS EN 12697-24:2018][8]. “This European Standard specifies the methods for characterizing the fatigue of bituminous mixtures using alternative tests, including bending tests and direct and indirect tensile tests. The tests are performed on compacted bituminous material under a sinusoidal loading or other controlled loading, using different types of specimens and supports”.

These tests will be described in the following sections. However, this thesis will focus on the four point bending test, which will be presented in detail.

2.2 Fatigue tests across the standards

2.2.1 Introduction:

Fatigue phenomenon is one of the most important distresses in bituminous pavement structures, occurring beneath recurrent traffic loading. Repetition of loading leads to a loss of rigidity of the fabric, resulting in failure. Fatigue resistance of bituminous mixture is its ability to resist recurrent loading while not failure or crack. The lifetime of pavements is directly associated with this phenomenon, that should be properly studied so as to confirm adequate structural design.[9]

Even if fatigue has been examined by several researchers, this phenomenon remains not fully understood. numerous strategies are applied within the laboratory to characterize fatigue of bituminous mixtures, involving both homogenous and nonhomogeneous tests.

In the following section the characterization tests will be presented following the **European standards**, as well as the **American standards.**

2.2.2 Characterization methods:

Homogeneous tests have the advantage of enabling direct access to material behaviour with none back-calculation or hypothesis, that isn't the case for nonhomogeneous tests. sinusoidal loading is typically applied for determination of bituminous mixture fatigue properties. it's doable to regulate either constant axial strain amplitude (controlled strain mode) or constant axial stress amplitude (controlled-stress mode). In any case, the midvalue of strain and stress should be checked throughout cycles. as an example, considering a centred sinusoidal loading, this midvalue is controlled and remains equal to zero. however, in several studies, this midvalue doesn't stay null (either for controlled loading, if solely compression is applied or for response signal), making permanent strain accumulation, that results in failure. The fatigue phenomenon is then utterly hidden by the other phenomenon. Such tests mustn't be analysed as strictly fatigue tests.

Fatigue tests are usually carried out by employing the same equipment and configuration used for stiffness testing, however in fatigue tests we use a higher number of load cycles **until we damage the material**.

2.2.3 Fatigue characterization methods according to the [EN 12697-24:2018]:

2.2.3.1 scope:

“This European Standard specifies the methods for characterizing the fatigue of bituminous mixtures using alternative tests, including **bending tests** and **direct and indirect tensile tests**. The tests are performed on compacted bituminous material under a sinusoidal loading or other controlled loading, using different types of specimens and supports”[8]

The procedure is used to:

a) Classify bituminous mixtures on the premise of its fatigue resistance.

b) Manual to relative performance in the pavement.

c) Acquire data meant for assessing the structural behaviour of the road.

d) Judge test data according to specifications for bituminous mixtures

Because this European normative doesn't enforce a particular sort of testing device, the exact selection of the test configuration depends on the probabilities and the operating range of the device used. For the selection of specific test conditions, the constraints of the merchandise standards for bituminous mixtures have to be compelled.

2.2.3.2 Conventional criteria of failure:

According to the [EN 12697-24:2018], the failure criteria is defined as the number of load cycles, *N*f/50, when the absolute value of the complex stiffness modulus *S*mix (stiffness modulus) has decreased to half its initial value *S*mix,0

Note 1 to go: In this normative not exclusively the standard criteria of failure, based on the reduction of stiffness, is conferred. Also, different failure criteria like the prevalence of macro cracks or the energy-based failure mechanism are used.

Note 2 to go: Different test strategies and various failure criteria would possibly produce results that aren't comparable.

Note 3 to go: In a strain-controlled fatigue test the reduction to half of the initial stiffness is a gradual process. In a stress-controlled test in nearly all cases there will be a progressive failure of the sample.

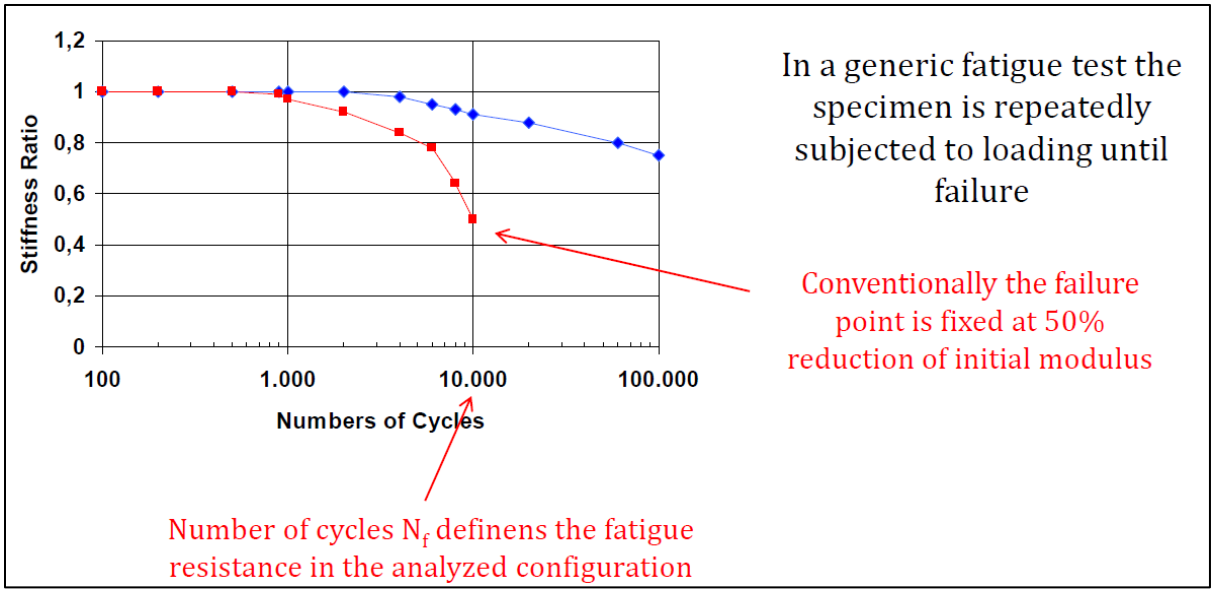

Figure 8 Conventional criteria of failure

It is experimentally observed that the number of cycles to failure (Nf) is related to the initial strain (εt) to which the material is subjected.

$\varepsilon_t = a.N_f^b$ Fatigue line in bi-logarithmic plane.

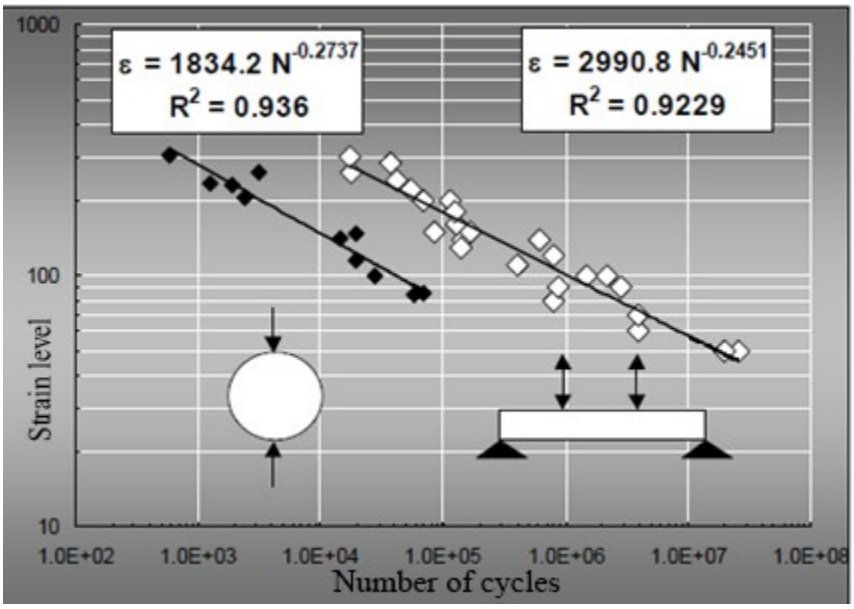

Figure 9 Example of fatigue curves

Each point corresponds to a single test carried out in different conditions (temperature, initial stress and / or strain, frequency). Different test configuration lead to different results.

Experimentally, it is observed that strain-controlled tests lead to higher number of cycles to failure than the stress-controlled tests.

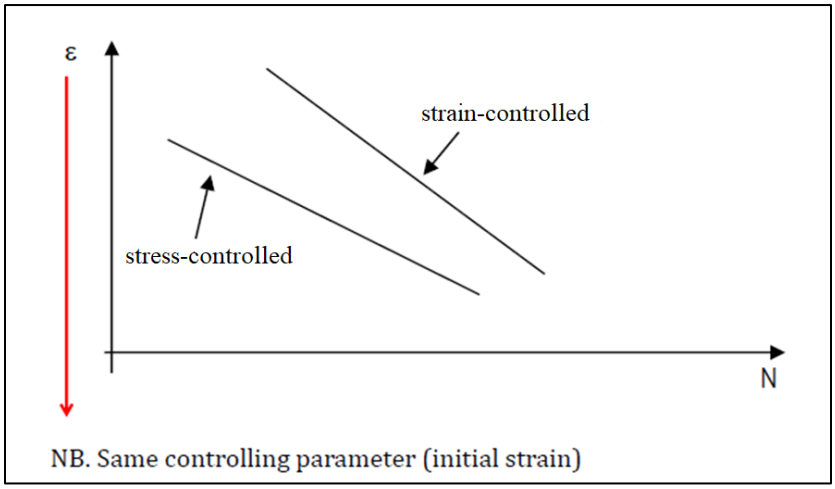

Figure 10 stress-strain controlled tests

2.2.3.3 Summary of the procedures:

All of the following tests will be briefly described, since it is not a main concern of this thesis, except the four-point bending test which will be addressed in detail.

The full testing protocol is described in the [EN 12697-24:2018][8]

- **Two-point bending test on trapezoidal shaped specimens (2PB-TR)**

"This method characterizes the behaviour of bituminous mixtures under fatigue loading with controlled displacement by two-point bending using trapezoidal shaped specimens. The method can be used for bituminous mixtures with a maximum aggregate size of up to 20 mm on specimens prepared in a laboratory or obtained from road layers with a thickness of at least 40 mm. For mixtures with an upper size D between 20 mm and 40 mm, the test can be performed using the same principle but with adapted specimen sizes. For a given frequency of sinusoidal displacement, the method shall be carried out on several elements tested in a ventilated atmosphere at a controlled temperature"[8]

An element test shall consist of:

- Enacting a constant amplitude sinusoidal displacement at the top of an isosceles trapezoidal console test piece, as shown in Figure (11)
- recording the change in the force at head amplitude relative to the reaction of the test piece.
- gauging the fatigue life of the test piece when the failure criterion is reached.

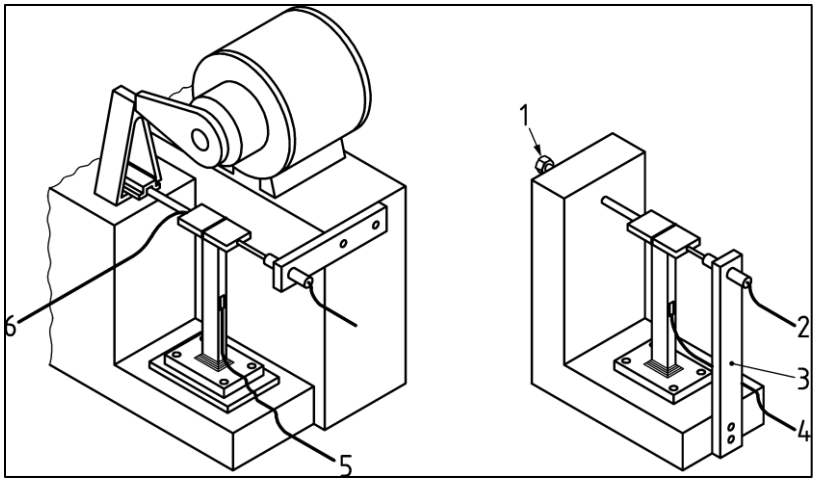

Figure 11 Sinusoidal displacement at the head of specimen

Key:

1- Screw to apply the deformation.
2- Displacement measurement.
3- Support.
4- Measured strain.
5- Recorded strain.
6- Recorded stress.

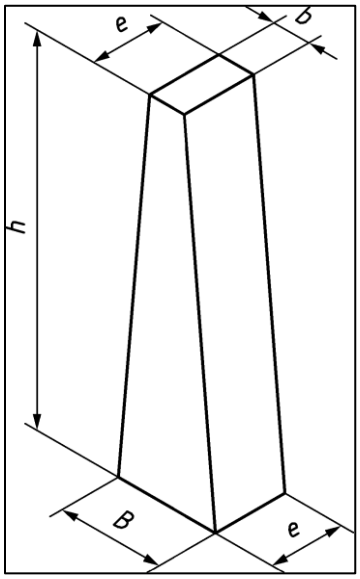

Figure 12 The trapezoidal shaped specimens

Dimensions of the specimens	Nominal maximum aggregate diameter in the mixture		
	$D \leq 14$ mm	$14 < D \leq 20$ mm	$20 < D \leq 40$ mm
B	56 ± 1 mm	70 ± 1 mm	70 ± 1 mm
b	25 ± 1 mm	25 ± 1 mm	25 ± 1 mm
e	25 ± 1 mm	25 ± 1 mm	50 ± 1 mm
h	250 ± 1 mm	250 ± 1 mm	250 ± 1 mm

Table 9 Dimensions of the 2PB-TR specimens

The test machine shall include a system enabling the applying of a sinusoidal displacement to the top of the specimen with constant frequency. The displacement shall vary but 0,12 µm/N throughout the test. The test machine shall be capable of applying the load to specimens at a frequency of (25 ± 1) Hertz and, if needed for special goals, at alternative frequencies ± 4 percent. If a frequency apart from 25 Hertz is employed, it ought to be enclosed within the test report. Results derived from tests at completely different frequencies may not be directly comparable.

The sample *i* will be pushed sinusoidally at its top at the enforced displacement amplitude ± 5 µm up to the failure criterion will been achieved. Between 100 cycles and 500 cycles, the response forces shall be recorded to ± 2 % and the average reaction force determined. The displacement *z*i shall be measured and *ε*i calculated for this element test. The number of cycles *N*i at the failure criterion shall be measured with a precision of 300 cycles.

The fatigue line of the mixture element tests at the various strain amplitude levels that the tests are performed shall be represented. The fatigue line shall be assessed in a dual decimal logarithmic system as a linear regression of fatigue life vs amplitude levels. Using these results, the strain corresponding to an average of one million cycles ε_6 and the slope of the fatigue line 1/b shall be defined. The standard deviation of the residual dispersion of fatigue life *sN* and the quality index relative to *ε*6, Δ*ε*6 may also be calculated.

The deformations *ε*i shall be selected so that either:

- The strain levels are roughly evenly spaced on a logarithmic scale.
- at least three strain levels, with a homogeneous number of at each level must be tested. The mean values shall be approximately regularly spaced on a logarithmic scale.

A minimum of 18 element tests must be carried out to estimate the result.

- **Two-point bending test on prismatic shaped specimens (2PB-PR)**

"This method characterizes the behaviour of bituminous mixtures under fatigue loading by 2-pointbending using square-prismatic shaped specimens. The method can be used for bituminous mixtures with a maximum aggregate size of up to 20 mm and on specimens prepared in a laboratory or obtained from road layers with a thickness of at least 40 mm" [8]

The test device shall carry with it a system allowing the applying of a sinusoidal displacement to the top of the specimen with a pre-defined frequency. The displacement shall vary less than 0,1 μm/N throughout the test. The test machine shall be capable of applying the displacement to specimens at a frequency of (25 ± 1) Hertz and, if needed for special goals, at different frequencies ± 4 percent. If a frequency aside from 25 Hertz is employed, it ought to be enclosed within the test report. Results obtained from tests at totally different frequencies don't seem to be directly comparable.

Dimensions of the specimens mm	Type of mixture	
	$D \leq 22$ mm	$D > 22$ mm
B	40 ± 1	80 ± 1
E	40 ± 1	80 ± 1
H	160 ± 1	320 ± 1

Table 10 Dimensions of the 2PB-PR specimen

Minimum of three levels of tension with a minimum of six duplicates per level must be carried out. The levels of tension shall be selected for the material in order to obtain a mean fatigue life of the series lies between 10^4 and 10^6 cycles for not less than 2 levels, and between 10^6 and 10^7 for a minimum of one level.

- **Three-point bending test on prismatic shaped specimens (3PB-PR)**

"This method characterizes the behaviour of bituminous mixes under fatigue loading, with controlled displacement by three-point bending using prismatic beam shaped specimens. The behaviour is characterized through the determination of the fatigue law in terms of strain (relation between strain and number of load cycles at failure) and the associated energy law. The method can be used for bituminous mixture specimens with maximum aggregate size of 22 mm or for samples from road layers with a thickness of at least 50 mm. For a given frequency of sinusoidal displacement, the method shall be carried out on several elements tested at a controlled temperature" [8]

An element test shall consist of applying a constant amplitude sinusoidal displacement to the mid-span point of a beam shaped specimen supported at both of its ends. The result shall be obtained from the correlation of the maximum initial strain at the mid-span section of the specimen, and the number of cycles needed to reduce to half the initial stiffness of the specimen. Throughout the element test, the strain at the mid-span section of the specimen shall be recorded regularly against the number of cycles.
Any machine could be used if it is occupied with a servo-hydraulic control press able to produce sinusoidal cyclic loading of the desired frequency and amplitude.

Test replicates shall be carried out on specimens taken from a homogenous group at different strain amplitudes. A fatigue line of the mixture under test shall be drawn by a rough calculation of the results of the element tests.

- **Indirect tensile test on cylindrical shaped specimens (IT-CY)**

"This method characterizes the behaviour of bituminous mixtures under repeated load fatigue testing using an Indirect Tensile Test (ITT). A cylindrical specimen manufactured in a laboratory or cored from a road layer can be used in this test. A cylinder shaped test specimen shall be subjected to repeated compressive loads with a (ha)versine load signal through the vertical diametral plane. This loading develops a relatively uniform tensile stress perpendicular to the direction of the applied load and along the vertical diametric plane, which causes the specimen to fail by splitting along the central part of the vertical diameter. The resulting horizontal deformation of the specimen shall be measured, and an assumed Poisson's ratio shall be used to calculate the tensile strain at the centre of the specimen. Fracture (fatigue) life shall be defined as the total number of load cycles before a fracture of the specimen occurs. Further failure criteria can be defined according to the dissipated energy during loading" [8]

The testing device shall allow applying repeated (ha)versine load pulses with rest periods at a load range of at least 15 kN with an accuracy of 0.25 %.

Sensor for measuring the displacements along the horizontal diametral plan, capable of measuring to an accuracy of at least ± 2 µm over a recommended measuring range of ± 2.0 mm.

The thermostatic chamber shall be capable of controlling a temperature range from −10 °C to 30 °C and with an accuracy of at least ± 0.5 °C.

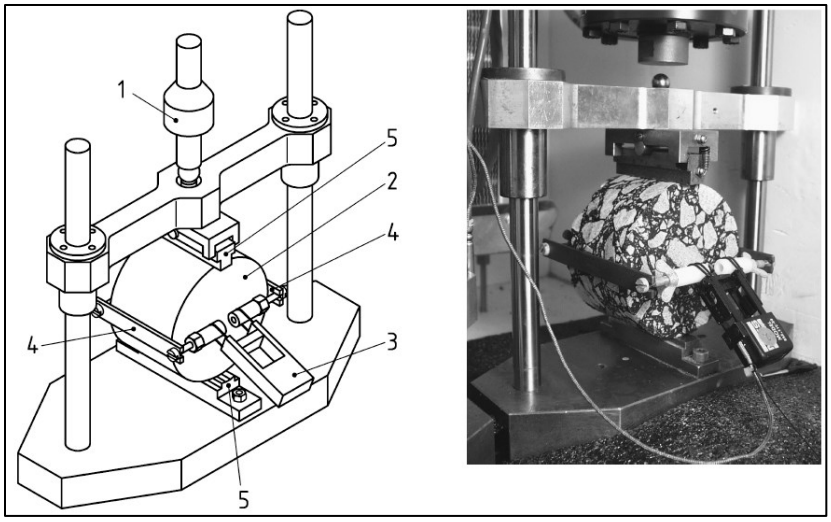

Figure 13 Indirect tensile test on cylindrical shaped specimens (IT-CY)

Key

1- load cell
2- asphalt specimen
3- extensometer
4- deformation strips
5- loading strips

15 to 18 specimens shall be prepared. The cylindrical specimens subject to the test shall be obtained in accordance with:

Laboratory Gyrator compactor according to [EN 12697-31] [10]
Cored samples from laboratory-prepared slab of asphalt according to [EN 12697-33] [11]
Cored samples taken from the road according to [EN 12697-27] [12]

The specimen shall have either:

- a thickness ≥ 40 mm and a diameter of (100 ± 3) mm for a maximum aggregate size of 16 mm; or

- a thickness ≥ 60 mm and a diameter of (150 ± 3) mm for a maximum aggregate size of between 16 and 32 mm.

- a thickness of ≥ 90 mm and a diameter of (150 ± 3) mm for a maximum aggregate size greater than 32 mm.

- The end sides of the specimens shall be plan parallel and at 90° to the surface of the specimen. A minimum divergence of less than 3° the right angle should be respected. The measurement shall be performed using a protractor at each end face at the quarter points on the circumferential line. The surfaces of the specimens shall be flat.

Approximately 70 µm/m to 400 µm/m initial tensile strain range is recommended for fatigue tests. The consequent fatigue life of the tested material shall fall within a range between 10^3 and 10^6 per number of load cycles.

A minimum of three stress levels must be carried out, with at least five replicates at every single level.

The fracture life could be assessed using two methods:

- Deformation method.
- Energy concept.

Deformation method

The fracture life is obtained from the relationship between log number of load cycles and the total horizontal deformation (Figure 14). The fracture life is at the intercept of the vertical line (1) with the horizontal axis.

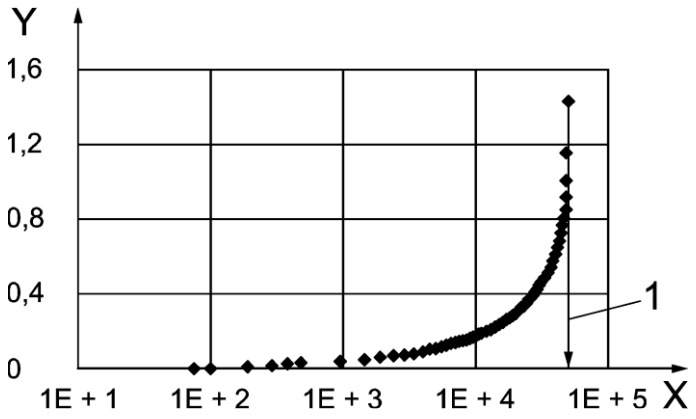

Figure 14 Determination of the fracture life of a specimen (Method 1)

Key

Y horizontal deformation in millimetres (mm).
X number of load cycles.
1 fracture life.

Energy concept

The fracture life is obtained from the relationship between decimal logarithm of the number of load cycles and the energy ratio. The fracture life is at the maximum energy ratio, shown in Figure (15)

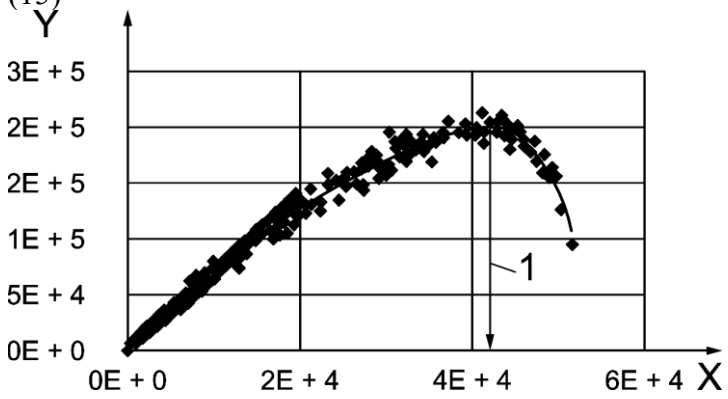

Figure 15 Determination of the fracture life of a specimen (Method 2)

Key

Y energy ratio in n/strain
X number of load cycles
1 fracture life

In Figure (16) the differences between the deformation and energy concept in the fatigue line determination is illustrated:

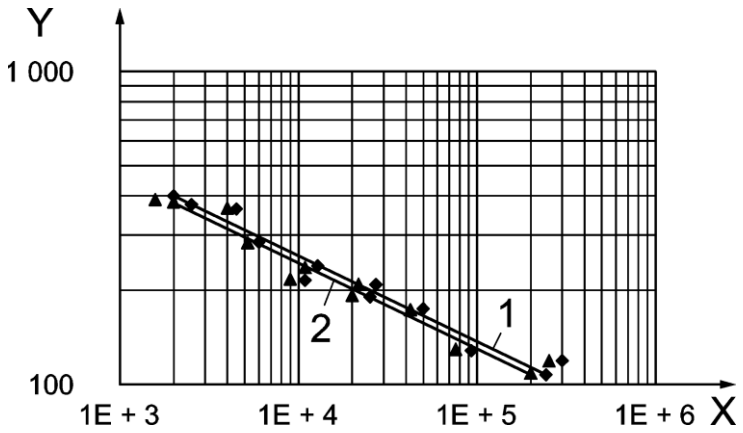

Figure 16 Initial total strain versus fracture life at different strain levels describing Method 1and Method 2

- **Cyclic indirect tensile test on cylindrical shaped specimens (CIT-CY)**

“A cylinder shaped test specimen shall be subjected to sinusoidal (cyclic) compressive load through the vertical diametral plane. This loading develops a relatively uniform tensile stress perpendicular to the direction of the applied load and along the vertical diametric plane, which causes the specimen to fail by splitting along the central part of the vertical diameter. The resulting horizontal deformation of the specimen shall be measured, and an assumed Poisson's ratio shall be used to calculate the tensile strain at the centre of the specimen. As failure criterion, the energy ratio concept based on dissipated energy shall be applied” [8]

A test equipment that allows a sinusoidal loading of the specimen among the desired accuracy shall be applied. A computer and software for measuring and saving the data are required.

The measuring system to record the horizontal deformation of the specimen ought to embody a minimum of 2 displacement transducers that required to be attached on to the specimen. The displacement transducers shall be positioned centrical on the cross sectional area of the specimen. The minimum measuring range for displacement transducers shall be 4 millimetre (each displacement transducer 2 mm) with an accuracy of 1,0 µm. Additionally, for test control the vertical specimen deformation shall be assessed by displacement transducers. The measuring range for displacement transducers shall be a minimum of 7 millimetre with associate degree of accuracy of at least 1 µm.

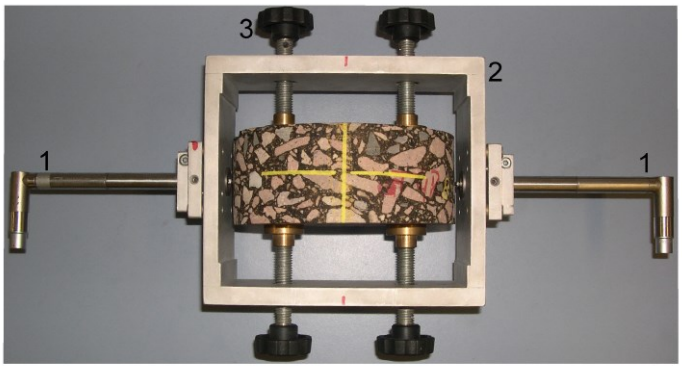

Figure 17 Example for the measurement of the horizontal deformation – frame with LVDTs

Key

1- LVDT
2- Frame
3- Set screws to fix the frame to the specimen

Thermostatic chamber, in which the required test temperature can be maintained within an accuracy of ± 0.5 °C in the vicinity of the specimens.

The cylindrical specimens subject to the test shall be obtained in accordance with:

Cored specimen from laboratory-prepared slab of asphalt according to [EN 12697-33] [11]
Gyrator compaction according to [EN 12697-31] [10]
Cored specimen taken from the road according to [EN 12697-27] [12]

Cored samples must be extracted from the pavement in longitudinal direction. The layers must be divided by sawing if the cores are taken from the pavement comprising several layers. The sample dimensions should conform with the obligations listed in Table (11). Damaged specimens shall be averted. Only intact specimens shall be tested.

Maximum grain size mm	**Specimen diameter** Ω mm	**Specimen height** h mm
≤ 16	100 ± 3	40 ± 2
> 16 to < 32	150 ± 3	60 ± 2
≥ 32	150 ± 3	90 ± 2

Table 11 Specimen dimensions foe the cyclic indirect tensile test on cylindrical

The test temperature is usually +20 °C.
Conditioning to test temperature must be prior to testing. The length of conditioning period is depending on the sample size and the tested material. The temperature in the sample must be fixed within ± 1 °C of the test temperature for a minimum of 10 minutes.

A cyclic vertical load shall be applied until the sample fails. This load is characterized by a specific frequency, lower force level and force amplitude. The loading must be interrupted when the vertical deformation goes above 7 mm. Through the test, the load and horizontal deformation shall be scrutinised continually and noted at pre-selected intervals to allow the estimation of the horizontal strain and stiffness modulus progress during the whole test.

The fracture life is found from the relationship between the number of load cycles and the energy ratio. The fracture life is at the maximum energy ratio, shown in Figure (18).

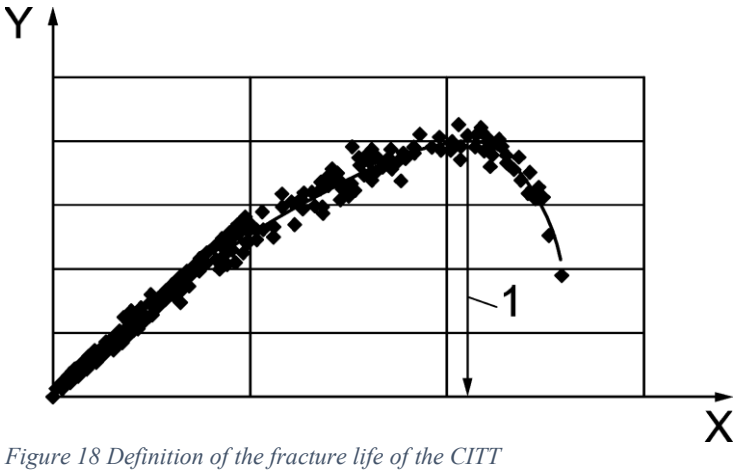

Figure 18 Definition of the fracture life of the CITT

Key
Y energy ratio.
X number of load cycles.
1 fracture life.

2.2.4 Four point bending machine.

- **Four-point bending test on prismatic shaped specimens (4PB-PR)**

"This method characterizes the behaviour of bituminous mixtures under fatigue loading using four-point-bending test equipment in which the inner and outer clamps are symmetrically placed, and slender rectangular shaped specimens (prismatic beams) are used. The prismatic beams shall be subjected to four-point periodic bending with free rotation and translation at all load and reaction points. The bending shall be realized by loading the two inner load points (inner clamps) in the vertical direction, perpendicular to the longitudinal axis of the beam. The vertical position of the end bearings (outer clamps) shall be fixed. This load configuration shall create a constant moment, and hence a constant strain, between the two inner clamps. The load shall be applied in the form of a sine function. During the test, the load required to bend the specimen, the deflection, and the phase lag between these two signals shall be measured as a function of time. Using these measurements, the fatigue characteristics of the material tested shall be determined" [8]

Two inner and two outer clamps shall be evenly located with respect to the centre of the prismatic sample. Constant and equal loads shall be applied at the middle third. All of the applied force, deflection and phase lag shall be recorded. The fatigue life of the test sample shall be estimated according to the chosen failure condition, as will be described in the following chapters.

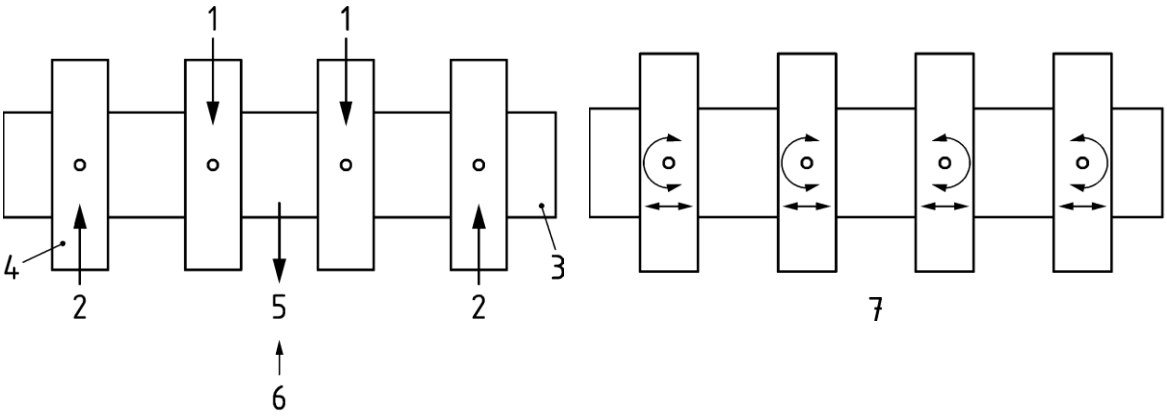

Figure 19 Basic principles of 4-point bending

Key

1- Applied load.
2- Reaction.
3- Specimen.
4- specimen clamp.
5- Deflection.
6- Return to original position.
7- Free translation and rotation.

- **Test machine**

The machine which is employed for this thesis is able to apply a sinusoidal load to a sample by an appropriate mechanism thanks to the two inner clamps attached on the specimen (Figure 21). The frequency of the load shall be between 0,1 to 60 Hz with an accuracy of 0,1 Hertz. **In our case we used a constant frequency of 10 Hertz**. The equipment is made of corrosion-resistant metal. Furthermore, the testing system is equipped with a system to monitor the loading mode of the sample in order to meet the specifications for the implementation of the test. The load cell has a measuring range of ± 2 000 N and conforms with the requirements for transducers of accuracy class 0,2. The measurement of the force is taken place in the mid-third area, and the measurement of the displacement is taken at the bottom surface of the sample (Inversed LVDT) between the two inner clamps. The displacement transducer has a measuring range of ± 1.0 mm fulfilling the specification for transducers of accuracy class 0.2

The deflection is measured at the centre of the bottom surface. In order to verify the necessary pure bending of the sample, the deflections of the two inner clamps are also be measured.

Figure 20 Four point bending machine with thermostatic chamber

- **Clamping device**

The clamping device is an equipment able of securing the sample (beam) in the bending frame so to provide horizontal translation and rotation at the four supports. The outer and inner clamps are designed to enable rotation freedom and horizontal translation of the beam within the clamps. The assumed pure bending in the middle third is checked by measuring the deflections at the inner clamp, $x = A$, and in the middle of the specimen, $x = L/2$.

Distance (A) should be selected in the range 0,25 < A/L < 0,4 and if possible close to one third of the effective length L (ASTM configuration). Here, the ratio will be 1,15. If A/L is chosen outside this range.

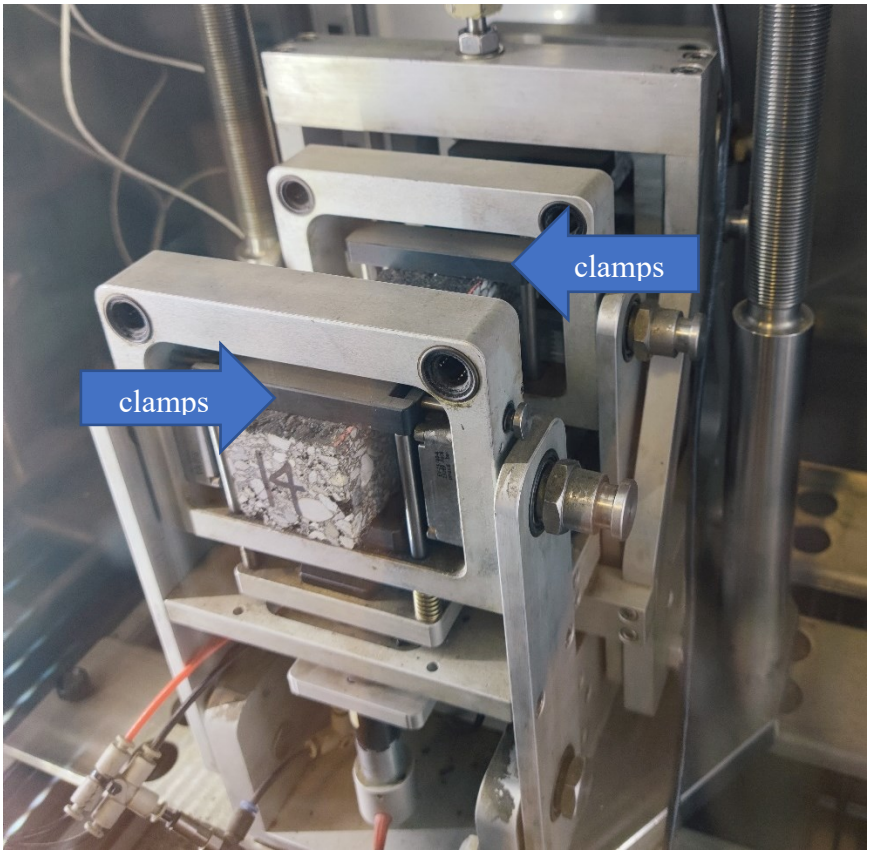

Figure 21 Clamping device

- **Thermostatic chamber**

Our thermostatic chamber is capable of keeping the mean temperature of the air flow at least 10 mm from the sample with an accuracy of ± 1 °C (during the testing period). Regulation shall be to an accuracy of 0.5 °C.

- **Electronic data registration equipment**

We have an electronic data acquisition system where transducer signals are amplified by low-noise amplifiers, so that a value of 10 V or ± 10 V corresponds to the full-scale deflection of the measuring scale of the transducer.

Output outlets are provided for connecting data acquisition and processing instruments. A resolution of 1 N for the force and 0.1 μm for the deformation is adopted with an accuracy class 0.2 %.

For the calculation of the strain, stress, dynamic stiffness modulus and (material) phase lag, the values of the frequency components at the test frequency are also recorded.

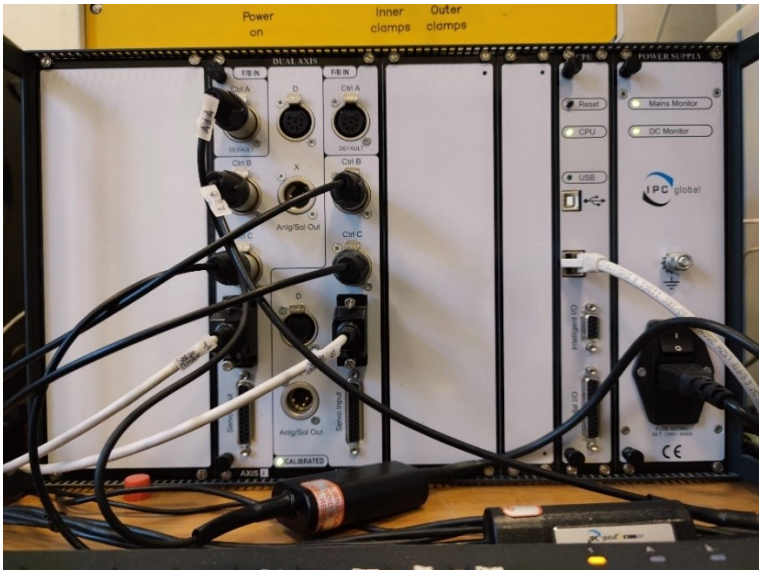

Figure 22 Electronic data registration equipment

- **Specimen Dimensions**

The beams have a prismatic shape with the following nominal proportions and tolerances:

- total length does not go above the effective length by more than 10 %.

(**The effective length of our testing device is 380.5 mm**)

- the difference between maximum and minimum measured value of the width and of the height is not greater than 1.0 mm ; the difference between minimum and maximum measured value of the length shall not be greater than 2.0 mm. (**beams fail to satisfy those limits were discarded**)

- The angle between adjacent longitudinal surfaces does not deviate from a right angle by more than 1°.

- The effective length *is* not less than six times whatever the highest value is for the width or the height.

- The width and the height are always more than three times the maximum grain size in the tested material.

The full length is determined four times with a ruler with an accuracy of 1.0 mm in the centre of the top and the bottom surfaces. The height and the width are measured with vernier callipers with an accuracy of 0.1 mm **at the places where the clamps are to be installed** ($x = 0$, $x = A$, $x = L - A$, $x = L$). The length of the test specimen is calculated as the arithmetic mean of the length measurements. The width and the height of the specimen are calculated similarly. **Beams not fulfilling the specimen specification are not tested**.

Figure 23 Four point bending beams

Figure 24 4PB measurement points

- **Sawing**

The beams are attained by cutting from slabs made in laboratory from the wheel compactor. From each slab we obtained three beams. Those beams are verified later in terms of density and voids ratio. The longitudinal axis of the beam shall be parallel with the axis of compaction.

The beams are checked visually for concerning non-homogeneity, compaction, void content, or the presence of large aggregate particles. **Beams with obvious irregularities are excluded.**

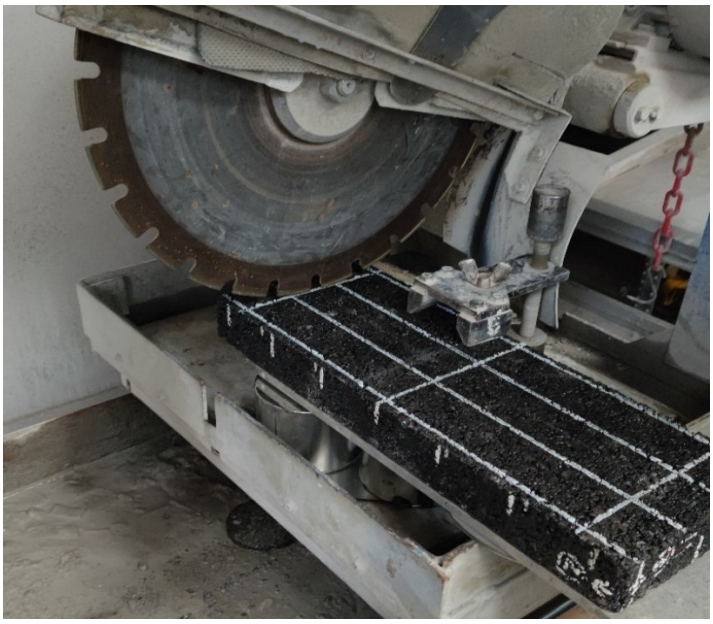

Figure 25 Slab sawing

- **Procedure**

The beams, thermostatic chamber and the loading equipment are set to the test temperature prior to the test. The minimum required conditioning time of the beams is shown in Table (12). For our case we used minimum 1 hour conditioning since our testing temperature is 20 °C.

Test temperature °C	**Time** h
0	2
20	1

Table 12 Minimum time required to bring specimens to test temperature

The beam with the two outer and two inner clamps shall be attached into the load frame. The beam is then pushed sinusoidally at the chosen frequency *(10Hz)* at the initial imposed strain level. The necessarily force is applied through the load frame connected to the two inner clamps. The strain controlled loading mode is guaranteed by a view of the measured force or displacement. The force, displacement and phase lag are recorded in the first 100 cycles (Cycles of the initial stiffness) and regularly thereafter (logarithmic capture).

The initial value of the modulus Smix is calculated at the hundredth cycle (n = 100). The fatigue test is carried out until the calculated modulus Smix dropped to 80% of its initial value (20% residual stiffness)

- **Choice of test conditions**

For a given temperature and frequency, the test is performed three levels (140, 200, 300) in the strain-controlled with six replicates per level. The levels for the chosen loading mode are chosen in such a way that the fatigue lives are within the range 10^4 to $2x10^6$ cycles.

- **Data processing**

Using the obtained data of the force, deflection, and phase lag between these two signals measured at load cycles n(i), the relevant results shall be calculated using the formula given in 3.5. The relevant test results shall be tabulated and graphically presented and related to the load cycle number $n(i)$ at which they are measured. These test results are:

- strain amplitude.
- stress amplitude.
- modulus of the complex modulus (dynamic stiffness modulus).
- (material) phase lag.
- dissipated energy per cycle.
- cumulated dissipated energy up to cycle $n(i)$.

- **Calculation and expression of results**

On the basis of the results representing the length of life $N_{i,j,k}$ for the chosen failure criteria j and the set of test conditions k, the fatigue line is drawn by making a linear regression between the decimal logarithms of $N_{i,j,k}$ and the decimal logarithms of the initial strain amplitude (strain amplitude at the 100th cycle). The shape of the fatigue line is expressed in the following formula:

$$\log\left(N_{i,j,k}\right) = A_0 + A_1.\log(\varepsilon_i)$$

where:

i is the specimen number.
j represents the chosen failure criteria.
k represents the set of test conditions.
ε_i is the initial strain amplitude measured at the 100th load cycle.

The most important outcome of this test is the strain correspondent with a fatigue life of 10^6 cycles, for the chosen failure criteria and set of test conditions since this ε_6 is considered a crucial input parameter for pavement design.

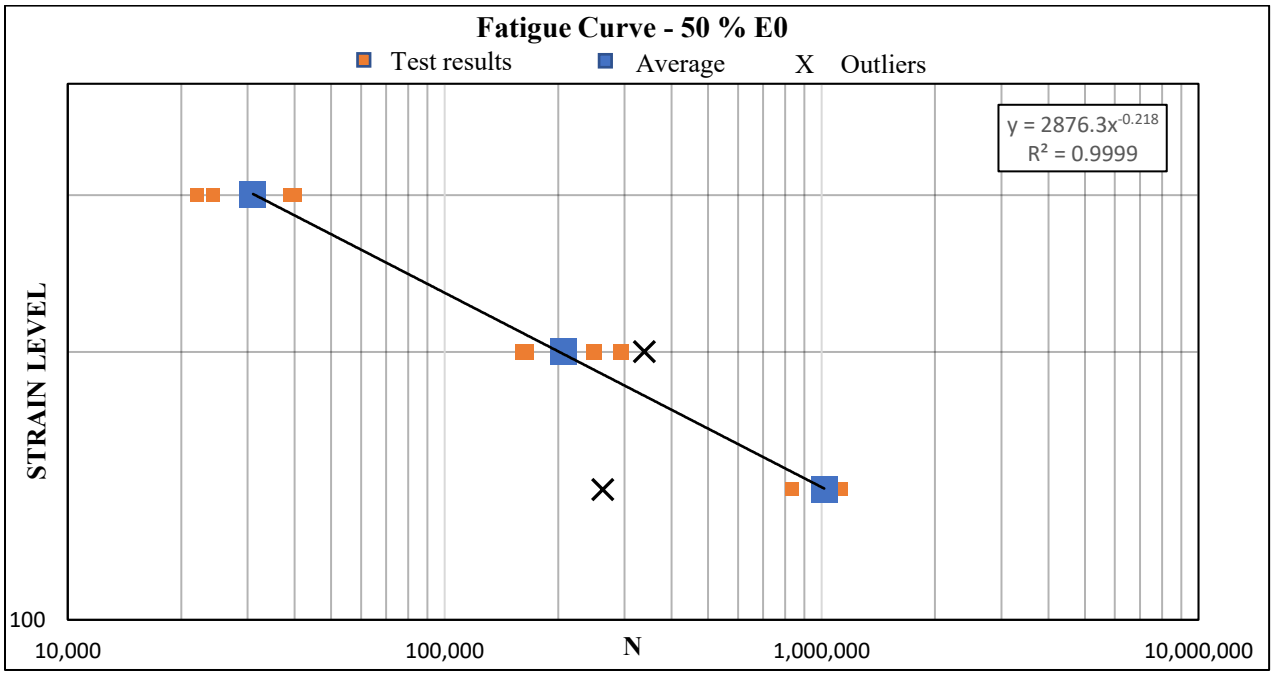

Figure 26 Typical fatigue curve

2.2.5 Fatigue tests in the American standards

The aim of this thesis is to characterize the fatigue of bituminous mixtures according to the European standards; however, a brief of the American characterization methods will be introduced.

We can characterize the fatigue of bituminous mixtures according to the American standards, i.e.: American Society for Testing and Materials (ASTM), and American Association of State Highway and Transportation Officials (AASHTO). 23

2.2.5.1 Fatigue characterization in the "ASTM"

- **Standard Test Method for Determining Fatigue Failure of Asphalt-Aggregate Mixtures with the Four-Point Beam Fatigue Device:**

- **scope**

According to the last **designation: D8237−21.** "This test method provides a procedure for determining a fatigue curve that is developed using three or more strain levels. The resulting data can be used in the fatigue models for mechanistic-empirical pavement design (that is, Pavement ME). Failure points are determined for estimating the fatigue life of 380 mm long by 50 mm thick by 63 mm in breadth (width) asphalt mixture beam (rectangular prism) specimens sawed from laboratory or field-compacted asphalt mixture, which are subjected to repeated flexural bending"[13]

- **Summary of test method**

It is a flexural bending test carried out on compacted prismatic beam samples to assess the fatigue properties of viscoelastic asphalt mixtures using a fixed reference target. A cyclic sinusoidal loading form is introduced with no rest periods from the start position. A completely peak-to-peak displacement is induced at the articulating H-frame mid third. The outer third points are detained in an articulating fixed spot around the neutral axis of the beam. The test in conventionally performed at frequency of 10 Hertz and a test temperature of 20 °C. This results in a constant bending moment at the middle span from 119 mm 60.5 mm (distance may differ between producers). The strain level is defined ahead as an input value for the device peak-to-peak deflection. This deflection at middle point location of a beam specimen is controlled by the closed-loop control system measured from the target position (neutral axis). The peak-to-peak deflection is measured in correspondence to a secure reference point placed at the outer articulating fixed position.

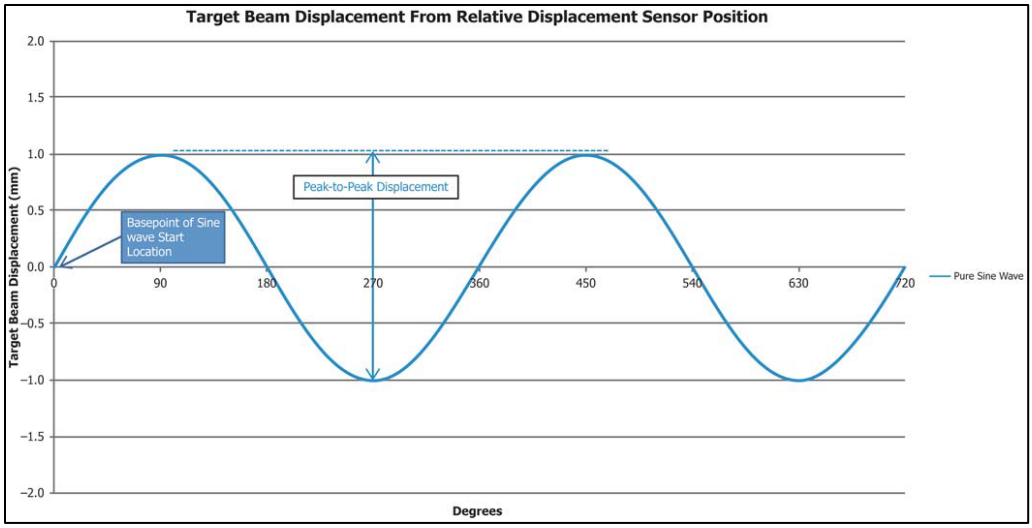

Figure 27 Illustration of Actuator Response of Repeated Sinusoidal Peak-to-Peak Defection

- **Significance and use:**

The in-LAB fatigue lifespan estimated by this normative for beam samples is used to calculate the fatigue life of asphalt mixtures subjected to recurrent traffic loading. Even if the field performance of those mixtures is affected by many factors (traffic configuration, loading rate, lateral wander, climate disparity; rest periods between loads, aging, etc.), it has been more precisely foretold when laboratory properties are identified besides an evaluation of the applied strain level at the layer depth by the traffic wheel load application over the pavement.

Note:

The data quality presented by this normative are reliant on the skill of the technician, the procedure and the competence, calibration, and maintenance of the used device.

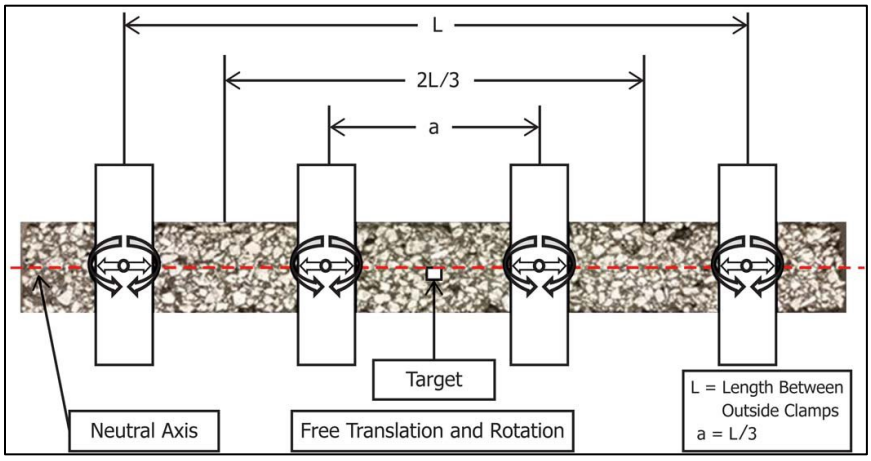

Figure 28 Specimen Articulation and Dimensioning (4PB-ASTM)

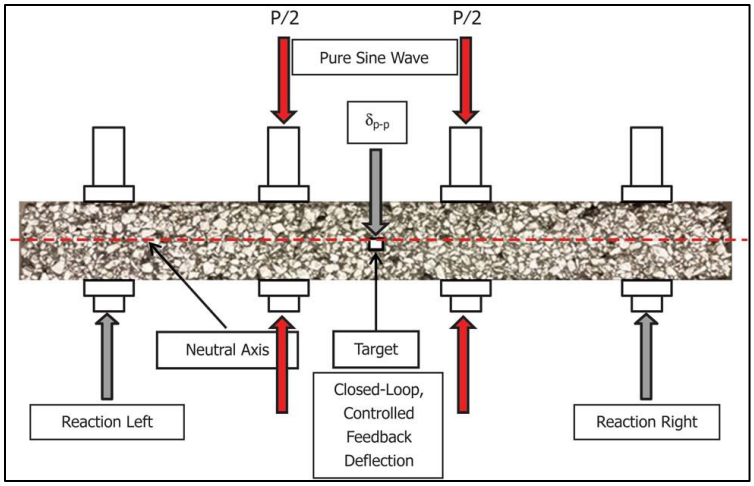

Figure 29 Load Characteristics of Fatigue Test Apparatus Illustrated as Pure Sine Wave (4PB-ASTM)

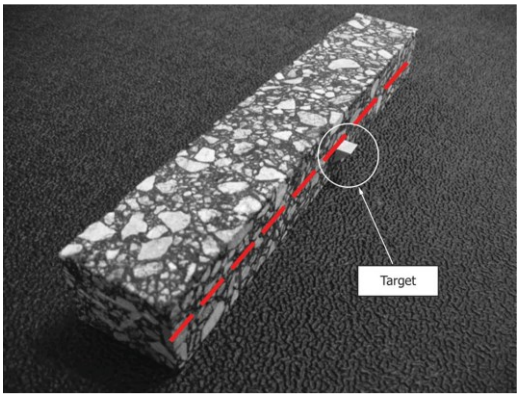

Figure 30 Target Attached to the Beam Neutral Axis (Mid-Height, Mid-Length) (4PB-ASTM)

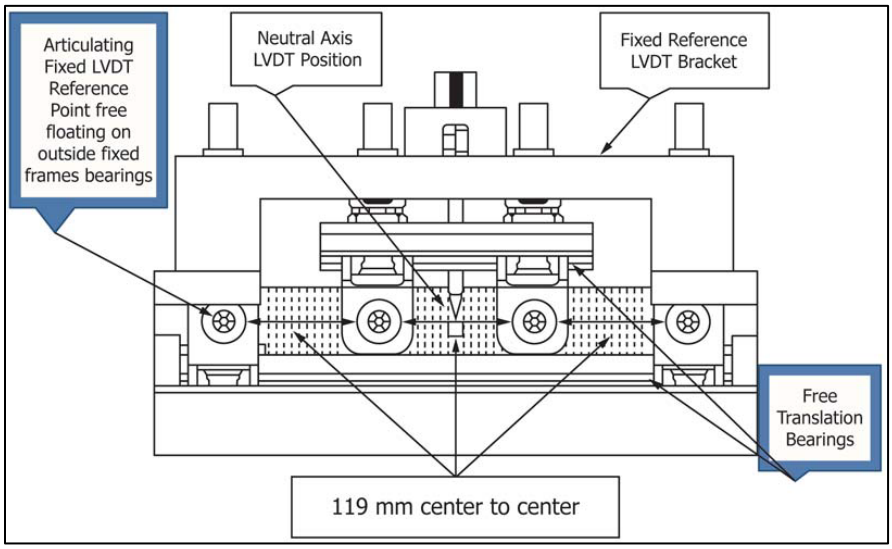

Figure 31Schematic of Fixed Reference Displacement Sensor of Flexural Beam Fatigue Test Apparatus (Side View) (4PB-ASTM)

- **Sampling and Test Specimen Preparation:**

"Laboratory-Mixed and Compacted Specimens—Sample asphalt binder in accordance with Practice D140/D140M, and sample aggregate in accordance with Practice D75/D75M. **If a complete fatigue curve is desired, prepare six to nine replicate asphalt mixture beam specimens**, compacted in accordance with Practice D7981 or D8079, or active AASHTO compaction standards for slab(s) or beam(s). Otherwise, prepare as many specimens as desired for individual beam test results. Laboratory-prepared mixtures are conditioned with a short-term oven aging (STOA) process, such as defined in Section 7.2 of AASHTO R 30 (condition loose mixture for 4 h at 135 °C). Determine the theoretical maximum specific gravity in accordance with Test Method D2041/D2041M. Determine the bulk specific gravity in accordance with Test Method D2726/D2726M. Calculate the percent air voids in accordance with Test Method D3203/D3203M. Test at least six replicate asphalt mixture beam specimens at different strain levels in order to develop a fatigue curve. The extra specimens may also be tested as desired if the data appears to include an outlier or if a beam failure occurs directly at a clamp. A linear relationship on a log-log plot exists between Nf and the level of tensile strain (με, micro strain = strain × 10^6)" [13]

2.2.5.2 Fatigue characterization in the "AASHTO"

- **Standard Method of Test for Determining the Damage Characteristic Curve and Failure Criterion Using the Asphalt Mixture Performance Tester (AMPT) Cyclic Fatigue Test:**

- **Scope**

According to the AASHTO Designation: "TP 107-18 $(2020)^1$, This test method covers procedures for preparing and testing asphalt concrete mixtures to determine the damage characteristic curve and failure criterion via direct tension cyclic fatigue tests in the Asphalt Mixture Performance Tester (AMPT). This standard is applicable to laboratory prepared specimens of mixtures with nominal maximum size aggregate less than or equal to 25.0 mm (0.98 in.). Mixtures with a nominal maximum aggregate size greater than or equal to 25.0 mm (0.98 in.) may experience lower success rates" [14]

- **Summary of test method**

A displacement-controlled actuator and recurring cyclic loading is applied to a cylindrical asphalt concrete sample till the failure is reached. The induced stress and on-specimen axial strain response are recorded and used to estimate the needed quantities. The relationship between the damage (S) and the pseudo secant modulus (C) is calculated and stated as the damage characteristic curve. **It is crucial to consider this normative connect to direct tension testing in an AMPT**. Test manufactures will vary if using other equipment and it is suggested more dedicated measures be established for these loading devices.

The equations used to calculate the pseudo strain, pseudo secant modulus, damage parameter, and failure criterion for the fatigue test specimens are found in the **AASHTO Designation: TP 107-18 (2020)[1],** calculation section.

- All the calculations can be automatically performed using the AMPT control software, ALPHA-Fatigue software, or the FlexMAT-Cracking spreadsheet defined in the FHWA report.

- **Significance and use:**

The damage characteristic curve represents the vital relationship between damage and material integrity for asphalt concrete mixtures. This property is independent of temperature, frequency, and mode of loading. Jointly with the linear viscoelastic properties of asphalt concrete, the damage characteristic curve can be used to examine the fatigue characteristics of asphalt those mixtures. Damage characteristic curves can also be combined with the failure criterion and further pavement response models to forecast the fatigue behaviour of in-service asphalt concrete mixtures.

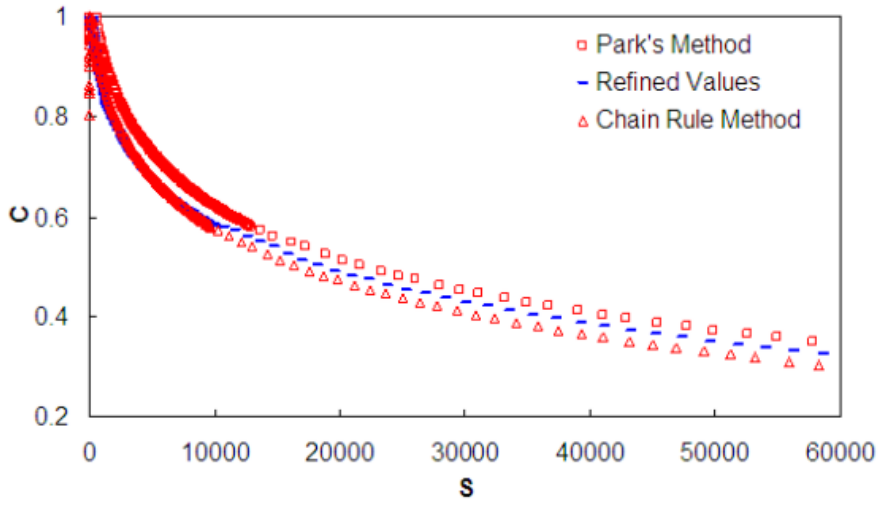

Transportation Research Board, National Academy of Science. From *Appendixes to NCHRP Report 547: Sample Performance Tests and Advanced Materials Characterization Models* (2005)

Figure 32 Typical damage characteristic curve

- **Apparatus**

Asphalt Mixture Performance Tester or any equivalent system meeting or surpassing the requirements of Equipment Specifications for the Simple Performance Test System, NCHRP Report 629, Appendix E, with the additional capability to conduct direct tension testing, as shown in Figure (33).

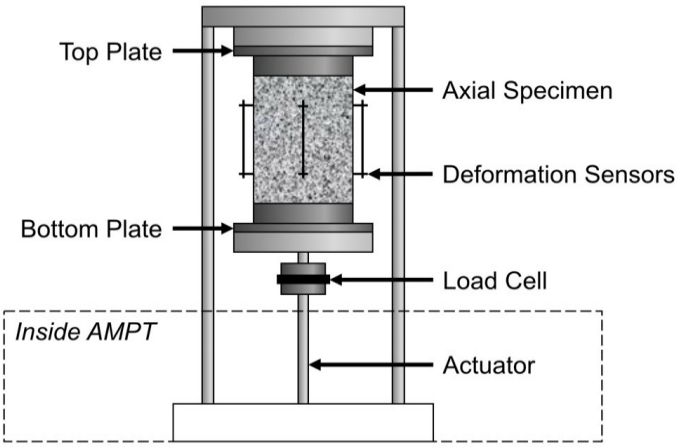

Figure 33 General Schematic of Direct Tension Test Setup

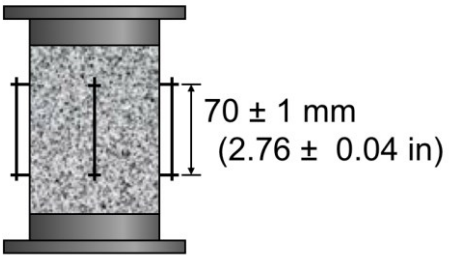

Figure 34 General Schematic of Gauge Points

- **procedure for estimating on-specimen strain levels in the AMPT**

Strain levels for fatigue tests are estimated based upon the **fingerprint dynamic modulus** of the mixture, as shown in Table (13).

The first thing is to perform a fingerprint dynamic modulus test, from which we can estimate |E*|fingerprint. Then we should use table X1.1 to estimate the programmed actuator micro strain.

Fingerprint Dynamic Modulus (units in MPa)	ε_{os1} (units in microstrain)
$\lvert E^* \rvert_{fingerprint} > 8{,}800$	300
$4{,}400 < \lvert E^* \rvert_{fingerprint} < 8{,}800$	500
$\lvert E^* \rvert_{fingerprint} < 4{,}400$	800

Table 13 Target On-Specimen Strain Levels for the First Specimen

Based on the estimated number of cycles to failure Nf for the first test specimen, we can use the following table to select a target on-specimen strain level for the following samples. Relying on the database used to develop this procedure, the mixture should be located within one of the families of curves in Table X1.1.

The intent is to choose different strain levels to get a range of cycles to failure which are properly spread out in loglog space for successive fatigue analyses. Because there is difficulty of finding exact Nf values, it is impossible to deliver fixed guidance on strain selection procedures. If this approach does not produce a satisfactory range of Nf values, users are fortified to regulate the strain inputs in increments of about 50 µs to acquire values in an acceptable range.

Table X1.1—Tool for Identifying Target On-Specimen Strain Levels for Second, Third, and Fourth Specimen of a Mixture Set. Note underlined a values only correspond to the example described in Section X1.5.

Target On-Specimen Microstrain	**If the $\|E^*\|_{fingerprint}$ is greater than 8,800 MPa, select 300 microstrain as the first specimen's strain**				**If 8,800 > $\|E^*\|_{fingerprint}$ > 4,400 MPa, select 500 microstrain as the first specimen's strain**					**If the $\|E^*\|_{fingerprint}$ is less than 4,400 MPa, select 800 microstrain as the first specimen's strain**			
Estimated cycles to failure for test specimen													
200	62,500	129,000	258,700	503,800	-	-	-	-	-	-	-	-	-
250	4,200	11,000	27,200	64,500	145,900	315,000	-	-	-	-	-	-	-
300	**500**	**1,500**	**4,300**	**12,000**	31,500	77,500	180,000	-	-	-	-	-	-
350	-	-	900	2,900	8,600	23,700	60,800	144,800	-	-	-	-	-
400	-	-	-	850	2,800	8,500	23,700	61,000	144,500	-	-	-	-
450	-	-	-	-	1,000	3,400	*10,500*	28,500	71,400	163,500	-	-	-
500	-	-	-	-	**500**	**1,500**	***4,900***	**14,400**	**38,000**	91,000	-	-	-
550	-	-	-	-	-	750	*2,500*	7,800	21,500	53,500	119,600	-	-
600	-	-	-	-	-	-	*1,400*	4,400	12,800	33,000	75,850	155,700	-
650	-	-	-	-	-	-	800	2,600	7,900	21,000	49,900	104,600	-
700	-	-	-	-	-	-	-	1,600	5,100	14,000	33,900	72,400	136,400
750	-	-	-	-	-	-	-	1,000	3,400	9,500	23,600	51,400	98,000
800	-	-	-	-	-	-	-	700	2,300	**6,700**	**16,900**	**37,300**	**72,000**
850	-	-	-	-	-	-	-	-	1,600	4,800	12,300	27,600	53,900
900	-	-	-	-	-	-	-	-	1,200	3,500	9,100	20,800	41,000
950	-	-	-	-	-	-	-	-	800	2,600	6,900	15,900	31,600
1,000	-	-	-	-	-	-	-	-	-	1,900	5,300	12,300	24,700
1,050	-	-	-	-	-	-	-	-	-	1,500	4,100	9,700	19,600
1,100	-	-	-	-	-	-	-	-	-	1,100	3,200	7,700	15,700
1,150	-	-	-	-	-	-	-	-	-	900	2,500	6,200	12,700
1,200	-	-	-	-	-	-	-	-	-	-	2,000	5,000	10,300
1,250	-	-	-	-	-	-	-	-	-	-	1,600	4,100	8,500
1,300	-	-	-	-	-	-	-	-	-	-	1,300	3,300	7,000

Table X1.1—Tool for Identifying Target On-Specimen Strain Levels for Second, Third, and Fourth Specimen of a Mixture Set. *(Continued)*

Target On-Specimen Microstrain	If the $\|E^*\|_{fingerprint}$ is greater than 8,800 MPa, select 300 microstrain as the first specimen's strain				If 8,800 > $\|E^*\|_{fingerprint}$ > 4,400 MPa, select 500 microstrain as the first specimen's strain					If the $\|E^*\|_{fingerprint}$ is less than 4,400 MPa, select 800 microstrain as the first specimen's strain			
	Estimated cycles to failure for test specimen												
1,350	-	-	-	-	-	-	-	-	-	-	1,100	2,800	5,900
1,400	-	-	-	-	-	-	-	-	-	-	900	2,300	4,900
1,450	-	-	-	-	-	-	-	-	-	-	750	2,000	4,200
1,500	-	-	-	-	-	-	-	-	-	-	-	1,700	3,600
1,550	-	-	-	-	-	-	-	-	-	-	-	1,400	3,000
1,600	-	-	-	-	-	-	-	-	-	-	-	1,200	2,600
1,650	-	-	-	-	-	-	-	-	-	-	-	1,000	2,300
1,700	-	-	-	-	-	-	-	-	-	-	-	900	2,000
1,750	-	-	-	-	-	-	-	-	-	-	-	750	1,700
1,800	-	-	-	-	-	-	-	-	-	-	-	-	1,500
1,850	-	-	-	-	-	-	-	-	-	-	-	-	1,300
1,900	-	-	-	-	-	-	-	-	-	-	-	-	1,150
1,950	-	-	-	-	-	-	-	-	-	-	-	-	1,000
2,000	-	-	-	-	-	-	-	-	-	-	-	-	900

- **Note**

The same test could be used with a smaller specimen, 38-mm (1.50-in.) diameter by 110-mm (4.33-in.) height. The same previous steps shall be carried out, using approximately the same equations as before. The full test procedure is described in the **AASHTO Designation: 133-19A[1]**, which covers measures for making and testing compacted and field cored asphalt mixture samples to estimate the damage characteristic curve and the corresponding fatigue parameters using the direct tension cyclic fatigue test accompanied by the asphalt mixture performance tester.

A smaller test equipment is also used in this case.

- **Standard Method of Test for Rutting and Fatigue Resistance of Asphalt Mixtures Using Incremental Repeated Load Permanent Deformation (iRLPD):**

- **Scope**

According to AASHTO Designation: TP 116-20[1], "This standard describes a test method for measuring the resistance of asphalt mixtures to rutting and fatigue cracking using minimum strain rates (m*) from an incremental repeated load permanent deformation (iRLPD) test conducted by means of a dynamic testing system (DTS). This practice is intended for dense- and gap-graded mixtures with nominal maximum aggregate sizes to 37.5 mm" [15]

- **Summary of the test method**

The procedure is based on measuring the minimum strain rate (m*) at the critical temperature and different load levels using the repeated load permanent deformation method. This test is performed at one test temperature and in several increments. The deviatoric load is kept fixed during each increment and is raised for each successive increment. The load pulse is 0.1 s every 1.0 s. permanent strain rates are determined by the actuator. The minimum strain rate for each increment is defined as the permanent axial strain due to the last cycle. The fatigue test is carried out in 12 increments of 100 cycles making use of an indirect-tensile setup on a 150-mm (6.0-in) diameter by 50-mm (2.0-in) high disk. The test is usually continued up to failure.

- **Significance and use**

The minimum strain rate (m*) is represents the fatigue resistance at intermediate temperature due to a repeated heavy-axle load. The fatigue test mimics field situations by employing the same loading magnitude and loading configuration as in the field. The sample, at its intermediate temperature, is incrementally loaded using a repeated load until the failure point is reached. The m* from the fatigue test is well associated with fatigue performance in the field.

Equations to estimate m* are described in detail in the AASHTO Designation: TP 116-20[1], calculations section, for both fatigue resistance and rutting

- **Apparatus:**

We can use any dynamic test system which can apply up to 20 KN (4500 lbf) of repeated load (0.1 s load/0.9 s unload). This dynamic testing system must have a controlled thermostatic testing chamber capable of keeping the temperature of the sample over a temperature range from 4 to 70°C (39 to 158°F) with a precision of ±0.5°C (1°F) and if possible capable of containing the test replicates and a dummy specimen with a temperature sensor attached in the center for temperature verification.

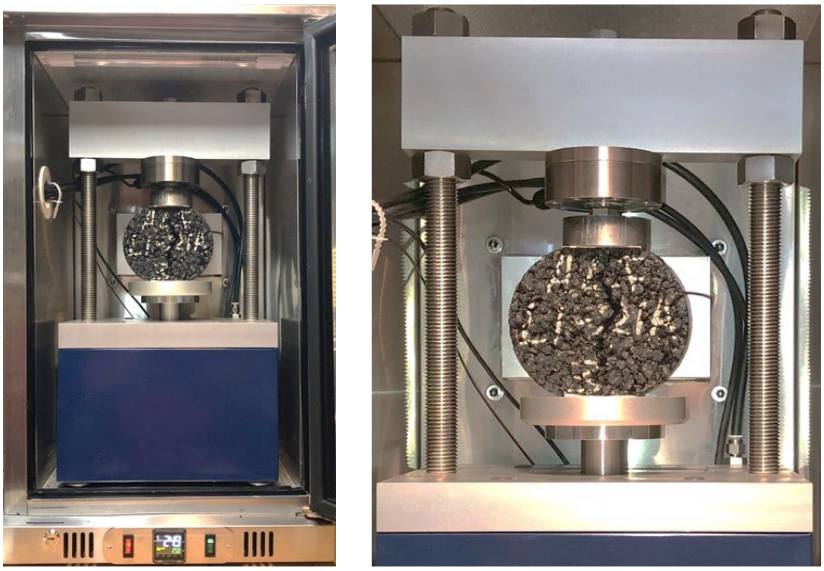

Figure 35 Testing Diametral Specimens to Failure in Accordance with the iRLPD

The m* at the increment before tertiary flow happens is the amount of fatigue resistance and indicated as fatigue index (FI). Figure (36) illustrates an example of FI values for three different mixtures. Lane 1 is the control section with the highest FI (37). Lane 5 with 50% RAP has FI of 20, and lane 3 with 20% RAS has the smallest value of FI of 19.

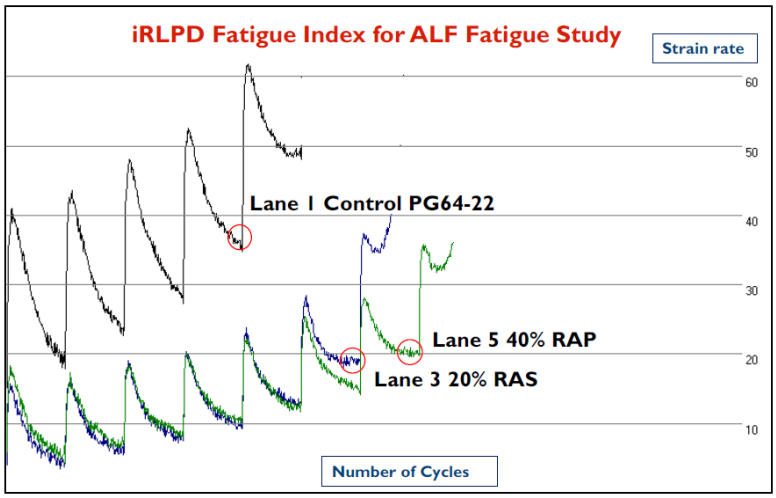

*Figure 36 Example of Fatigue Index (FI) determination using m**

- **Summary of test methods**

Since fatigue characterization is a fundamental problem in asphalt mixtures, we can clearly see it is widely discussed among different standards. The British standards have many tests to characterize the fatigue, starting from the simple 2-point bending test and ending with the 4-point bending test which is the last and most common standard. In the American standards the testing devices are mainly focused on the 4-point bending as well as the Asphalt Mixtures Performance Tester (AMPT), which is gaining interest in the asphalt industry as a tool capable of characterizing asphalt mixtures and closing the gap between pavement design and mixture design. In addition to the previously mentioned tests, the Incremental Repeated Load Permanent Deformation (iRLPD) is also used to estimate the fatigue resistance of asphalt mixtures.

2.3 Fatigue modelling

2.3.1 Introduction

The primary mechanisms of fatigue of flexible pavements are problematic. Generally, fatigue is the accumulation of damage inside the material under the impact of repeated load applications. This accumulated damage leads to fatigue cracking, which is a substantial distress in flexible pavements. A detailed description of the damage triggered by the fatigue turns out to be crucial if mechanistic pavement design approach is to be accurately adopted. The fatigue-related parameters of AC are usually achieved by repeated-load LAB testing. The preliminary fatigue models of asphalt mixtures are simple phenomenological expressions of fatigue under cyclic loading. Paris's law plays a vital role in associating the rate of crack growth to tensile strain developed in asphalt mixture. Nevertheless, continuum damage fatigue, and fracture mechanics models have been established. Paris's law was similarly used to relate the rate of crack growth to the deprivation of fracture toughness indicators such as the stress intensity factor when linear elastic fracture mechanics is used. Dissipated energy or surface energy models were also reviewed and proposed considering the shape of the phenomenological formula or incorporated in the Paris's law. [16]

Many models have been introduced for the fatigue problem. In the following section some of the models will be introduced.

2.3.2 Empirical Phenomenological Models

This category comprises models that were created relying on the experimental data to relate fatigue life (maximum allowable number of load repetitions or cycles *Nf*) to tensile strain ε_t and the dynamic modulus *E** of the mixtures. A conventional formulation can be represented as:

$$N_f = k_1 \varepsilon_t^{-k2} |E^*|^{-k3}$$

In which *k1, k2, k3* are regression coefficients. A common failure criterion for fatigue life at a particular strain is the loading repetition at which the mixture drops its modulus by 50%. If *k2, = k3* and for direct tension tests:

$$N_f = k_1 (\varepsilon_t E^*)^{-k2} = k_1 \sigma_t^{-k2}$$

There are many models in this category. Following are two examples. The current Mechanistic Empirical Pavement Design Guide (MEPDG) uses a model shown below:

$$N_f = 0.00432 * \beta_{f1} * C * \left(\frac{1}{\varepsilon_t}\right)^{3.291\beta_{f2}} * \left(\frac{1}{E}\right)^{0.854\beta_{f3}}$$

$$C = 10^{4.84*\left[\frac{V_b}{V_a+V_b}-0.69\right]}$$

β_{f1}, β_{f2}, β_{f3}= calibration factors
C = laboratory to field adjustment factor
et = critical tensile strain
E = stiffness of the AC surface layer
V_a = air voids (%)
V_b = effective binder content (%)

The model is similar to that by El-Basyouny et al. (2005):

$$N_f = 0.00432 * C * \left(\frac{1}{\varepsilon_t}\right)^{3.291} * \left(\frac{1}{E}\right)^{0.854}$$

$$C = 10^M$$

$$M = 4.84 * \left[\frac{V_b}{V_a + V_b} - 0.69\right]$$

where *Nf* = number of repetitions to fatigue cracking,
t = tensile strain at the critical location,
C = correction factor,
E = stiffness of the material (psi),
M = power factor,
V_b= effective binder content (%), and
V_a= air voids (%)

Sousa et al. (1998) [17], conducted a set of phenomenological fatigue models under an agreement with the SHRP. shift factors have been applied to calibrate those models, and this calibration was relying on field observations to deliver rational assessments of the in-service life of a pavement. Order 10 and more shift factors are required to correct the shortcomings in the methodology. An example of these vulnerability is the neglected crack propagation phase, which is usually mis-represented or simulated in the conventional laboratory fatigue tests, and hence the phenomenological models.[16]

Several other models are included in this category, among which we can list:

- **The Shell Model**

$$N_f = \left[\frac{\varepsilon_t}{(0.856V_b + 1.08) * S_{mix}^{-0.36}}\right]^{-5}$$

Where *Nf* = fatigue life; ε_t = tensile strain; *Smix* = mixture flexural stiffness; and *Vb* = asphalt content by volume.

- **The Asphalt Institute Model**

$$N_f = S_f * 10^{[4.84(VFB-0.69)]} * 0.004325 * \varepsilon_t^{-3.291} * S_{mix}^{-0.845}$$

Where *Nf* = fatigue life; *Sf* = shift factor to convert laboratory test results to field expected results (the recommended factor is 18.4 for a 10% cracked area); ε_t = tensile strain applied; *Smix* = flexural stiffness of a mix (psi); and *VFB* = voids filled with bitumen.

- **The Tayebali (1996) Model (SHRP Project A-003A)** [18]

$$N_f = S_f * 2.738 * 10^5 * e^{0.077VFB} * \varepsilon_t^{-3.6224} * S_0^{''-2.720}$$

Where *Sf* = shift factor to convert laboratory results to field expected results (the recommended factor is 10 for 10% cracked area and 14.0 for 45% cracked area), *e* = base of natural logarithm, *VFB* = percentage of voids filled by bitumen, *e*0 = strain level, and $S_0^{''}$ = loss of stiffness as measured in flexure.

2.3.3 Fracture Mechanics Models

Those models exploit the cracking propagation law for both linear and non-linear elastic fracture mechanics. For linear elastic fracture models, the Paris law is usually applied. For the non-linear elastic mechanics, the *J* integral is often used. An example of these models is:

- **The Uzan Model**

Uzan (2007) [19] modelled the fatigue cracking as a double-stage process containing crack initiation and crack propagation. The crack initiation stage is characterized by conventional laboratory fatigue tests, while the crack-propagation stage is described using the Paris-Erdogan law. Uzan adopted the model developed by Tayebali et al. in SHRP Project A-003A as the crack-initiation model.

The Paris-Erdogan law $\frac{dc}{dN} = A(\Delta K)^n$ was adopted as the crack-propagation model for estimating the number of load repetitions required to propagate the crack. Where, *c* = crack length; *N* = number of load repetitions; Δ*K* = difference between maximum and minimum stress intensity factor *K*; and *A*, *n* = Paris law fracture parameters for AC. In the case of Δ*K* = *K,* it is given by the following equation:

$$N_p = \frac{1}{A} . \int_{c0}^{h} \frac{dc}{K^n} = \frac{1}{A} . I_k$$

Where *Np* is number of load repetitions to propagate a crack of initial length *c*0 to the surface; *h* is layer thickness; *c*0 is initial crack length; *K* is stress-intensity factor (*K*I for Mode I and *K*II for Mode II); *n, A*, are material properties; and I_k = *Np A*.

2.3.4 Damage-Based Models

The models falling in this category rest on the accumulative damage concept. An example of these models is:

- **Castro and Sanchez Model**

Castro and Sanchez (2008) [20], suggested a phenomenological model based on the continuum damage theory. The 3-point bending fatigue test was adopted to estimate the parameters in the equation presented below:

$$\mathrm{N} = \mathrm{a}.\,\varepsilon_0^{\mathrm{b}}.\,\mathrm{D}^{\mathrm{c}}$$

N is the number of loading cycles and *e*0 is the initial strain; *a, b* and *c* are the parameters of asphalt concrete determined experimentally; *D* is the damage parameter.

$$D = \frac{|E_0^*| - |E^*|}{|E_0^*|}$$

defined as the loss of the norm of the complex modulus that takes place in a specimen during a test.

- **Bodin Model**

Bodin, et al. (2004) [21], suggested a non-local damage model to forecast pavement fatigue cracking, which was employed in a finite-element code along with a self-adaptive jump-in-cycle procedure for high-cycle fatigue computations. The mathematical model used to illustrate mechanical damage is an elasticity-based damage model for fatigue.

$$N_{crit} = \frac{F(d_{crit})(\beta + 1)}{{\varepsilon_a}^{\beta+1}}$$

$$F(d_{crit}) = constant$$

$$F(d) = \sum_{cycle\ 1}^{N} \frac{{\varepsilon_a}^{\beta+1}}{\beta + 1}$$

Where *d* is the damage variable; ε_a is the amplitude of the equivalent strain over one cycle; *f* (*d*) is the function of damage and *F*(*d*) is the scalar function of damage; and *b* is a model parameter.

2.3.5 Dissipated Energy-Based Model

Based on the relationship between total dissipated energy and the number of cycles up to fatigue or fracture, the following energy model was developed by van Dijk (1975) [22]

$$N = \left(\frac{\pi S_{fat} sin\phi}{A_\varphi}\right)^{\frac{1}{z-1}\frac{2}{\varepsilon_0^{z-1}}}$$

Where *N* is the number of load applications to fatigue; *Sfat* is initial stiffness modulus; ϕ-phase angle between stress and strain; and *z* and *A* are material constants.

Ghuzlan et al. (2000) [23] offered a dissipated energy model to model the fatigue of asphalt mixtures. The following equation is used to calculate dissipated energy in the flexural fatigue test:

$$W_i = \pi \sigma_i \varepsilon_i sin\varphi_i$$

Where *Wi* = dissipated energy at load cycle *I*; σ_i= stress amplitude at load cycle *I*; ε_i = strain amplitude at load cycle *i*; and φ_i = phase angle between stress and strain. Then the total (cumulative) dissipated energy at failure will be as follows:

$$W_{fat} = \sum_{i=1}^{n} W_i$$

Conventionally, fatigue life was related to the total dissipated energy in the fatigue test as follows, where *N* is the number of cycles to failure and *A*, *z* are experimentally determined coefficients:

$$W_{fat} = A.(N)^z$$

The conventional failure criterion in fatigue testing, 50% reduction in modulus, however, was discovered to provide a non-consistent indicator of the onset of failure when various modes of loading are used. Dissipated energy, when assessed as a change between two load cycles, offers a more profoundly correct indication of damage from one load cycle to the next than does cumulative dissipated energy.

A new failure criterion has been introduced for fatigue characterization relying on the assumption that the change in dissipated energy between two consequences cycles is the proper indicator of the damage induced to the material by that load cycle. This new failure criterion was identified as the change in dissipated energy between subsequent cycles divided by the total dissipated energy to first load cycle. For the reason of equipment data limitations, this change was usually calculated roughly every 100 load cycles. The new failure criterion is stated as follows, where *N* is the number of cycles to failure and *A*, *z values* are coefficients which are experimentally estimated.

$$\frac{\Delta DE}{\Delta E} = A.(N)^z$$

The damage accumulation ratio ($\Delta DE/DE$) provides a reliable failure indicator that appears to be independent of the loading mode.

Bonnetti et al. (2002) [24] implemented fatigue tests on a series of unmodified and modified binders and the results were evaluated using the dissipated energy ratio concept. The number of cycles to crack propagation, *Np*, was used as the fatigue criterion for the analysis. Using the initial dissipated energy per cycle (*Wi*) as the primary independent variable for modelling fatigue of binders appears to be a favourable technique to standardize some of the testing conditions. The parameter *Np*20, defined as the number of cycles at which the dissipated energy ratio shows 20% divergence from the no-damage ratio, appears to be a promising parameter to define failure.

It was observed that the most appropriate way of assessing the influence of modifiers in the fatigue response of the binders is using the **cumulative dissipated energy ratio (DER):**

$$DER = \frac{\sum_{i=1}^{n} Wi}{Wn}$$

Where *Wi* = dissipated energy per cycle; *Wn* = dissipated energy at cycle *n;* and $\sum_{i=1}^{n} Wi$ = total sum of dissipated energy up to cycle *n.* Then fatigue life, based on the DER criterion, can be represented as:

$$N_f = k_2 \left(\frac{1}{Wi}\right)^{k1}$$

Where *K*1 and *K*2 are the slope and the *Y* intercept, respectively, of the fitted fatigue curves (*Wi* versus *Np*) for a given asphalt binder. The slope and the *Y* intercept from fatigue curves obtained from different types of fatigue testing were used in the equation to determine the number of cycles to failure (*Nf*).

The most important limits for all the fatigue models comprise the failure criteria, the testing boundary conditions, and the absence of basic mechanism at microscopic levels.

2.4 Fatigue failure criteria

Substantial work has been administered over the last 20 years in developing the fatigue test equipment and analysis techniques. On the instrumentation aspect the enhancements to the four-point bending, and the trapezoidal fatigue equipment were created throughout the strategic highway research program, A003 project, offering a major breakthrough. Testing requirements in these devices need solely 4 to 6 specimens to capture the fatigue performance of a given mixture (constructing the fatigue curve). This analysis scheme furthermore provides the chance to quantify the rate of micro-cracks formation, besides the corresponding effect on the apparent stiffness of the mixture. This upgraded testing instrumentation permits to precisely estimate the point where fatigue failure happens.[25]

The fatigue life of a sample is defined as a number of cycles that brings sample to failure under a specific fatigue criterion. Many criteria have been introduced to face this problem, some criteria are based on the reduction of the modulus to a certain value, while others focused on the energy concepts, or other parameters away from the stiffness like the phase angle for example.

In the following passages, five different criteria will be presented.

2.4.1 The conventional criterion (50% of E_0):

The fatigue failure definition of asphalt concrete in LAB tests has perpetually been arguable, particularly within the strain-controlled cyclic loading configuration once no calamitous failure or fracture is ascertained. ancient fatigue analysis identifies failure as the point when we have 50% reduction in material's modulus of its initial value, and the corresponding number of cycles is indicated as Nf_{50}. This failure criterion is deemed to be reliable for the application of continuum damage models however might not offer a coherent prediction for the damage state as a result of its arbitrary assumption (Modulus reduction to half its initial value) [26]

The classical criterion reflects only the sample stiffness, neglecting the material properties and the fatigue phenomenon itself. Some scholars point out other effects such as non-linearity, self-heating and thixotropy (Mangiafico et al. 2015) [27]. Every so often, a 50% decrease in stiffness is not associated with cracking for one material, while for another one it is equivalent to a considerable micro or even macro cracking.

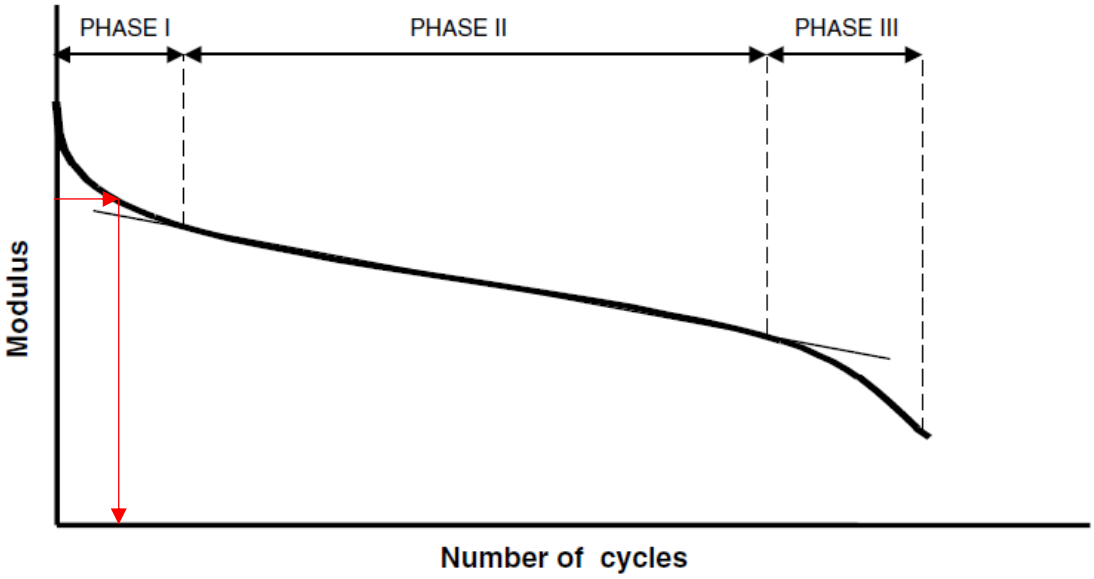

Figure 37 Conventional failure criterion

2.4.2 linear damage evolution criterion (50% of E_{00}):

"The first proposed developments, made at ENTPE, supposed a linear variation of the modulus with the number of cycles in well-chosen intervals. A fatigue slope associated with a given interval could be used to characterize fatigue." [28]

The method developed at the laboratory "DGCB" of ENTPE was used to characterize fatigue in this approach. The method assumes a linear evolution of the modulus with number of applied load cycles within given intervals.

In a typical fatigue test the relationship between the Modulus and the number of cycles can be identified using three disparate phases:

- Phase I: This phase is distinguished by a rapid reduction in the modulus due to the tedious excitation of load application. Nevertheless, the reduction is not mainly justified by fatigue damage. Heating and other phenomenon like thixotropy can take place.

- Phase II: Throughout this phase, the fatigue contribution is dominant on the stiffness decrease. Even if the parasitic effect (thermal heating and thixotropy) is tiny in this phase, it has to be taken into account. In the "DGCB" practice, this Phase, is examined to characterize the fatigue damage evolution, from which we can estimate the modulus (E_{00}) value by linear extrapolation when we have a linear reduction of the modulus. The E_{00} represents the intercept of this line, as shown in Figure (38).

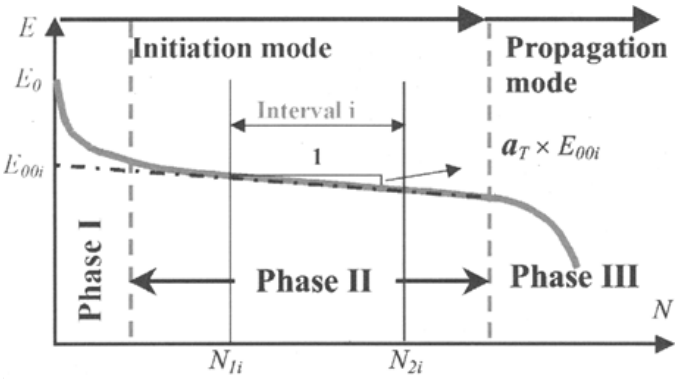

Figure 38 Stiffness Modulus versus cycles

- Phase Ill: if we can describe the first two phases crack-initiation phases, this third phase is considered as crack propagation, where the macro-cracks start to grow, until the global failure is achieved at the end of this phase.

This failure criterion is the number of cycles corresponding to 50% reduction of the modulus value (E_{00}) obtained through linear extrapolation of the stage at which we have linear reduction of the modulus when drawn versus the number of cycles.

2.4.3 Peak in phase angle criterion:

Reese (1997) [29] proposed a new methodology to describe fatigue failure using the peak of the phase angle. During a typical fatigue test under cyclic loading, the measured phase angle usually undergoes a steady increase if damage happens, this stage is then followed by a sharp reduction. Fatigue life, or number of cycles to failure N_f, is defined as the cycle at which this sharp reduction takes place (Figure 39). This method is believed to be more based on theoratical aspects, since it is traced through the viscoelastic property of the material, and this reduction indicates an alteration in the governing mechanism inside the material. [30]

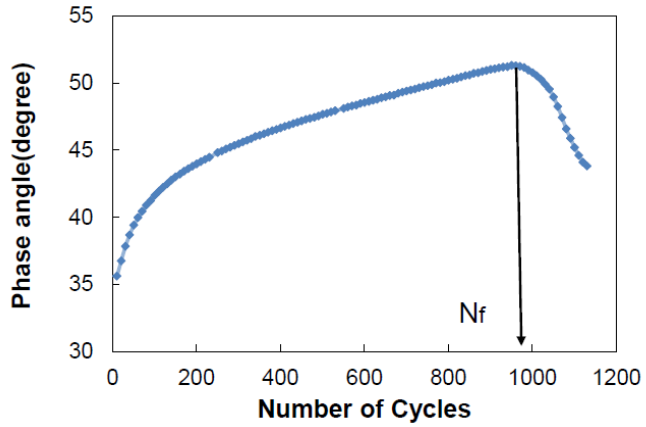

Figure 39 Fatigue life defined by Reese's (1997) approach.

2.4.4 Energy ratio criterion:

Hopman et al. (1989) [31] recommended the use of an "energy ratio" to define the number of cycles (N_1) at which we have the formation or macro-cracks in a strain-controlled test (macro-cracks results when the microcracks merge to form a sharp crack, which then propagates up to failure), Figure 40. The energy ratio, Wn, is defined as follows:

$$W_n = \frac{n \,.\, w_0}{w_n}$$

Where:
n = cycle number
wo = dissipated energy in first cycle
wn = dissipated energy in *n*-th cycle

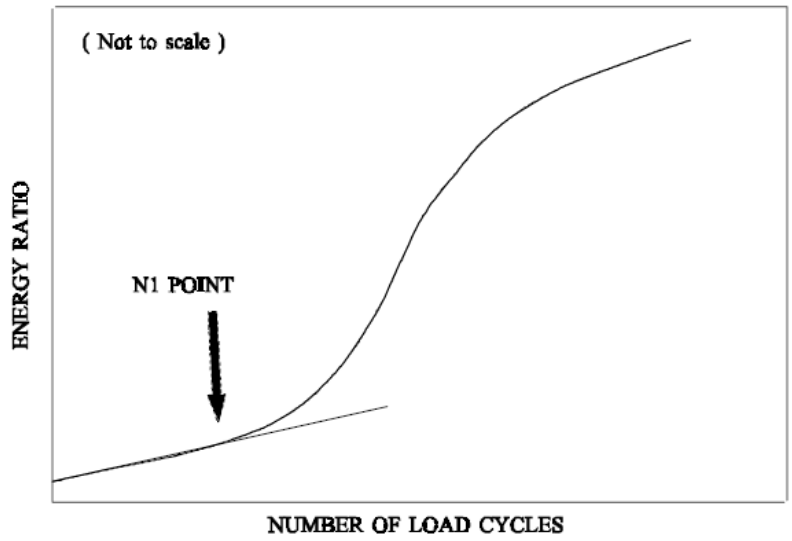

Figure 40 Energy Ratio (after Hopman, 1989)

When we plot the energy ratio versus the number of cycles, a noticeable change of the slope can be clearly seen at a critical number of cycles, N_1. This usually corresponds to a 40% drop in extensional complex modulus and was suggested to accord with the sharp crack formation. The energy ratio can be written as:

$$W_n = \frac{n(\pi\sigma_0\varepsilon_0 sin\delta_0)}{\pi\sigma_n\varepsilon_n sin\delta_n}$$

where:
n = cycle number
σ***0*** = stress in the initial cycle
σ***n*** = stress in ***n***-th cycle
ε***0*** = strain in the initial cycle
ε***n*** = strain in ***n***-th cycle
δ***n*** = phase lag in cycle ***n***

If the stress term is substituted by ($\varepsilon \cdot E^*$) we get (for a strain- controlled test) the energy ratio, as follows:

$$W_n = \frac{n(\pi\ {\varepsilon_0}^2 E^* sin\delta_0)}{\pi {\varepsilon_0}^2 E^* sin\delta_n}$$

All constant terms in this equation could be shortcut into one single constant. Furthermore, the change in sin δ is insignificant compared to the change in E^* as indicated by (Rowe, 1993) [32] and, therefore, the ratio of the sinδ can be taken as unity. So, the reduced energy ratio for a strain-controlled fatigue test, R_n^{ε}, could be written as follows:

$$R_n^{\varepsilon} = \frac{n}{E_n^*}$$

For strain- controlled test the value of N_1 is identified in the point at which the slope of the (R_n^{ε}) versus (n) diverges from a straight line (Figure 40).

For a stress- controlled test the same approach yields R_n^{σ} as follows:

$$R_n^{\sigma} = nE_n^*$$

In a stress- controlled test, the amount of the load stays fixed, and after the phase of crack initiation when we have the presence of crack tips, the stress increases sharply. Accordingly, the value of N_1 can be easily estimated from the peak of R_n^{σ} vs n graph (Figure 41). This idea of identifying fatigue life by the N_1 peak point is extremely desirable because the data attained from either stress/strain controlled test configuration characterizes the material in the same state of damage instead of the modulus reduction criteria (The classical approach), which is an arbitrary definition.

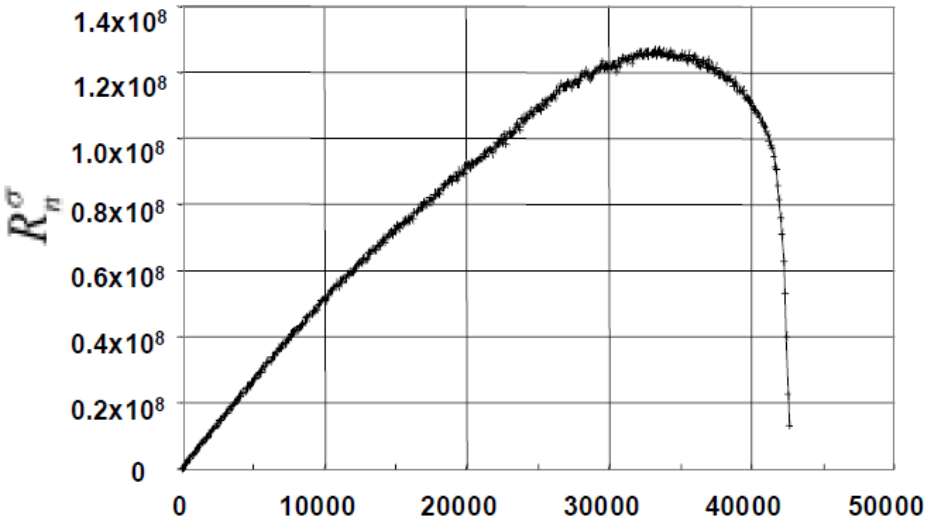

Figure 41 Energy ratio of stress-controlled fatigue test

A typical graph could be achieved if the data from strain-controlled test is plotted, However, a further stage of behaviour is noted. This later stage is linked with the slow crack propagation over the specimen as the stress drops in the controlled strain test.

the N_1 condition is very much difficult to define for strain- controlled than to stress- controlled tests (This is because of the decrease of the stress at the crack tip as the crack progresses, resulting in a reducing rate of crack propagation). This problem could be surpassed by employing the same analysis for the controlled stress method as previously stated. Although the fatigue tests are carried out using strain-controlled tests a modified version of Hopman's analysis for stress-controlled tests can be used. When plotting the product (n·E*) versus n we get a noticeable peak at failure $N_1[25]$.as shown in Figure (41).

In the phase of micro-crack formation, the reduction in modulus is linear (*dE*/dn* = constant). As cracks develop and start to propagate the relative damage, which is the slope (*dE*/dn*) accelerates and, therefore, the product (*n·E**) declines, as follows:

$$E^* = 1 + n\frac{dE^*}{dn} + \frac{n^2}{2!}.\frac{d^2E^*}{dn^2} + R$$

$$R \ll \left(1 + n\frac{dE^*}{dn} + \frac{n^2}{2!}.\frac{d^2E^*}{dn^2}\right)$$

$$E^*n \approx n + n^2\frac{dE^*}{dn} + \frac{n^3}{2!}.\frac{d^2E^*}{dn^2}$$

In the phase of micro-crack formation, the second differential equals zero and $n{\cdot}E^* = n\,(1+ n{\cdot}E^*)$. When the damage rate accelerates as a sharp crack develops, the second differential becomes negative and the product $n{\cdot}E^*$ decreases. The resulting peak implies the transition point between micro-crack formation and the propagation of a macro-crack.

2.4.5 Dissipated Energy ratio criterion:

The implementation of the dissipated energy approach for fatigue damage analysis has been supported by numerous authors. this methodology permits an independent fatigue law to be developed no matter loading mode, frequency, rest periods and temperature. once viscoelastic materials are exposed to cyclic loading, they produce different routes for the loading and unloading cycles resulting in hysteresis loops [33]. The dissipated energy per cycle is calculated as the area within the hysteresis loop and computed through the following equation:

$$wi = \pi \, \sigma i \, \varepsilon i \, sin \, \delta i$$

where wi is the dissipated energy at cycle i while σi, εi, δi are the stress amplitude, strain amplitude and phase angle at cycle i, respectively.

It is noticeable that this methodology comprises the main viscoelastic parameters (stress, strain, and phase angle) and hence monitoring the change in these parameters throughout the fatigue evolution permits an inherent fatigue law to be developed. Van Dijk and his colleagues were the first researchers to employ the dissipated energy approach for fatigue characterization in asphalt mixtures. They demonstrated that the relationship between accumulated dissipated energy (Wfat) at failure and number of cycles Nf to failure depends exclusively on material properties and it is constant regardless of the mode of loading, frequency, and temperature. After n cycles, the expression for the accumulated dissipated energy could be estimated as:

$$Wn = \sum_{i=0}^{n} wi$$

The relationship between cumulative dissipated energy to the number of load cycles to failure was found to follow a power law relation as following:

$$Wfat = A.N_{fat}^{z}$$

Where:

Wfat =total dissipated energy until failure due to fatigue cracking.
Nfat = number of loading cycles to fatigue.
A and z= material constants.

The major worry with this approach is that the sum of dissipated energy calculated using the first equation contains energies that are not liable for fatigue damage like recoverable viscoelastic energy and heat energy. Consequently, Ghuzlan and Carpenter [34] suggested the use of the Dissipated Energy Ratio (DER) to investigate the fatigue behaviour.

As a result of repeated cyclic loading, the fatigue life should correspond to the transition point between crack initiation and crack propagation. As we saw in the previous sections, several approaches have been adopted to correctly identify the fatigue failure point. The conventional approach of a 50% reduction in the initial stiffness is the most frequently used method to identify the fatigue failure in bituminous materials. Nevertheless, several researchers indicated that this criterion may not always be suitable for evaluating fatigue properties. Furthermore, the various stress/strain loading modes do not always generate a distinctive intrinsic fatigue law if this arbitrary definition is adopted. Consequently, it was crucial to find other approaches that are not subjective but can explain the fatigue failure based on a more fundamental analysis. The Dissipated Energy Ratio concept shown below was suggested to offer a rational criterion for identifying the fatigue failure of bituminous mixtures [14].

$$DER = \frac{\sum_{i=1}^{n} Wi}{Wn}$$

Where:
Wi = dissipated energy per cycle.
Wn = dissipated energy at cycle n.

The graph of the correlation between DER and number of cycles in the stress-controlled mode offers a unique approach to assess the stage of fatigue damage at which the material experiences a transition from crack initiation to crack propagation. Figure (42) indicates the relationship between DER and loading cycles. Throughout the first part the damage is negligible and $DER = n$ (the dissipated energy is roughly equal for successive cycles). As the relative difference in dissipated energy between successive cycles becomes substantial, the dissipated energy ratio starts deviating from the equality line which is interpreted as crack initiation. The fatigue failure Nf point in Figure (42) is characterized by the sudden change in DER which can be linked to the point of transition from crack initiation to crack propagation. This change is believed to be highly material-specific and independent of the mode of loading. For the strain-controlled test configuration the failure point Nf is described by the intersection of two tangents as shown in the following figure:

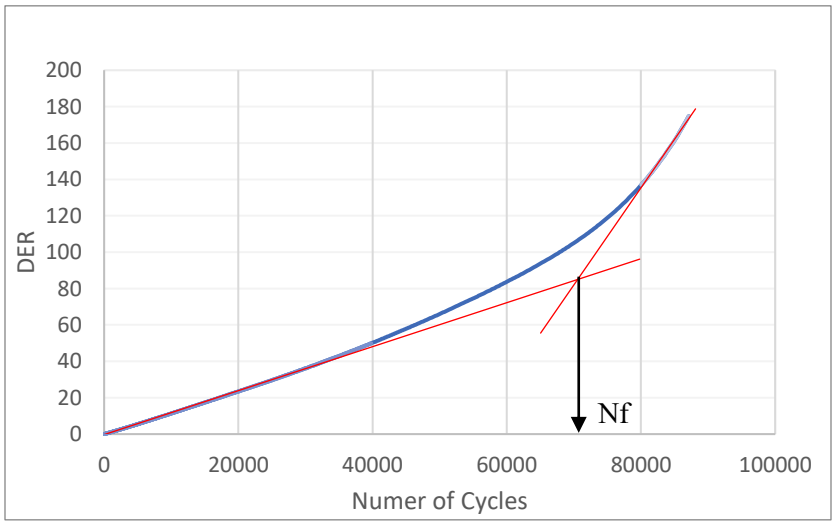

Figure 42 DER approach

2.5 pavement design

Even if pavement design has step by step developed from art to science, empiricism yet plays a crucial role up to the current day. before the early 1920s, the thickness of pavement was established strictly by experience. Constant thickness was used for all over the road even though broadly various soils were confronted. All through the following years, experience has been achieved, consequently leading to develop various ways for determining the required thickness of pavement. [35]

Firstly, pavement types will be presented, then the most important are presented, and finally the design methods are introduced for both flexible and rigid pavements. The last part will be dedicated to describing the KENLAYER software for pavement design.

2.5.1 Pavement types:

Three main types of pavements could be listed: flexible or asphalt pavements, rigid or concrete pavements, and composite pavements.

2.5.1.1 Flexible pavements:

flexible pavements are bedded systems with superior materials on top wherever the intensity of stress is high and inferior materials at the bottom wherever the intensity is low. Adherence to this design principle makes possible the employment of local materials and typically ends up in a most economical design. this is often notably true in regions wherever high-quality materials are expensive however local materials of inferior quality are readily out there.

Figure (43) shows a typical cross section of a flexible pavement. Starting from the top, the pavement consists of seal coat, surface course, tack coat, binder course, prime coat, base course, subbase course, compacted subgrade, and natural subgrade. The use of the various courses is based on either necessity or economy, and some of the courses may be omitted.

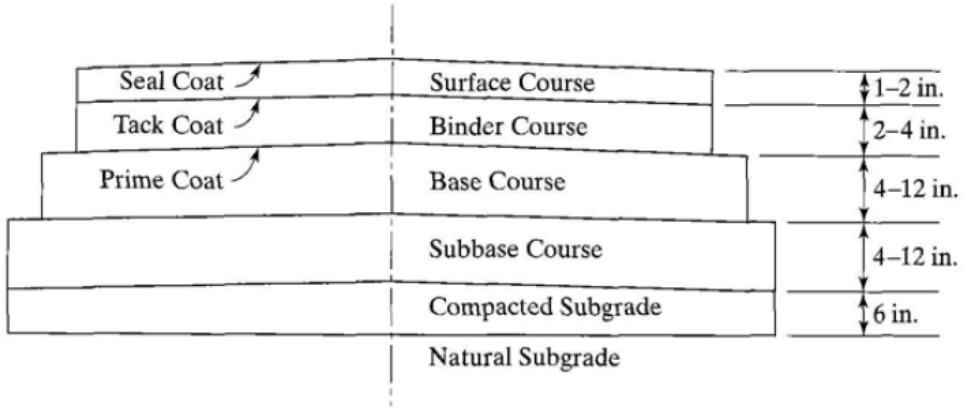

Figure 43 Typical cross section of a flexible pavement

- **Seal Coat**

This layer is a thin asphaltic emulsion used to provide waterproofing to the surface or to offer skid resistance if the aggregates were polished by traffic and become slick. As a function of the purpose, seal coats could or couldn't be covered with aggregate.

- **Surface Course**

It is that the top course of an asphaltic pavement, generally known as the wearing course. it's typically made of dense graded hot mixed asphalt. It should be robust to resist distortion due to traffic and supply a sleek and skid-resistant riding surface. It should be waterproof to safeguard the whole pavement and subgrade from the deteriorating action of water. If the previously mentioned requirements couldn't be achieved, the employment of a seal coat is usually recommended.

- **Binder Course**

This layer is generally known as the asphalt base course, is that the asphalt layer beneath the surface course. There are two excuses that a binder course is employed additionally to the surface course. First, the hot mixed asphalt is very thick so it can't be compacted in one layer, therefore it should be laid in two layers. Secondly, the binder course usually comprises bigger aggregates and fewer asphalt with a less quality compared to the surface course. Therefore, replacing a part of the surface course by the binder course leads to a more economical design. If the binder course is over 76 mm, it's typically laid in two layers.

- **Tack Coat**

It is used to ensure bond between bituminous layers increasing the adhesion at the interface and to provide waterproofing effects. It is made with a light application of bitumen, usually in the form of emulsion. The bituminous emulsion is a dispersion of bitumen in water. Scientifically, it is a heterogenous thermodynamically unstable system in which a phase (bitumen) is dispersed in another (water) in little drops. There are two kinds of emulsion: cationic (+) and anionic (-). Breaking is the term used to indicate the moment in which water separates from bitumen and the taking starts. In a tack coat, it is usually used a slow break emulsion.

- **Prime Coat**

It is an application of emulsion of cutback bitumen on an untreated granular layer which penetrates in it. It is used to ensure bond between bituminous and granular layers and to provide waterproofing effects. In a prime coat, it is usually used a slow break emulsion.

- **Base course and subbase Course:**

The base course is the stratum of material directly below the surface or binder course. It is made of crushed stone, crushed slag, or different natural or stabilized materials. The subbase course is the layer of material underneath the base course. The implementation of two various granular materials is mainly due to economic reasons. Instead of employing the costlier base course material for the whole layer, local and cheaper materials are recommended to be used as a subbase course on the top of the subgrade. If the base course is open graded, the subbase course containing more fines will act as a filter between the subgrade and also the base course.

- **Subgrade**

It is the soil than is found in situ. The top part of this layer (150 – 300 mm) should be adequately compacted. Its function is to support the entire pavement.

2.5.1.2 Rigid pavements:

This type of pavements is usually built from ordinary Portland cement concrete and the analysis approach is depending on the plate theory, as a substitute of the multi-layer principle. Plate theory is a streamlined version of the multi-layer which assumes that plain elements (slab modelled as thick plate) will remain plain after the bending. The plate theory or layered theory can be employed if the application of wheel load is in the internal part of the slab, and in this condition both theories generate approximately the same flexural stress or strain. On the other hand, If the load application is close to the slab edge, of less than 0 .61 m from the edge, only the plate theory can be adopted for rigid pavements. The sense behind the fact that the layered theory is appropriate to flexible pavements, but not too rigid pavements is that the Portland cement concrete is much stiffer than hot mixed asphalt and hence distributing the load over a significantly broader area. Therefore, a distance of 0.61 m from the edge is believed to be pretty far in a flexible pavement however not sufficiently far in a rigid pavement. The presence of joints in rigid pavements also limits the application of the layered theory. Figure (44) shows a typical cross section for rigid pavements.

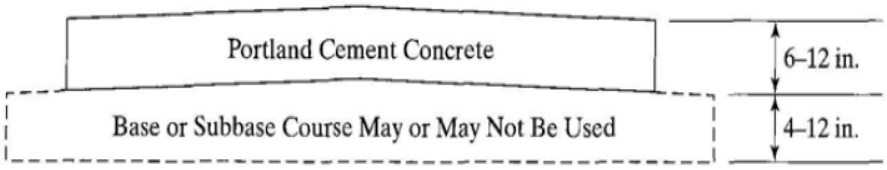

Figure 44 Typical cross section for rigid pavements

Compared to flexible pavements, rigid pavements can be placed directly on the subgrade or on one layer of granular or stabilized material. This one maybe called base or subbase.

There are four types of cement concrete slabs which divide rigid pavements into four types: Jointed (JPCP), Jointed and reinforced (JRCP), Continuous and reinforced (CRCP), Prestressed (PCP).

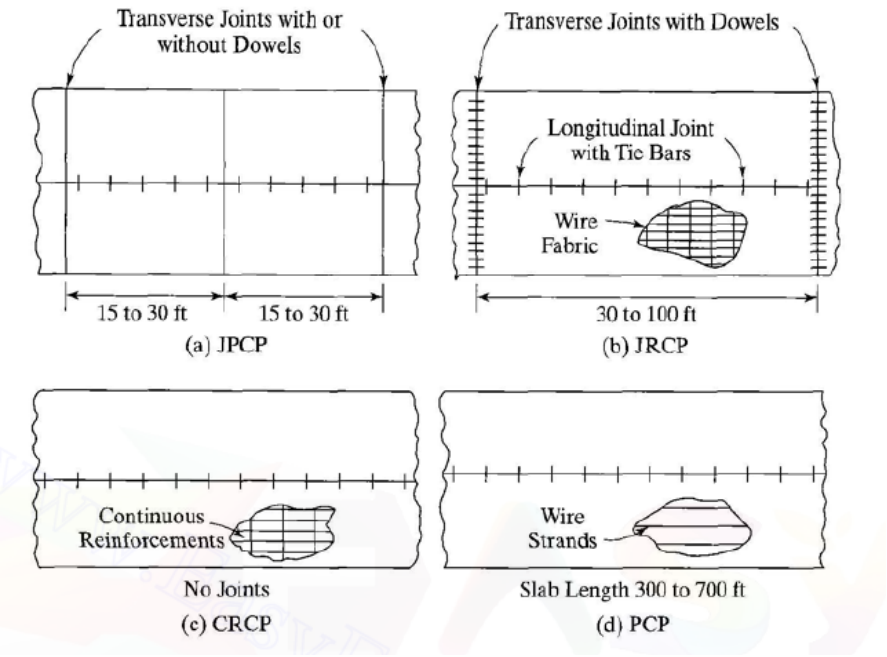

Figure 45 Four types of concrete pavements

- **Jointed plain concrete pavements (JPCP):**

it is characterized by closely spaced contraction joints without steel or reinforcements. Load transfer is ensured by dowls or by aggregate interlock (there is a little cut on the surface of the pavement and the joint is completed by the breaking of the pavement). Load transfer mode affects the maximum joint spacing. In fact, for un doweled joints, the maximum spacing is 4.6 m while for doweled joints the maximum spacing is 6.1 m because, even if the joint opens, there is still an adequate load distribution due to the dowel length.

- **Jointed reinforced concrete pavements (JRCP):**

There are steel reinforcements (wire mesh or bars) used to increase the maximum joint spacing which becomes of about 9 – 30 m. the amount of steel in designed to hold the slabs together after cracking. Dowels are required for load transfer.

- **Continuous reinforcement concrete pavements (CRCP):**

In this case there are no joints but there is the formation of transversal cracks at close intervals in the pavement which become the joints. The spacing and the width of the cracks are controlled by steel reinforcements.

- **Prestressed concrete pavements:**

They bring to a reduction of tensile stresses which cause a thickness decrease so that thickness depends only on steel covering. These pavements are still in an experimental stage, and they are very expensive. They are more frequent for airport pavements.

2.5.1.3 composite pavements:

These types of pavements are constructed with both cement concrete, which provides a strong base, and bituminous mixtures, which provide a smooth and non-reflecting surface. They are very expensive and rarely used as a new construction.

2.5.2 Pavement distresses:

Pavement distress must be given a crucial care in pavement design. In the mechanistic empirical methods, any failure criterion should be developed distinctly to reflect each specific distress. Tactlessly, several distresses are resulting from deficits in construction, materials, and maintenance which are not directly linked to the design. However, an adequate knowledge of the different distress types is significant to pavement designers because it gives the helping hand to recognise the reasons of the distress. In the case of inappropriate design because of distresses, enhancements in the design method can be presented. Besides, pavement management system is directly liked to those distresses since they can affect the choice of the best strategies for maintenance and rehabilitation which could be developed. [35]

The Highway distress identification manual [36] is divided into three sections, each focusing on a particular type of pavement: (1) Asphalt concrete-surfaces, (2) Jointed Portland cement concrete, and (3) Contiguously reinforced Portland cement concrete.

Since the description of those distresses is not thesis-related topic, we will just list the most common types.

- **Distresses for pavements with asphalt concrete surfaces**

This type is divided into 5 sub-categories:

1. Cracking (Fatigue cracking, Block cracking, Edge cracking, Longitudinal Cracking, Reflection cracking, Transverse cracking).
2. Patching and potholes.
3. Surface deformation (Rutting, Shoving).
4. Surface defects (Bleeding, Polishing, Ravelling)
5. Miscellaneous distresses (Lane-to-shoulder drop-off, Water bleeding, Pumping)

- **Distresses for pavements with jointed Portland cement concrete surfaces**

This type is divided into 4 sub-categories:

1. Cracking (Corner breaks, Durability cracking, Longitudinal cracking, Transverse cracking).
2. Joint Deficiencies (Transverse and Longitudinal joint seal damage, Spalling of longitudinal and transverse joints)
3. Surface deficiencies (Map cracking, Scaling, Polishing, pop-outs)
4. Miscellaneous distresses (Blow-ups, Faulting of transverse joints and cracking, Lane-to-shoulder drop-off, Lane-to-shoulder separation, Patch/ Patch deterioration, water Bleeding, Pumping)

- **Distresses for pavements with jointed Portland cement concrete surfaces**

This type is divided into 3 sub-categories:

1. Cracking (Durability cracking, Longitudinal cracking, Transverse cracking).
2. Surface defects (Map cracking, Scaling, Polishing, pop-outs).
3. Miscellaneous distresses (Blow-ups, Transverse construction joint deterioration, Lan-to-shoulder drop-off, Lan-to-shoulder separation, Patch/Patch deterioration, Water bleeding, Pumping, Spalling of longitudinal joints, Longitudinal joint seal damage, Punch-outs)

2.5.3 Design methods for flexible pavements:

Since it is not convenient to list all of the methods that have been used pavement design. Only a few typical methods will be presented to signify the overall trend.

These design methods can be categorized into five groups: empirical methods, limiting shear failure methods, Limiting deflection methods, Road test methods, and mechanistic–empirical methods.

- **Empirical methods**

Empirical method has been without implementing a strength test since the introduction of the Public Roads (PR) soil classification system (Hogentogler and Terzaghi, 1929), in which the subgrade was categorized as uniform from A-1 to A-8 and nonuniform from B-1 to B-3. The PR system was then edited by the Highway Research Board, in which soils were categorized from A-1 to A- 7 and a group index was included to distinguish the soil inside each class. California Highway Department was the first body to implement the use of empirical method accompanied by strength test. The thickness of pavements was associated to the California Bearing Ratio (CBR), which is the penetration resistance of a subgrade soil relative to a standard crushed rock. during the second world war, the CBR approach of design was examined broadly by the U.S. Corps of Engineers and turns to be a very trendy technique after the war.

The main drawback of empirical methods is that it can solely be applicable for a pre-defined environmental, material, and loading configuration. The design won't be valid if these conditions are altered, consequently a new method must be established using trial and error to match the new situations.

- **Limiting shear failure methods**

This technique is employed to work out the thickness of pavements in order that shear failures won't happen. the main properties of pavement elements and subgrade soils to be thought of are their cohesion and angle of internal friction.

- **Limiting deflection methods**

This method is employed to estimate the thickness of pavements to prevent the vertical deflection from exceeding a permissible threshold. For instance, The Kansas State Highway Commission (1947) limited the deflection of subgrade to 2.54 mm, while the U.S. Navy (1953) restricted the surface deflection to 6.35 mm. The main apparent advantage of this approach is that the deflection can be effortlessly quantified in the field. Regrettably, pavement failures are instigated by excessive stresses and strains rather than of deflections.

- **Road test methods**

The AASHTO method, can be a clear example of this methods. The drawback of the method is that the design equations is exclusively applicable to the configuration at the road test site. Massive adjustments based on theory or experience are necessary if any alteration of test conditions took place. These methods relate a parameter to the performance.

- **Mechanistic–empirical methods**

This method of design is depending on the mechanics of materials which links an input, like the wheel load, to an output or pavement response, like the stress or strain. The response values are used to forecast distress from laboratory-test and field-performance data. Reliance on perceived performance is crucial because theory alone proven to be insufficient to design pavements convincingly.

Vertical compressive strain on the surface of subgrade was firstly suggested by Kerkhoven and Dormon (1953) as a failure criterion to limit the rutting. horizontal tensile strain at the bottom of asphalt layer was suggested by Saal and Pell (1960) to diminish fatigue cracking, as shown in Figure (43). The use of the previously mentioned notions for pavement design was first presented in the United States by Dormon and Metcalf (1965).

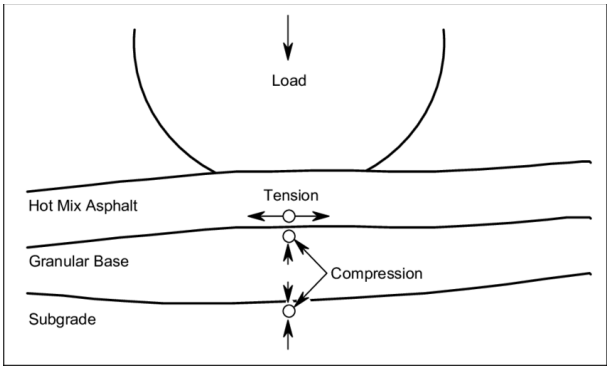

Figure 46 Tensile and compressive strains flexible pavement

The idea of implementing the vertical compressive strain to control the rutting is centred upon the reality that plastic strains are proportional to elastic strains in paving materials. Therefore, by reducing the elastic strains on the subgrade, the elastic strains in the upper components will also be monitored; consequently, the amount of rutting on the pavement surface will be controlled in return. These two criteria have later been implemented by Shell Petroleum International and by the Asphalt Institute in their mechanistic–empirical methods of design. The benefits of mechanistic methods are the enhancement in the reliability of a design, the capability to foretell the types of distress, and the possibility to extrapolate from limited field and laboratory data.

The phrase "hot mix asphalt" indicated in Figure (43) is equivalent to the typically used term "asphalt concrete." It is an asphaltic aggregate mixture manufactured at a batch or drum mixing equipment that must be mixed, spread, and compacted at high temperature.

Other developments in flexible pavement design include the application of computer programs, the inclusion of serviceability and reliability, and the consideration of dynamic loading. One of these software (KENLAYER) will be presented in the following section and will be used in this thesis to design a typical flexible pavement.

2.5.4 KENLAYER software pavement design:

The KENLAYER software can be used only for the design of flexible pavements without the presence of joints or rigid layers. For pavements with rigid layers, such as Portland cement concrete and composite pavements, the KENSLABS program must be adopted. The software is based on the solution for an elastic layered system subjected to a circularly loaded area. If we have multiple wheel configurations, the superimposition aspect is applied iteratively for non-linear layers and lumped at different times for viscoelastic layers. So, KENLAYER can be applied to layered systems subjected to single, dual, dual-tandem, or dual-tridem wheels with a different behaviour of each layer, either linear elastic, nonlinear elastic, or viscoelastic. Damage analysis can be made by splitting each year into a maximum of 12 periods, with a distinct set of material properties. Each of the previously mentioned periods are associated with 12 load bands as maximum. Those load groups could be either single or many. The damage generated by fatigue cracking and rutting in each period of the load bands is added up to assess the design life. [35]

Damage analysis is carried out for both fatigue cracking and permanent deformation.
The failure criterion for fatigue cracking is expressed as:

$$N_f = f_1(\varepsilon_t)^{-f_1}(E_1)^{-f_3}$$

Where:
N_f is the allowable number of load repetitions to prevent fatigue cracking.
ε_t is the tensile strain at the bottom of asphalt layer.
E_1 is the elastic modulus of asphalt layer.
f_1, f_2, and f_3 are constants determined from laboratory fatigue tests, with f_1 modified to correlate with field performance observations.

The Asphalt Institute used 0.0796, 0.854, and 2.363 for f_1, f_2, and f_3, respectively, in their analytically based design approach. The Shell institute employed 0.0685, 5.671, and 2.363. Counting on the fact that the number of load repetitions needed to move from the phase of cracking to limiting failure conditions is less for thin asphalt layers compared thicker layers.

The failure criterion for permanent deformation is expressed as:

$$N_d = f_4(\varepsilon_t)^{-f_5}$$

Where:

N_d is the allowable number of load repetitions to limit permanent deformation,
ε_t is the compressive strain on the top of subgrade.
f_4 and f_5 are constants determined from road tests or field performance.

Values of f_4 and f_5 are suggested as $1.365\ x\ 10^{-9}$ and 4.477 by the Asphalt Institute.
$6.15\ x\ 10^{-7}$ and 4.0 by Shell Institute.
$1.13\ x\ 10^{-6}$ and 3.571 by the University of Nottingham.

Chapter 3: Materials and methods

3.1 Experimental campaign

The aim of this section is to highlight the experimental campaign starting from the material characterization ending up with obtaining the beams to be tested in the four-point bending test.

In order to obtain the final fatigue curve of our mixture, a minimum of six beams are prepared, to be tested for at least three strain levels (140 μm/m, 200 μm/m, 300 μm/m).

The first stage was characterizing the mixture that we received from the plant. The aggregate portions of the mixture are Sand, 3/8, 8/18, Filler. The employed bitumen is normal bitumen grade 50/70.

Knowing all of the previous information, the binder content was obtained by performing two ignition tests according to the standard [BS EN 12697-39-2020] [37] and the average binder content was recorded. From the burned mixture, two aggregate gradation tests we carried out according to [BS EN 933-1-2012] [38]. After that, the theoretical maximum density of the mixture, and the aggregate density were estimated according to [BS EN 12697-5-2018], [BS EN 1097-6-2013] [39] [40] using the pycnometer method.

To know the workability and the compatibility of the mixture, four gyratory tests were carried out according to [BS EN 12697-31-2019] [41]. Then, the slabs are created using the roller compactor according to [BS EN 12697-33-2019] [11].Finally the obtained beams are tested using the four-point bending device in accordance with [BS EN 12697-24-2018] [8].

3.2 Materials characterization

Mixture characterization tests are used to describe the vital mixture parameters. The most fundamental tests include:

1. Theoretical maximum density of the mixture.
2. Aggregate density.
3. Ignition test to estimate the binder content.
4. Sieve analysis to estimate aggregate gradation.
5. Gyratory compaction to estimate Compactability and workability of the mixture.
6. Roller compaction to get the slabs and then the 4PB beams.
7. Bulk density.

3.3.1 Theoretical maximum density of the mixture / Aggregate density:

The theoretical maximum specific gravity, or in other words could be indicated as the theoretical maximum density (TMD), is the hot mixed asphalt density excluding air voids. Therefore, if the air voids were theoretically excluded from a sample, the density of the remaining aggregate and asphalt binder would be the theoretical maximum density. TMD is a significant HMA characteristic because it is used to determine the air voids in compacted HMA and other volumetric-related properties of a compacted bituminous mixture, and also to offer a target values for the compaction.

- **Procedure:**

The estimation of the theoretical maximum density of the mixture is carried out in accordance with [BS EN 12697-5-2018], using the volumetric procedure.

The mass of the loose sample used for this test is taken greater than 50 times the numerical value of the nominal maximum aggregate size (12.5mm)

The mixture was placed in the oven at (110 ± 5) ºC, in order to disaggregate it. After that the sample was poured a table, and let down to cool, then it was loosened and separated manually into coarse particles.

Knowing the volume of already calibrated pycnometer (V_P), the weight of the empty pycnometer, and the accompanied cap is recorded (m_1). After that the sample is placed inside the pycnometer and the total weight is recorded (m_2). The pycnometer was filled with de-aired water up to 2/3 of its height. Then the pycnometer was placed in the vacuum system to evacuate the entrapped air. The vacuum was applied for a minimum of 1 hour, and the pycnometer was stirred each 15 min. after the entrapped air is removed, dismantle the vacuum system, place the pycnometer cap, and fill the pycnometer with water up to the top. Finally, dry the pycnometer surface and immediately record it weight (m_3), and take the temperature.

The same procedure is valid for the aggregate density.

Figure 47 Mixture disaggregation after cooled down

Figure 48 Asphalt particles inside the pycnometer

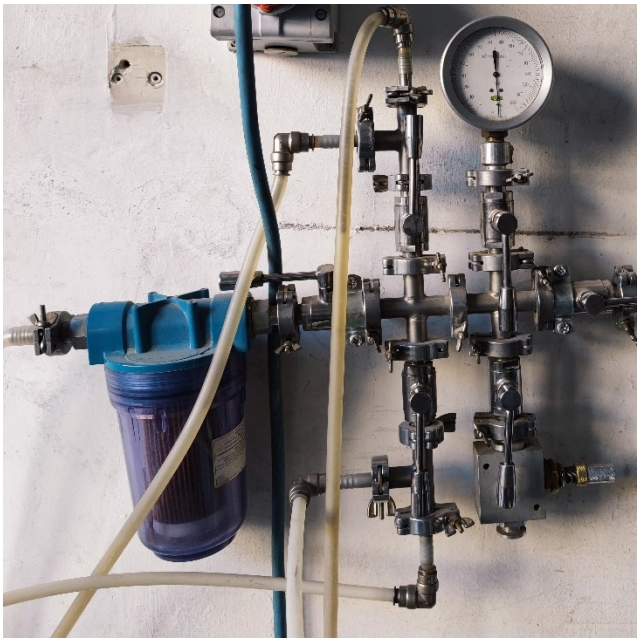

Figure 49 Vacuum system

- **Calculations:**

The density of the water is calculated as follows:

$$\rho_w = 1{,}00025205 + \left(\frac{7.59xt - 5{,}32xt^2}{10^6}\right)$$

Where:

ρ_w is the density of water at test temperature, in megagram per cubic metre (Mg/m3).
t is the temperature of the water in degrees Celsius (°C).

The maximum density ρ_{mv} of the bituminous mixtures determined by the volumetric procedure is calculated as follows:

$$\rho_{mv} = \frac{(m_2 - m_1)}{10^6 x V_P - \frac{m_3 - m_2}{\rho_w}}$$

Where:

ρ_{mv} is the maximum density of the bituminous mixture, as determined by the volumetric procedure, in megagrams per cubic metre (Mg/m3) to the nearest 0,001 Mg/m3.

m_1 is the mass of the pycnometer plus head piece, in grams (g).
m_2 is the mass of the pycnometer plus head piece, and test sample, in grams (g).
m_3 is the mass of the pycnometer plus head piece, test sample and water, in grams (g).
V_P is the volume of the pycnometer, when filled up to the top, in cubic metres (m3).
ρ_w is the density of the water at test temperature, in megagrams per cubic metre (Mg/m3) to the nearest 0,000 1 Mg/m3.

The same calculation is valid for the aggregate density.

Pycnometer	Cork	V_P
		[m^3]
6	F	0.0012830
K	15	0.0013383

Table 14 Pycnometer calibration

Asphalt		Pycnometer	Pycnometer + material	Pycnometer + material + water	Pycnometer volume	Temp	water density	Theoretical max density (TMD)
Pycnometer	Cork	M_P	M_{P+M}	$M_{P+M+H2O}$	V_P	T	ρ_w	ρ_{mw}
		[g]	[g]	[g]	[m^3]	[°C]	[kg/m^3]	[kg/m^3]
6	F	1041.4	1612.6	2665.6	0.0012830	21.0	998.1	2505
K	15	924.0	1419.4	2556.8	0.0013383	21.0	998.1	2494
6	F	1041.4	1542.1	2622.6	0.0012830	21.0	998.1	2498
K	15	924.0	1396.4	2544.0	0.0013383	20.9	998.1	2507

Table 15 Theoretical maximum density for Asphalt mixture

Mean TMD	2501
Standard deviation	6
Coefficient of variation	0.2

Table 16 Statistical parameters of TMD of the mixture

Aggregate		Pycnometer	Pycnometer + material + water	Pycnometer + material + water	Pycnometer volume	Temp	water density	Theoretical max density (TMD)
Pycnometer	Cork	M_P	M_{P+M}	$M_{P+M+H2O}$	V_P	T	ρ_w	ρ_{mw}
		[g]	[g]	[g]	[m^3]	[°C]	[kg/m^3]	[kg/m^3]
6	F	1041.4	1730.3	2760.9	0.0012830	18.6	998.6	2745
K	15	924.0	1635.4	2712.8	0.0013383	18.6	998.6	2744

Table 17 Aggregate density

Mean TMD	2744
Standard deviation	1
Coefficient of variation	0.0

Table 18 Statistical parameters of particles density

3.3.2 Ignition test:

The estimation of the binder content of asphalt mixtures through the ignition test come as an alternative to the old-fashioned method of separating the binder using solvents. The method can be used for evaluation of mixture composition because the remaining aggregate can be used for determining aggregate gradation and density, because the test temperature does not damage the aggregate particles. the outcomes can be used for quality assurance and quality control of the mixture.

- **Procedure:**

The estimation of the binder content by ignition test is carried out in accordance with [BS EN 12697-39-2020], using method (B) which permits the use of a furnace and external balance.

The size of the used sample is estimated as a function of the nominal maximum aggregate size according to the following table:

Nominal maximum aggregate size mm	Mass of sample g	Maximum constant mass limit g
4	1 000 to 1 400	0,15
5,6 or 6,3 or 8 or 10	1 000 to 1 600	0,15
11,2 or 12,5 or 14 or 16	1 000 to 1 700	0,20
20 or 22,4	1 000 to 2 400	0,25
31,5	1 000 to 3 000	0,30
40 or 45	1 000 to 4 000	0,40

Table 19 Size of the ignition test sample

The furnace was pre heated up to the test temperature (540 °C). Meanwhile, the weight of the empty sample baskets and catch pan (W_t) was recorded, and the sample was place and distributed evenly inside the baskets and the corresponding weight was recorded (W_{t+s}). After the furnace temperature was reached, the sample was placed inside the furnace. Stop the test after the mass loss equal to zero, take out the sample and let it to cool down at room temperature, and then record the mass of the sample + sample basket + catch pan (W_{t+a}).

- **Calculations:**

The total mass of bituminous mixture before the ignition ($W_{S,W}$) is calculated as:

$$W_{S,W} = W_{t+s} - W_t$$

Where:

$W_{S,W}$ is the total mass of bituminous mixture prior to ignition, in grams (g).
W_{t+s} is the mass of bituminous mixture, sample basket(s) and catch pan prior to ignition, in grams (g).
W_t is the mass of the sample basket(s) and catch pan, in grams (g).

The total mass of the remaining aggregate after the ignition test is:

$$W_a = W_{t+a} - W_t$$

Where:

W_a is the total mass of aggregate remaining after ignition, in grams (g).
W_{t+a} is the mass of bituminous mixture, sample basket(s) and catch pan after ignition, in grams (g).
W_t is the mass of the sample basket(s) and catch pan, in grams (g).

The corrected binder content by the mass of bituminous mixture is calculated as:

$$B = \frac{(W_s - W_a)}{W_s} x100 - C_F$$

where:

B is the corrected binder content of the bituminous mixture sample, in percent (%).
W_s is the dried total mass of the bituminous mixture prior to ignition, in grams (g).
W_a is the total mass of aggregate remaining after ignition, in grams (g).
C_F is the calibration value, in percent (%). (Was neglected in our calculations)

Figure 50 Ignition test furnace and the sample baskets

Figure 51 Sample distribution inside the basket and sample cooling

	1st sample	2nd sample
Empty basket wt. (g)	2844.4	2838.6
Mass before Ignition (g)	4242.8	4324.3
Mass after Ignition (g)	4162.3	4242.7
Mixture wt. (g)	1398.4	1485.7
Aggregate wt. (g)	1317.9	1404.1
Binder content (%) by wt. of Mixture	**5.76**	**5.49**
Binder content (%) by wt. of Aggregate	**6.11**	**5.81**

Table 20 Binder content

3.3.3 Sieve analysis:

The particle size distribution of an aggregate is one of the most prominent aggregate characteristics in estimating because it controls the overall pavement behaviour. In hot mixed asphalt, gradation helps to determine the most influencing pavement parameters such as the stiffness, stability, durability, permeability, workability, fatigue resistance, and frictional resistance. In Portland cement concrete, the gradation helps estimate durability, porosity, workability, cement and water requirements, strength, and shrinkage. Because of these crucial dependencies, particle size distribution is a vital concern in the mix design. Based on that that the limits provided by the specification must be always respected.

- **Procedure**

The estimation of the particle size distribution was carried out in accordance with [BS EN 933-1-2012], using washing and dry sieving.

The size of the test portion for the test was estimated as a function of the aggregate size according to the following table:

Aggregate size D (maximum) mm	mass of aggregates kg	volume of lightweight aggregates (litres)
90	80	-
32	10	2,1
16	2,6	1,7
8	0,6	0,8
≤ 4	0,2	0,3

Table 21 Minimum size of test portion for aggregate gradation

The weight of the estimated test portion was recorded (M_1). After that the sample was placed in a container and then washed, and the residual returned on 0.063 mm sieve was dried, and the corresponding weight was recorded (M_2). Then, the sample was poured in the sieving column, which consist of a number of sieves fitted together and arranged in a decreasing order from top to bottom. The column was placed in a mechanical vibration for shaking for 10 min. After that, the sieves were removed one by one, the weight of each sieve was recorded, along with the weight of the empty sieve.

Figure 52 Typical sieve

Figure 53 Sample washing

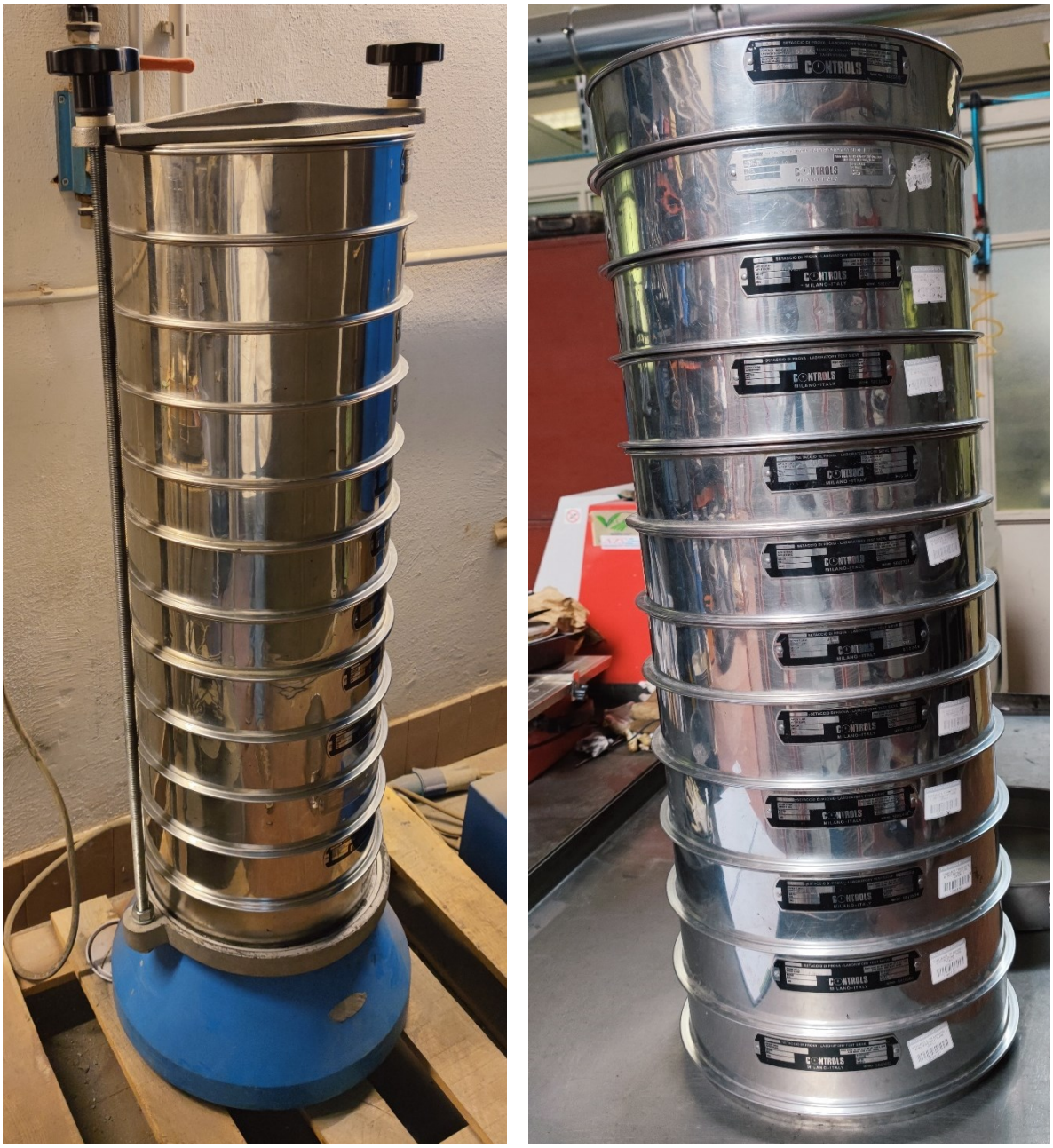

Figure 54 Sieves column and the mechanical vibrator

- **Calculations:**

All of the masses were recorded in a data sheet, and then the mass retained on each sieve was calculated as percentage of the original mass (M_1). The cumulative percentage of the original dry mass passing each sieve down to the 0.063 mm was calculated.

The percentage of fines (*f)* passing the 0.063 mm sieve was calculated as follows:

$$f = \frac{(M_1 - M_2) + P}{M_1} x100$$

Where:

M_1 is the dried mass of the test portion, in kilograms.
M_2 is the dried mass of the residue retained on the 0.063 mm sieve, in kilograms.
P is the mass of the screened material remaining in the pan, in kilograms.

The results were validated based on the difference between the sum of the masses and P, obtaining less than 1 % from mass M_2.

The limiting values for aggregate gradation was taken as follows:

Sieve size (mm)	Lower limit (% passing)	Upper limit (% passing)
32	100	100
16	90	100
10	73	85
4	45	56
2	28	38
0.5	16	24
0.25	11	18
0.063	4	8

Table 22 Aggregate gradation limits

Sieve size (mm)	Sieve Mass (g)	Sieve + soil (g)	Retained (g)	Retained (g) + Filler	cumulative R (g)	cumulative R (%)	Passing (%)
16	1303.6	1303.6	0	0	0	0	100
14	1058.1	1076.2	18.1	18.1	18.1	1.4	98.6
12.5	1053.7	1100.7	47	47	65.1	4.9	95.1
10	1029.4	1126.6	97.2	97.2	162.3	12.3	87.7
8	1071.6	1163.5	91.9	91.9	254.2	19.3	80.7
6.3	1193.5	1296.9	103.4	103.4	357.6	27.2	72.8
4	1108.7	1364	255.3	255.3	612.9	46.6	53.4
2	980.7	1233.3	252.6	252.6	865.5	65.8	34.2
1	866.2	1001.2	135	135	1000.5	76.1	23.9
0.5	784	888.5	104.5	104.5	1105	84	16
0.25	726.6	796.8	70.2	70.2	1175.2	89.3	10.7
0.063	773	830.9	57.9	57.9	1233.1	93.7	6.3
Pan	725	725.6	0.6	82.4	1315.5	100	0
Total	**12674.1**	**13907.8**	**1233.7**	**1315.5**			

Table 23 Sieve analysis of the 1st sample

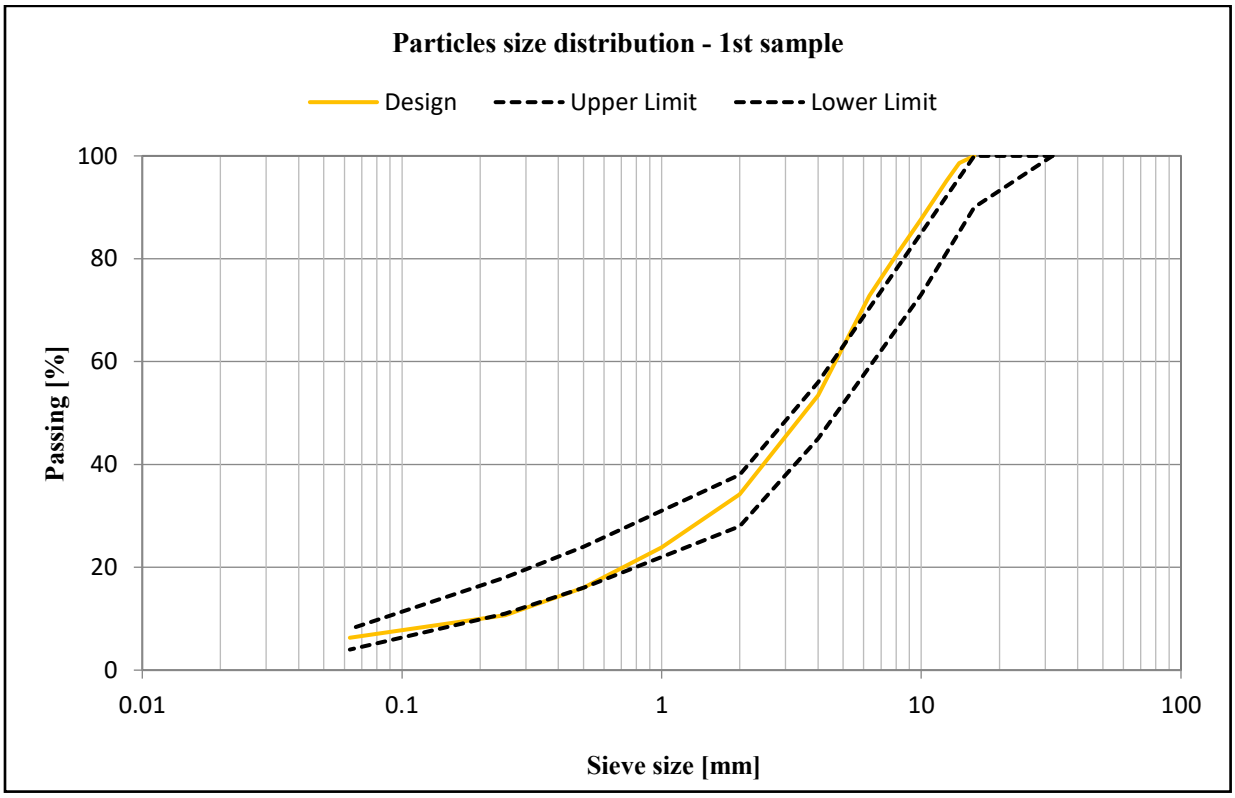

Figure 55 Aggregate gradation - 1st sample

Sieve size (mm)	Sieve Mass (g)	Sieve + soil (g)	Retained (g)	Retained (g) + Filler	cumulative R (g)	cumulative R (%)	Passing (%)
16	1303.6	1303.6	0	0	0	0	100
14	1058.1	1076.8	18.7	18.7	18.7	1.3	98.7
12.5	1184.2	1222.2	38	38	56.7	4	96
10	1029.4	1160.2	130.8	130.8	187.5	13.4	86.6
8	1071.6	1199.9	128.3	128.3	315.8	22.5	77.5
6.3	1193.6	1306.1	112.5	112.5	428.3	30.6	69.4
4	1108.8	1365.8	257	257	685.3	48.9	51.1
2	975.3	1219.7	244.4	244.4	929.7	66.4	33.6
1	866.2	1014.6	148.4	148.4	1078.1	77	23
0.5	783.9	891.3	107.4	107.4	1185.5	84.6	15.4
0.25	726.7	797.9	71.2	71.2	1256.7	89.7	10.3
0.063	773.1	832.1	59	59	1315.7	93.9	6.1
Pan	725	725.8	0.8	84.9	1400.6	100	0
Total	**12799.5**	**14116**	**1316.5**	**1400.6**			

Table 24 Sieve analysis of the 2nd sample

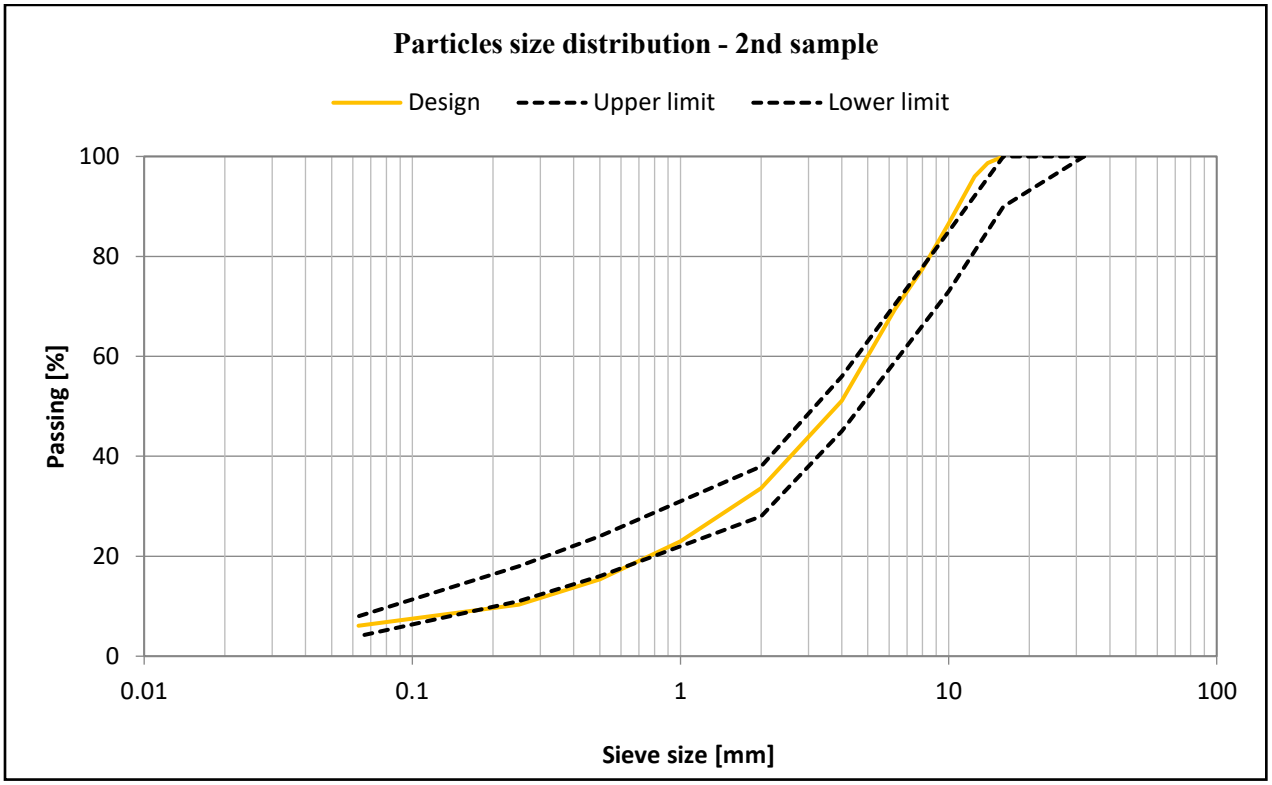

Figure 56 Aggregate gradation - 2nd sample

3.3.4 Gyratory compaction:

The Compactability and workability of the bituminous mixtures was estimated using the gyratory compactor. This method is used for estimating the air voids content (or compaction ratio) of a mixture for a given number of gyrations. It is also used to prepare specimens of a certain height for subsequent testing of their mechanical properties.

"The bituminous mixture is contained within a cylindrical mould limited by inserts and kept at a constant temperature within specified tolerances throughout the whole duration of the test. Compaction is achieved by the simultaneous action of a low static compression, and of the shearing action resulting from the motion of the axis of the sample which generates a conical surface of revolution, of apex O and of 2 ϕ angle at the apex, while the ends of the test piece should ideally remain perpendicular to the axis of the conical surface" [41]

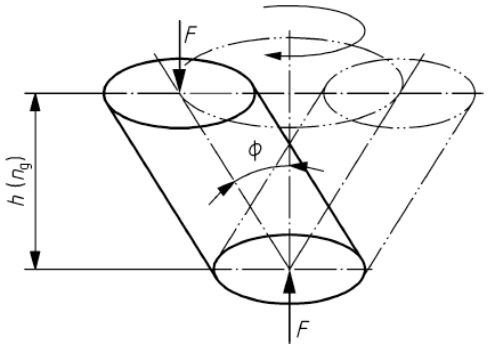

Figure 57 Test piece motion diagram

- **Procedure:**

The gyratory compaction was carried out according to [BS EN 12697-31:2019]

Fistly, he mass (M) to be implemented in the mould is calculated as follow:

$$M = 10^{-3}\pi\frac{D^2}{4}h_{min}\rho_M$$

Where:

M is the mass of a dry mixture to be introduced in the mould, in grams (g).
D is the internal diameter of the mould, in millimetres (mm).
h_{min} is the minimum height of compacted specimen, corresponding to zero percent of voids, in millimetres (mm).
ρ_M is the maximum density of the mixture, in Megagrams per cubic metre (Mg/m3).

h_{min} is a constant value and must be taken as 0.66D and 1.05D.

Since we used the 100 mm diameter mould, the value of h_{min} should be taken between 66 mm and 105 mm, and it was taken equal to 70 mm.

Based on that, the mass of the dry mixture to be put in the mould equals 1375 gm.

D (mm)	Hmin, MIN (mm)	Hmin, MAX (mm)	TMD (Kg/m3)	M, MIN (g)	M, MAX (g)
100	66	105	2501	1296.42	2062.49

Table 25 Gyratory sample's mass inside the mold

Since the nominal maximum aggregate size (12.5 mm) is less than 16 mm, a diameter of 100 mm was chosen for the specimen.

The molds and the inserts were put in the oven for conditioning for at least two hours to bring it to the reference compaction temperature ± 5 ºC, which is estimated as a function of the bitumen grade following the next table:

Paving grade of bitumen	Reference compaction temperature for: °C		Paving grade of bitumen	Reference compaction temperature for mixtures of types other than mastic asphalt °C
	Mixtures of types other than mastic asphalt	Mastic asphalt mixtures		
10/20 to 20/30	180	230	250/330	130
30/45	175	220	330/430	125
35/50	165	210	500/650	120
40/60	155	200	650/900	115
50/70	150	-	V12000	115
70/100	145	-	V6000	110
100/150	140	-	V3000	100
160/220	135	-	V1500	90

Table 26 Reference compaction temperature

At the same time the bituminous mixture was brought to the reference compaction temperature avoiding excessive heating in order to avoid additional aging of the loose mixture.

After the mold, inserts, and the mixture reach the target temperature; the mold with the bottom insert were placed in a balance, and a lubricant was applied to the inner surface. After that and the predefined mass was poured inside the mold by means of a funnel. The top level of the mixture was leveled, and the top insert was placed. The mold containing the mixture was put back inside the oven for at least 15 min to allow a homogenous temperature before running the test.

Then, the mold was placed inside the gyratory compactor and the test was run. After the test has finished, the compacted sample was then extracted from the mold and let to cool down. After that the thickness measurements were taken at four points along the diameter (each 90 º) as follows:

Sample 1, 100 GY			
Thickness measured at 90 º (mm)			
73.75	73.75	73.75	73.65
Average Thickness (mm)			73.7

Table 27 Thickness of the 1st gyratory sample

Sample 2, 100 GY			
Thickness measured at 90 º (mm)			
73.95	74.1	74.1	74.1
Average Thickness (mm)			74.0

Table 28 Thickness of the 2nd gyratory sample

Sample 3, 180 GY			
Thickness measured at 90 º (mm)			
72.45	72.45	72.65	72.75
Average Thickness (mm)			72.5

Table 29 Thickness of the 3rd gyratory sample

Sample 4, 180 GY			
Thickness measured at 90 º (mm)			
72.9	72.75	72.75	72.8
Average Thickness (mm)			72.8

Table 30 Thickness of the 4th gyratory sample

Figure 58 Typical gyratory molds and samples

The compactablilty and workability were estimated from the compaction curve as we can see in the following graphs:

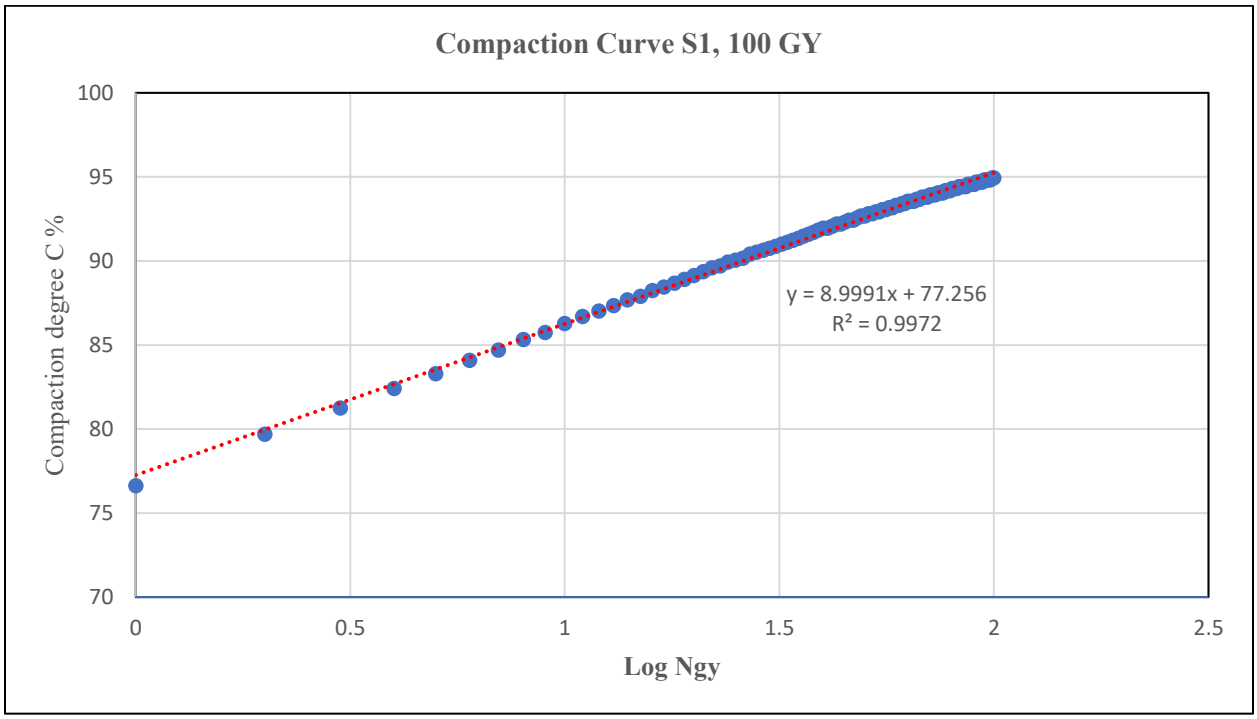

Figure 59 Compaction curve - 1st gyratory sample

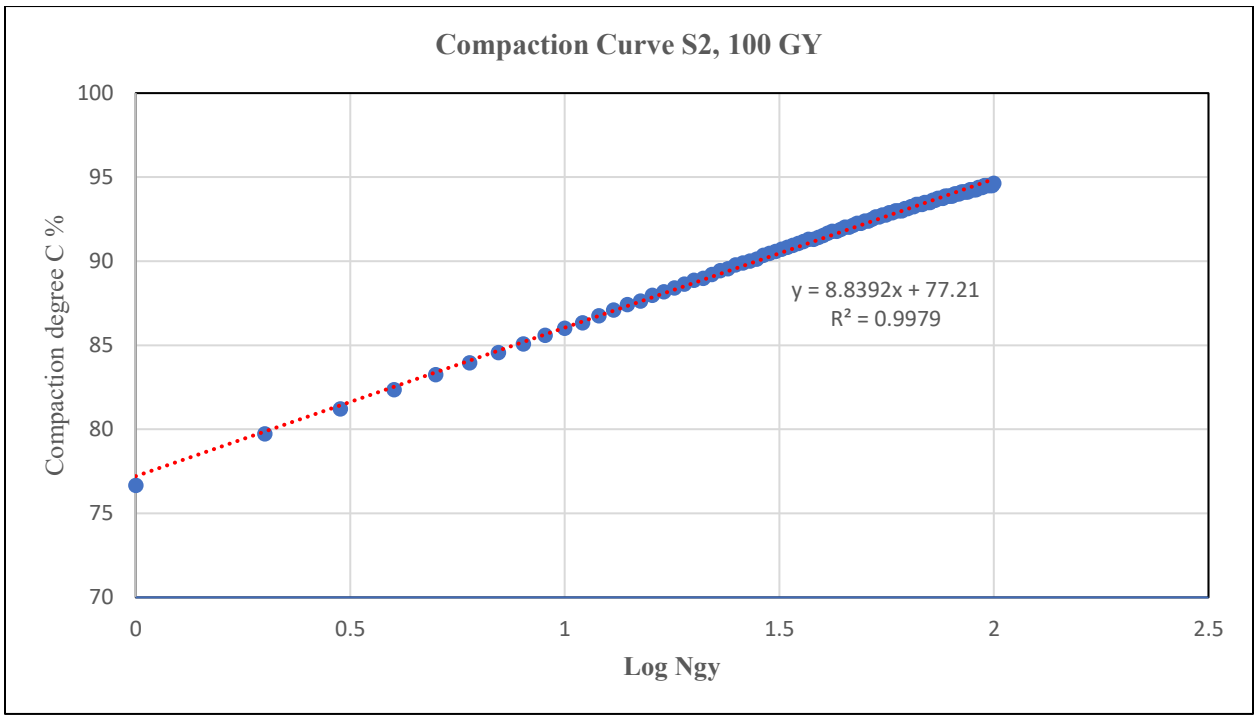

Figure 60 Compaction curve - 2nd gyratory sample

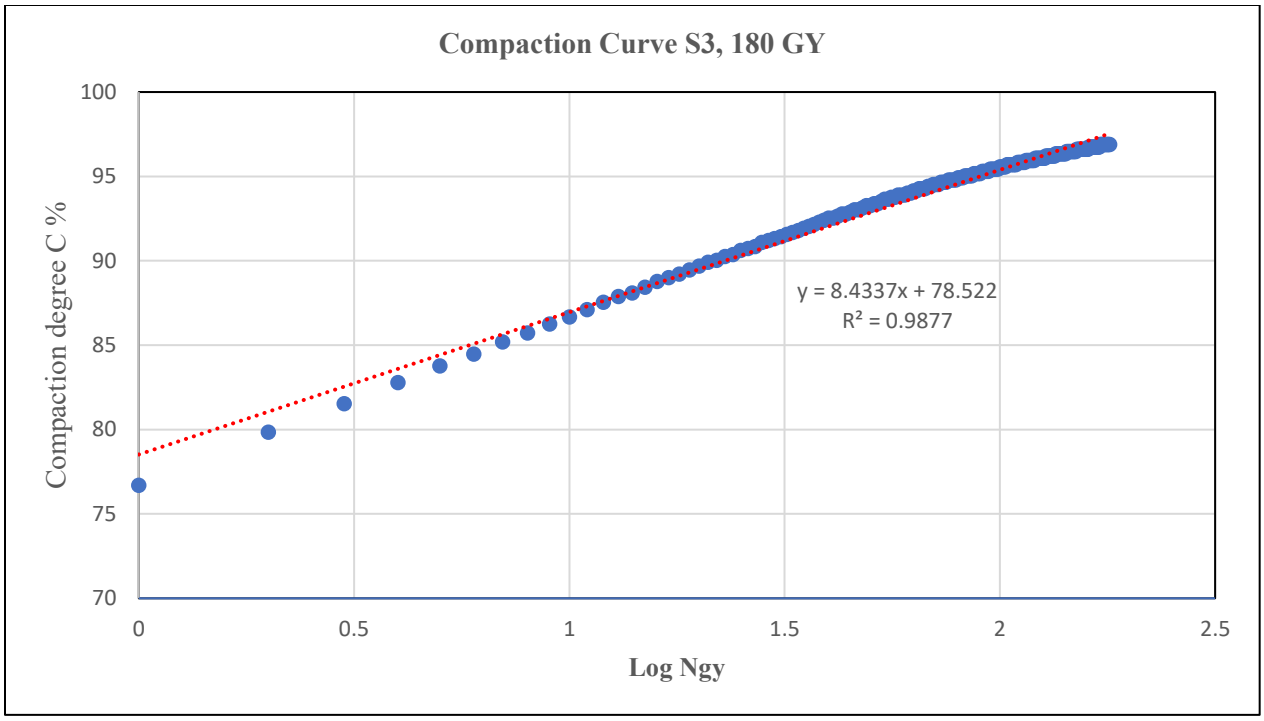

Figure 61 Compaction curve - 3rd gyratory sample

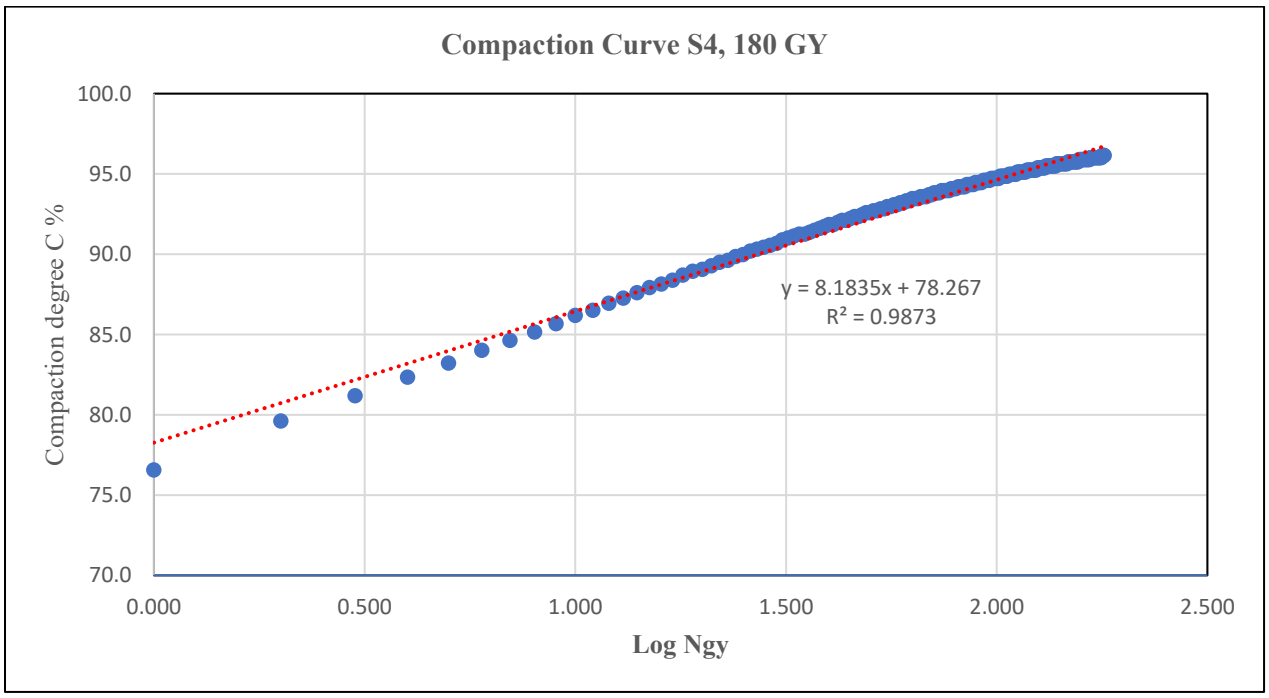

Figure 62 Compaction curve - 4th gyratory sample

The results are summarized in the following table:

Sample	1	2	3	4
Workablilty	9.00	8.84	8.43	8.18
Self compaction	77.3	77.2	77.5	77.3

Table 31 Samples workability and Compactability

3.3.5 Roller compaction:

The roller compaction is carried out to get slabs of bituminous mixture, which are used later to obtain the four point bending beams after sawing. The roller compaction is performed using a wheel fitted with pneumatic tires, until the specified volume is reached *(L=500 mm, l=180 mm, h= 50 mm*). the roller compaction is made in accordance with [BS EN 12697-33-2019].

- **Procedure:**

The mass of bituminous mixture to be introduced in the mold is calculated as:

$$M = 10^{-6}.L.l.e.\rho_m.\left(\frac{100 - v}{100}\right)$$

where:

M is the mass of slab, in kilograms (Kg).
L is the interior length of the mold, in (mm).
l is the interior width of the mold, in (mm).
e is the final thickness of slab, in (mm).
ρ_m is the theoretical maximum density of the mixture in (Mg/m^3).
v is the air voids content in slab, in percentage (%).

To be compacted mass							
%v	**Mould size**			**Volume**	**TMD**	**Mass**	**MV, geo**
(-)	**w [cm]**	**L [cm]**	**H [cm]**	**[cm^3]**	**[g/cm^3]**	**[g]**	**[g/cm^3]**
7.5	18.0	50.0	5.0	4500.0	2.501	**10410.4**	2.313

Table 32 Wheel compactor to be compacted mass

Before the compaction, the metal mold, the frame, and the base were preheated up to the reference compaction temperature for at least two hours. After the sample and the metallic parts reached the test temperature, it was taken out from the oven and immediately placed back in the compaction equipment. After that some Silicon was applied to the metallic parts covering the inner surface of the mold and the base. The mold was then filled with the mass (M+14 gm) of the bituminous mixture, and the material was spread evenly with a shovel removing any segregation.

In order to achieve the target air voids (taken as 7.5 %), we used a heavy compaction following the sweep plan indicated in table (31), which gives the closest result above the desired air voids content, the some additional passed are applied making sure that the sweep plan is even to avoid uneven compaction and surface deformations.

The passes in blocked axis at the end of sweep plan could be replaced with 4 to 6 passes using a smooth steel roller with no transverse displacement to further even the surface.

Figure 63 The roller compactor without the auxiliary elements

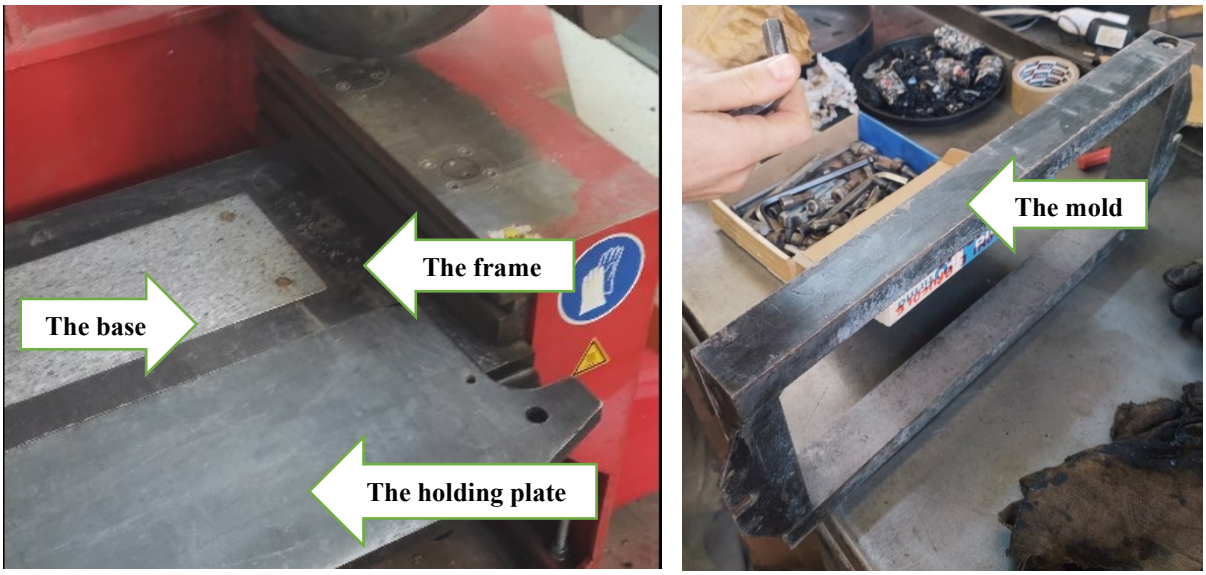

Figure 64 The wheel compactor auxiliary elements

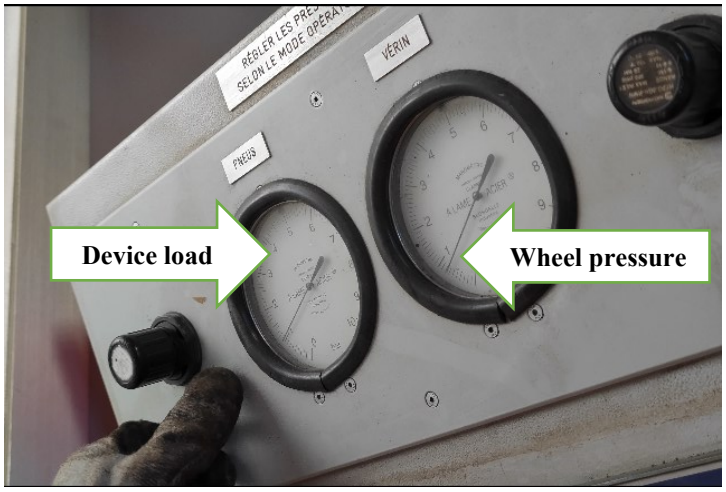

Figure 65 Setting device load and wheel pressure

Figure 66 The compacted slab

Number of passes						Tyre pressure MPa	Load F kN	Start	Extent of lateral translation a mm	Axis mode
Position of the wheel										
Front		Centre		Rear						
	Cumulative [a]		Cumulative [a]		Cumulative [a]					
1						0,1	1	right	75	blocked
				1						
		1								
1										
				1						
		1								
2	2					0,6	5	right	45	freed
				2	2					
		1	1							
2	4									
				2	4					
		1	2							
4	8									
				4	8					
		2	4							
8	16									
				8	16					
		4	8							
8	24									
				8	24					
		4	12							
4	28									
				4	28					
		2	14							
2	30									
				2	30					
		1	15							
2	32									
				2	32					
		1	16							
1						0,6	5		45	blocked
				1						
		1								
1										
				1						
		1								

[a] The cumulated number of passes is given only for the freed axis mode.

Table 33 Sweep plan, specimens 500 mm × 180 mm × e, heavy compaction,

After the compaction was finished, the slab was extracted from the roller compactor and let to cool down, then the measurements of the thickness were taken along the four sides of the slabs as we can see in the follow example:

1st wheel compaction						
Long Side 1 (mm)						
51.3	50.75	50.4	50.5	51	51	51.65
Long Side 2 (mm)						
51.6	51.45	51.25	51.5	50.9	50.95	52.15
Short Side 1 (mm)						
51.15	51.3	51.55				
Short side 2 (mm)						
52	51.9	51.45				

Table 34 Compacted slab thickness

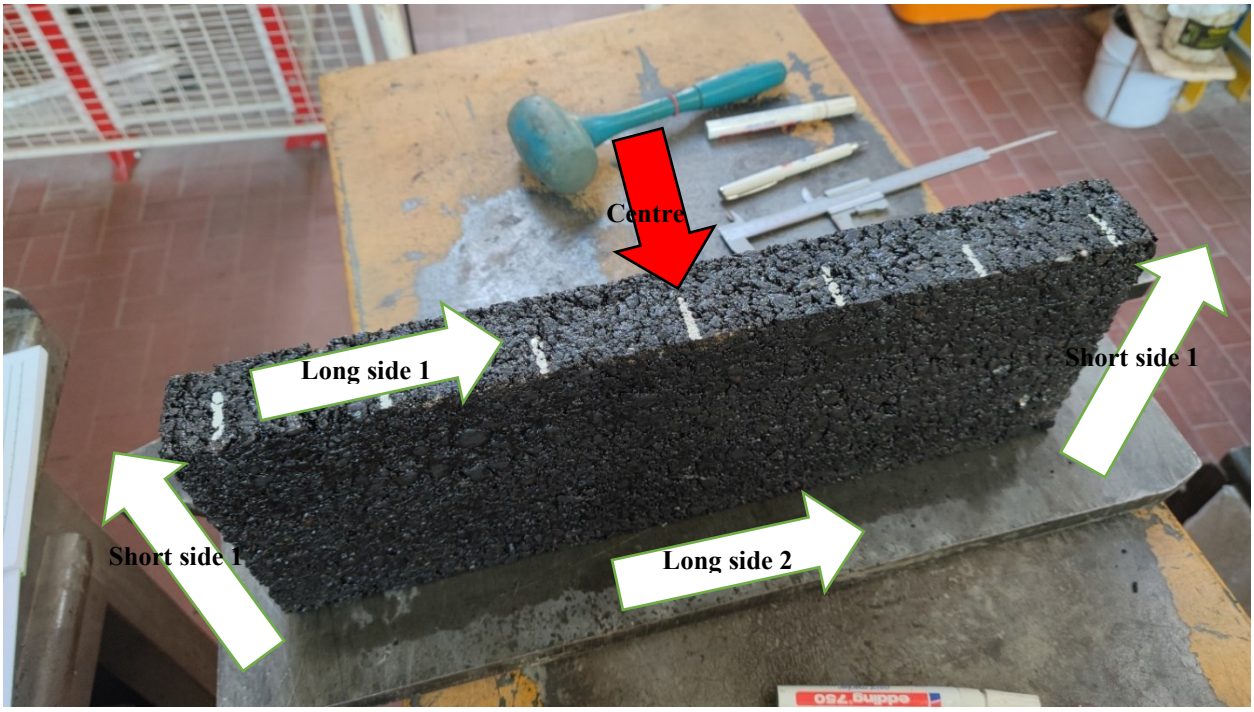

Table 35 Thickness measurements positions

The remaining tables are provided in the Appendix section.

3.3.6 Bulk density for gyratory samples, roller compacted slabs, and 4PB beams:

The bulk density is the density of a compacted hot mixed asphalt, and it is one of the most fundamental compacted mixture properties, since it is used to calculate the real air void in the mixture.

There are several different ways to measure bulk specific gravity, all of which use slightly different ways to determine specimen volume. In our case we used the saturated surface dry approach (SSD), which is the most common method to calculate the specimen volume by subtracting the mass of the specimen in water from the mass of a saturated surface dry (SSD) specimen. SSD is defined as the specimen condition when the internal air voids are filled with water and the surface (including air voids connected to the surface) is dry.

The compaction of the specimens was done using two different testing devices:

1. The gyratory shear compactor.
2. The wheel compactor.

And hence two bulk densities were estimated, according to [BS EN 12697-6-2020].

- **Procedure:**

The procedure is the same for the gyratory compactor samples, the roller compactor samples, and the obtained four-point bending samples. Firstly, the mass of the dry specimen was recorded (m_1), then the specimen was immersed in the water path to allow water to saturate the specimen sufficiently enough for the mass not to change. The sample was left in the water for about 1 hour, and then the weight in waster was recorded (m_2) taking care that no air bubbles adhered to the surface. Next, the specimen was removed from the water path, and its surface was dried by wiping the surface with a piece of chamois, and the corresponding weight was recorded immediately (m_3). Finally, the temperature of the water was recorded.

- **Calculations:**

The bulk density is calculated as follows:

$$\rho_{SSD} = \frac{m_1}{m_3 - m_2} x \rho_w$$

Where:

ρ_{SSD} is the bulk density (SSD), in megagram per cubic metre (Mg/m3).
m_1 is the mass of the dry specimen, in gram (g).
m_2 is the mass of the specimen in water, in gram (g).
m_3 is the mass of the saturated surface-dried specimen, in gram (g).
ρ_w is the density of the water at test temperature, in megagram per cubic metre (Mg/m3).

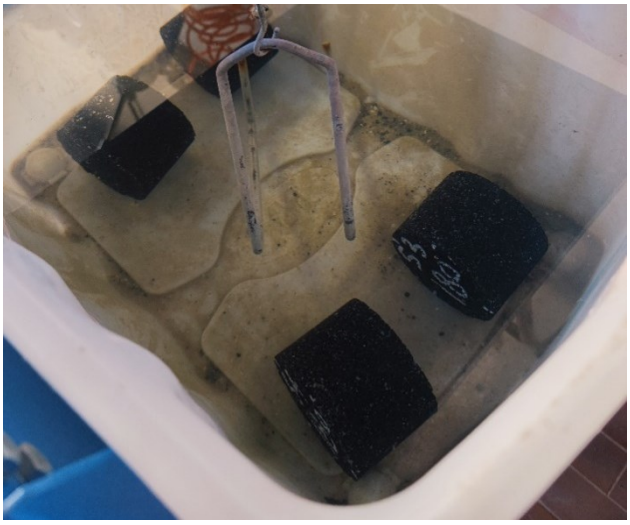

Figure 67 Gyratory samples inside the water path and temperature measurement

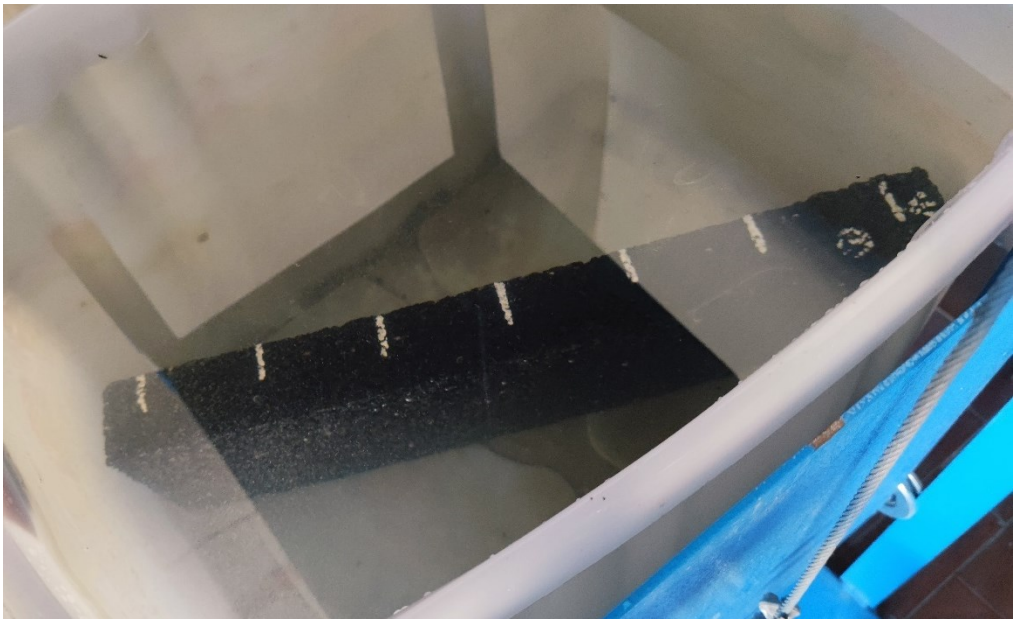

Figure 68 The slab inside the water path

Figure 69 The 4PB beams inside the water path

Figure 70 The water path and the balance

An example of the results is shown in the following tables, for both the gyratory compactor samples, roller compactor samples, and four-point bending samples:

Theoretical air voids (%)							
ID	**Thickness (H)**	**Diameter (D)**	**Volume (V)**	**Mass (M)**	ρ_{geo}	**TMD**	**V% Theo**
[-]	**[mm]**	**[mm]**	**[m³]**	**[g]**	**[kg/m³]**	**[kg/m³]**	**[%]**
1	73.7	100.0	0.000579	1372.5	2370.3	2501.0	5.2
2	74.1	100.0	0.000582	1371.8	2358.3	2501.0	5.7
3	72.6	100.0	0.000570	1374.0	2410.5	2501.0	3.6
4	72.8	100.0	0.000572	1373.2	2401.7	2501.0	4.0

Table 36 Theoretical air voids for gyratory samples

Real air voids (%)								
ID	**M 1**	**M 2**	**M 3**	**Temp.**	ρ_w	ρ_{SSD}	**TMD**	**V% real**
[-]	**[g]**	**[g]**	**[g]**	**[°C]**	**[kg/m³]**	**[kg/m³]**	**[kg/m³]**	**[%]**
1	1372.5	808.7	1375.4	17.6	998.7	2419	2501	3.3
2	1371.8	806.9	1375.0	17.6	998.7	2412	2501	3.6
3	1374.0	815.5	1375.5	17.6	998.7	2450	2501	2.0
4	1373.2	814.7	1375.6	17.6	998.7	2445	2501	2.2

Table 37 Real air voids of gyratory samples

Mould size			Volume	TMD	Mass	ρ, geo	V% geo
w [cm]	**L [cm]**	**H [cm]**	**[cm³]**	**[g/cm³]**	**[g]**	**[g/cm³]**	**(-)**
18.0	50.0	4.94	4441.7	2.501	10181.8	2.292	8.3

Table 38 Theoretical air voids of a typical wheel compactor slab

M 1 [g]	M 2 [g]	M 3 [g]	Temp. [°C]	ρ_w [kg/m³]	ρ_{SSD} [kg/m³]	TMD [kg/m³]	V% real [%]
10181.8	5937.5	10248.3	19.3	998.4	2358	2501	5.71

Table 39 Real air voids a typical wheel compactor slab

7th set of BEAMS								
ID [-]	**B** [mm]	**H** [mm]	**L** [mm]	**V** [m^3]	**M** [g]	**ρ geo** [kg/m^3]	**TMD** [kg/m^3]	**V% geo** [%]
19L	51.1	48.4	408.0	0.001010	2330.2	2308.1	2501.0	7.7
20C	50.2	49.3	408.5	0.001012	2370.0	2342.5	2501.0	6.3
21R	50.8	48.7	408.0	0.001009	2350.8	2329.6	2501.0	6.9

Table 40 Theoretical air voids of a typical set of beams

ID [-]	**M 1** [g]	**M 2** [g]	**M 3** [g]	**Temp.** [°C]	ρ_w [kg/m^3]	ρ_{SSD} [kg/m^3]	**TMD** [kg/m^3]	**V% real** [%]
19L	2330.2	1353.1	2335.3	19.0	998.5	2369	2501	5.3
20C	2370.0	1382.6	2372.3	19.0	998.5	2391	2501	4.4
21R	2350.8	1364.9	2355.0	19.0	998.5	2371	2501	5.2

Table 41 Real air voids of a typical set of beams

The remaining tables are presented in the Appendix.

Chapter 4: Analysis of the results

4.1 Introduction

Relying on the literature review presented in the second chapter, five failure criteria were selected. In the following passages the results from those failure criteria will be presented and compared up with the best path to follow for fatigue resistance characterization.

The first two failure criteria are based on the modulus reduction: 50 % reduction in the initial modulus taken at the 100^{th} cycle, and 50 % reduction in the modulus extrapolated from the phase of linear reduction of the modulus (Intermediate phase). The third failure criterion is the peak in the phase angle. The last two criteria are based on energy concepts, the first one is the energy ratio, and the second one is the dissipated energy approach.

Furthermore, some additional relationships will be introduced like the relationship between the visco-elastic-related modulus versus the void ratio of the beams, and fatigue-related modulus versus the void ratio. Also, the relationship between the positions of the beams derived from the wheel compacted slab and the corresponding air voids will be presented.

Statistical analysis will be made, dealing with the expected non-homogeneity of the results. Consequently, a sensitive pavement design will be carried out using KENLAYER non-linear analysis software. The design will be based on a fixed pavement configuration, adopting the mechanistic empirical pavement design fatigue model (Transfer function). The purpose is to see how pavement design is affected by the variability in fatigue resistance characterization.

4.2 1st failure criteria: 50% reduction of the initial stiffness:

This is one of the most used criteria to define the fatigue failure of bituminous mixtures, and it is defined as the point when we have 50% reduction in material's modulus of its initial value, which is taken at the 100th cycle, and the corresponding number of cycles is indicated as Nf_{50}. This failure criterion is deemed to be reliable for the application of continuum damage models however might not offer a coherent prediction for the damage state as a result of its arbitrary assumption (Modulus reduction to half its initial value).

The classical criterion reflects only the sample stiffness, neglecting the material properties, fatigue phenomenon itself, and other phenomenon like the self-heating and thixotropy. Every so often, a 50% decrease in stiffness is not associated with cracking for one material, while for another one it is equivalent to a considerable micro or even macro cracking.

This non-consistency was clear throughout the obtained results, since we obtained a scattered values, which are not related to any behavioural change in the material.

In this study, more than 18 different beams have been analysed by testing a minimum of 6 beams at each of the strain levels (300 µm/m, 200 µm/m, 140 µm/m). Those strain levels are selected by performing some trails. The idea was to obtain three strain levels that have a good distribution when plotted versus the number of cycles to failure, and to yield fatigue lives between 10,000 and $2*10^6$ cycles for the specific failure criteria, as indicated in the [BSI- resistance to fatigue] [8]

According to the ASTM [**Designation: D8237 – 21]** [42]**,** the desired initial peak-to-peak strain is between 50 µm/m to 3000 µm/m, with a typical values ranges from 200 µm/m to 800 µm/m. relying on this we decided to choose strain levels between 100 µm/m and 400 µm/m, which is half of the values suggested by the ASTM. This is because we are working with strain amplitude not peak-to-peak strain.

Some trail tests were conducted, starting with testing the extremes (100 µm/m, 400 µm/m), then intermediate values, and based on the obtained results we choose the above mentioned strain levels.

Next, we can see a typical test result after been analysed with respect to this failure criterion, and the number of cycles for each test:

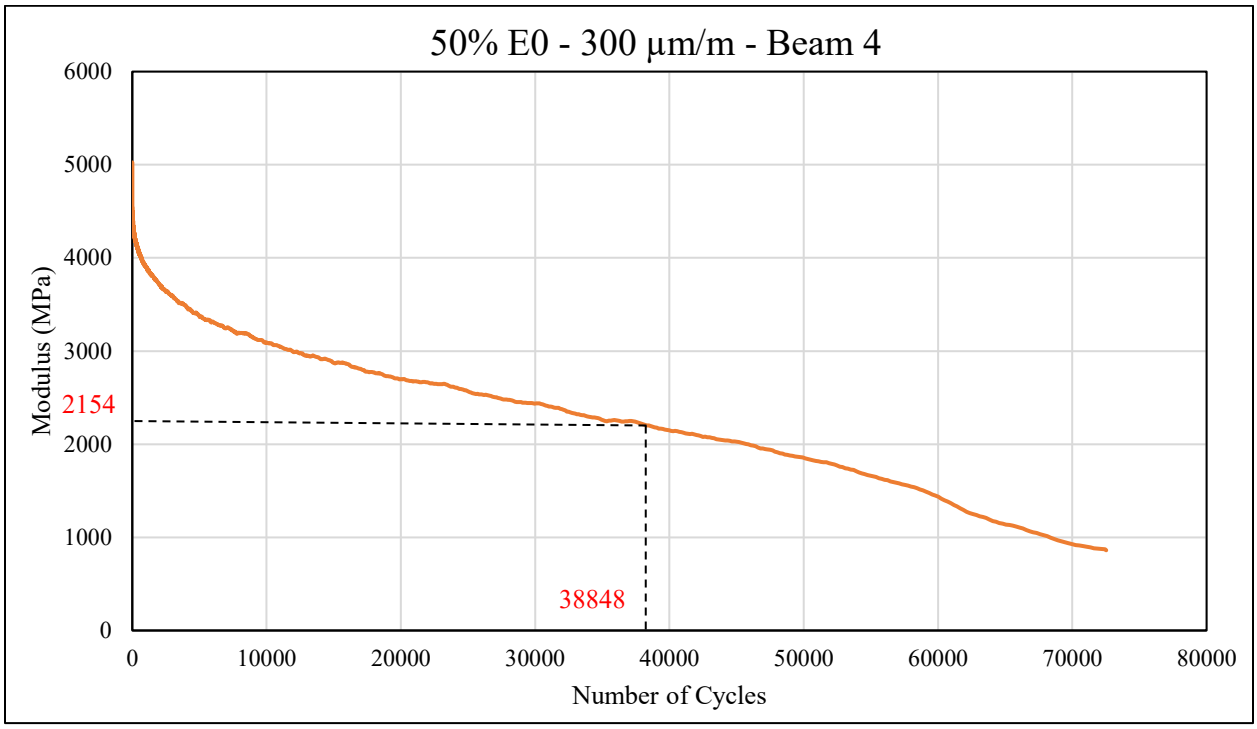

Figure 71 Typical fatigue test result using the 50%E0 criteria

In this case the initial modulus was (4,309 MPa), and the corresponding number of cycles by using this criterion (50% of 4309 MPa = 2,154 MPa) was (38,848 cycles).

The results are summarized in the following table:

Failure criterion	50% Reduction in the initial Stiffness (E0) - 300 µm/m					
Beam ID	Beam 4	Beam 7	Beam 8	Beam 9	Beam 10	Beam 12
Number of cycles	38,849	39,965	24,267	12,351	22,089	29,969

Failure criterion	50% Reduction in the initial Stiffness (E0) - 200 µm/m					
Beam ID	Beam 3	Beam 13	Beam 14	Beam 15	Beam 18	Beam 21R
Number of cycles	293,539	163,850	338,846	249,911	161,354	163,433

Failure criterion	50% Reduction in the initial Stiffness (E0) – 140 µm/m			
Beam ID	Beam 6	Beam 22L	Beam 24R	Beam 30R
Number of cycles	1,049,188	263,031	1,059,340	833,897

Table 42 Typical fatigue test result using the conventional criteria

4.3 2nd failure criteria: 50% reduction of the E00

As we saw in the literature chapter, this method assumes a linear evolution of the modulus with number of applied load cycles within given interval.

This failure criterion is the number of cycles corresponding to 50% reduction of the modulus value (E_{00}) obtained through linear extrapolation of the stage at which we have linear reduction of the modulus (intermediate stage) when drawn versus the number of cycles.

The definition of this interval is somehow subjective because it depends on the length of the intermediate stage which can differ from one test to another.

Next, we can see a typical test result after been analysed with respect to this failure criterion, and the number of cycles for each test:

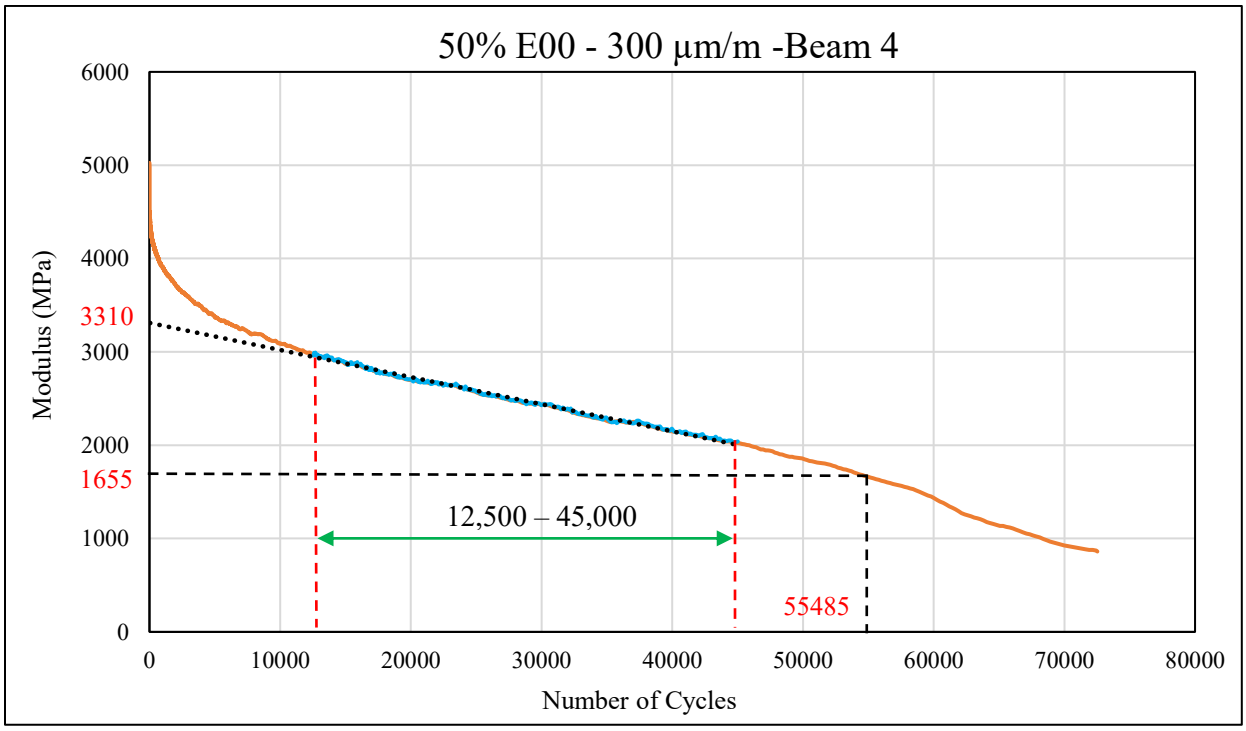

Figure 72 Typical fatigue test result using the 50%E00 criteria

In this case the extrapolated modulus was (3,310 MPa), and the corresponding number of cycles by using this criterion (50% of 3,310 MPa = 1,655 MPa) was (55,485 cycles).

The results are summarized in the following table:

Failure criterion	50% Reduction in the extrapolated Stiffness (E00) - 300 µm/m					
Beam ID	Beam 4	Beam 7	Beam 8	Beam 9	Beam 10	Beam 12
Number of cycles	55,486	114,818	51,485	15,021	37,012	46,417

Failure criterion	50% Reduction in the extrapolated Stiffness (E00) - 200 µm/m					
Beam ID	Beam 3	Beam 13	Beam 14	Beam 15	Beam 18	Beam 21R
Number of cycles	350,309	226,758	645,657	361,225	284,010	1,267,030

Failure criterion	50% Reduction in the extrapolated Stiffness (E00) - 140 µm/m			
Beam ID	Beam 6	Beam 22L	Beam 24R	Beam 30R
Number of cycles	1,853,854	1,689,577	1,689,577	1,801,174

Table 43 Typical fatigue test result using the 50%E00 criteria

4.4 3rd failure criteria: Peak in phases angle

During a typical fatigue test under cyclic loading, the measured phase angle usually undergoes a steady increase if damage happens, this stage is then followed by a sharp reduction. Fatigue life, or number of cycles to failure N_f, is defined as the cycle at which this sharp reduction takes place. This method is believed to be more based on theoretical aspects, since it is traced through the viscoelastic property of the material, and this reduction indicates an alteration in the governing mechanism inside the material.

Next, we can see a typical test result after been analysed with respect to this failure criterion, and the number of cycles for each test:

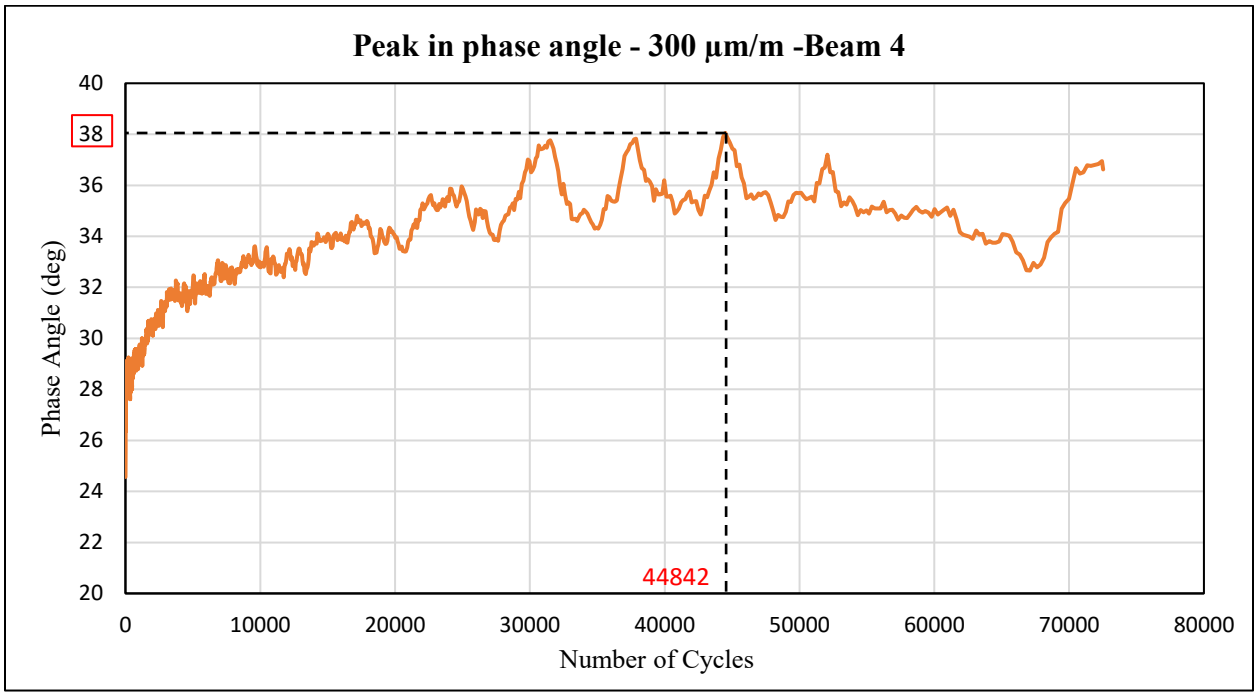

Figure 73 Typical fatigue test result using the peak in the phase angle criteria

In this case the peak took place at (38 º), and the corresponding number of cycles by using this criterion was (44842 cycles).

The results are summarized in the following table:

Failure criterion	Peak in the phase angle - 300 µm/m					
Beam ID	Beam 4	Beam 7	Beam 8	Beam 9	Beam 10	Beam 12
Number of cycles	44,842	40,037	73,861	19,166	19,125	61,203

Failure criterion	Peak in the phase angle - 200 µm/m					
Beam ID	Beam 3	Beam 13	Beam 14	Beam 15	Beam 18	Beam 21R
Number of cycles	243,312	180,118	399,965	235,475	117,266	138,828

Failure criterion	Peak in the phase angle - 140 µm/m			
Beam ID	Beam 6	Beam 22L	Beam 24R	Beam 30R
Number of cycles	790,285	230,859	238,659	230,859

Table 44 Typical fatigue test result using peak in the phase angle criteria

4.5 4th failure criteria: Energy ratio

As we saw in the literature chapter, in a stress- controlled test, the amount of the load stays fixed, and after the phase of crack initiation when we have the presence of crack tips, the stress increases sharply. Accordingly, the value of N_1 can be easily estimated from the peak of R_n^σ vs n This idea of identifying fatigue life by the N_1 peak point is extremely desirable because the data attained from either stress/strain controlled test configuration characterizes the material in the same state of damage instead of the modulus reduction criteria (The classical approach), which is an arbitrary definition.

A typical graph could be achieved if the data from strain-controlled test is plotted, However, a further stage of behaviour is noted. This later stage is linked with the slow crack propagation over the specimen as the stress drops in the controlled strain test.

the N_1 condition is very much difficult to define for strain- controlled than to stress- controlled tests (This is because of the decrease of the stress at the crack tip as the crack progresses, resulting in a reducing rate of crack propagation). This problem could be surpassed by employing the same analysis for the controlled stress method as previously stated. Although the fatigue tests are carried out using strain-controlled tests a modified version of Hopman's analysis for stress-controlled tests can be used. When plotting the product (NxE) versus N we get a noticeable peak at failure N_1, as we can see in the following example:

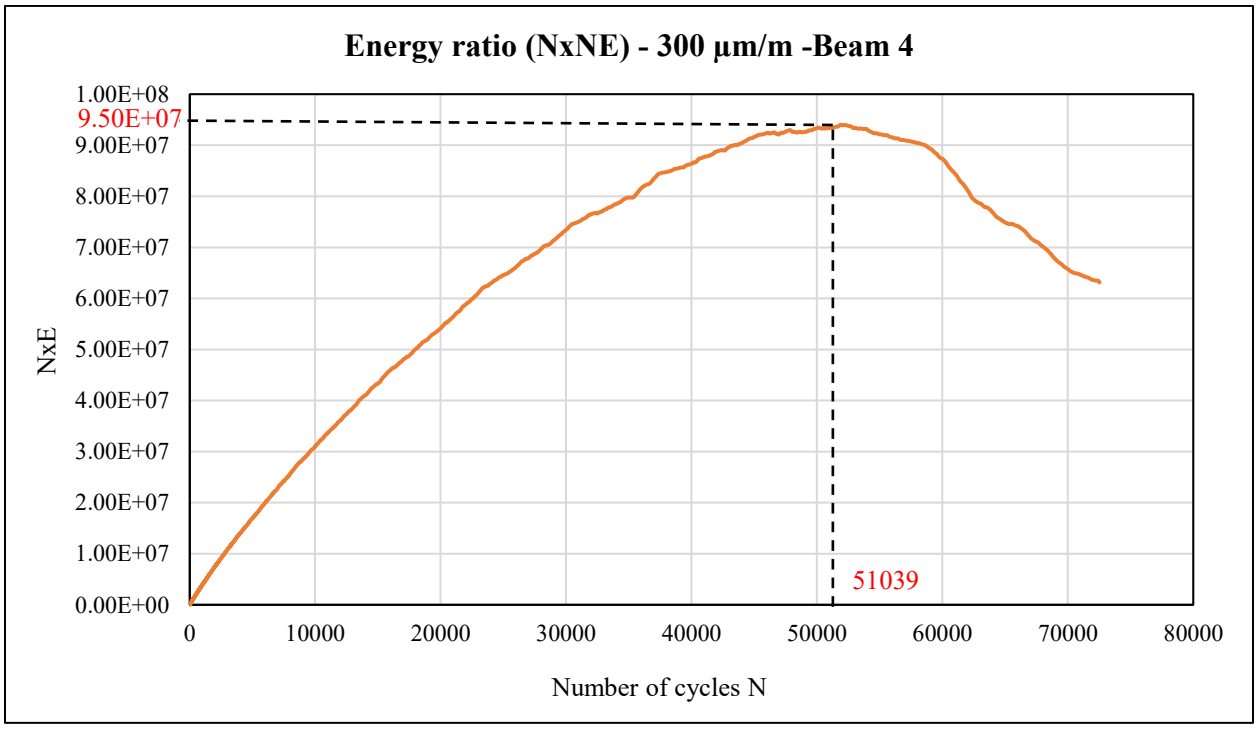

Figure 74 Typical fatigue test result using the energy ratio criteria

In this case the peak took place at (9.50E+07), and the corresponding number of cycles by using this criterion was (51039 cycles).

The results are summarized in the following table:

Failure criterion	Energy ratio - 300 µm/m					
Beam ID	Beam 4	Beam 7	Beam 8	Beam 9	Beam 10	Beam 12
Number of cycles	51,039	108,258	69,867	13,133	40,983	45,885

Failure criterion	Energy ratio - 200 µm/m					
Beam ID	Beam 3	Beam 13	Beam 14	Beam 15	Beam 18	Beam 21R
Number of cycles	296,506	197,022	558,927	317,867	279,684	1,207,666

Failure criterion	Energy ratio - 140 µm/m			
Beam ID	Beam 6	Beam 22L	Beam 24R	Beam 30R
Number of cycles	-	1,657,457	1,727,835	1,920,142

Table 45 Typical fatigue test result using the energy ratio criteria

4.6 5th failure criteria: Dissipated energy ratio

The graph of the correlation between DER and number of cycles in the stress-controlled mode offers a unique approach to assess the stage of fatigue damage at which the material experiences a transition from crack initiation to crack propagation. Throughout the first part the damage is negligible and $DER = n$ (the dissipated energy is roughly equal for successive cycles). As the relative difference in dissipated energy between successive cycles becomes substantial, the dissipated energy ratio starts deviating from the equality line which is interpreted as crack initiation. The fatigue failure Nf point is characterized by the sudden change in DER which can be linked to the point of transition from crack initiation to crack propagation. This change is believed to be highly material-specific and independent of the mode of loading. For the strain-controlled test configuration the failure point Nf is described by the intersection of two tangents as we can see in the following example. Those two tangents are somehow subjective, since the transitional phase differs from each sample to another [43].

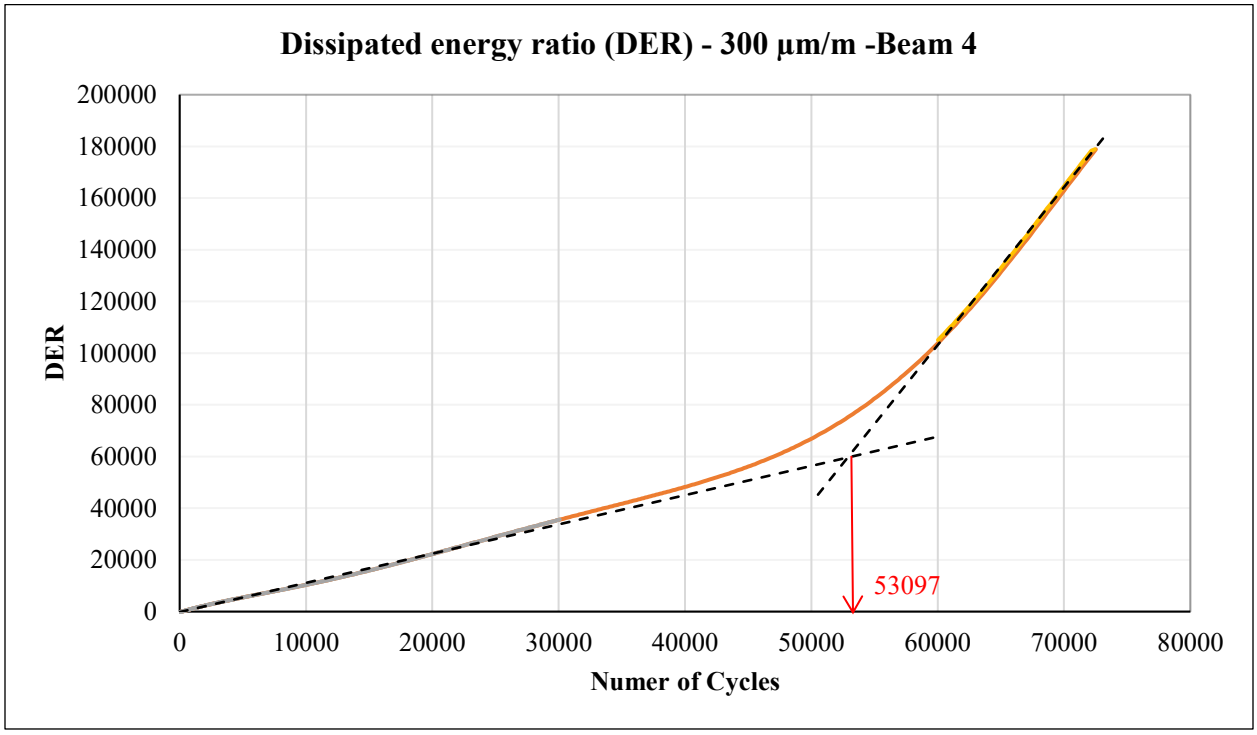

Figure 75 Typical fatigue test result using the dissipated energy ratio criteria

In this case the intersection took place at (DER = 59868), and the corresponding number of cycles by using this criterion was (53097 cycles).

The interpretation of the second line is a function from of the termination stiffness, which is in our case was 20% of the initial stiffness (E0)

The results are summarized in the following table:

Failure criterion	Dissipated Energy ratio - 300 µm/m					
Beam ID	Beam 4	Beam 7	Beam 8	Beam 9	Beam 10	Beam 12
Number of cycles	53,097	116,874	70,580	15,118	39,356	48,240

Failure criterion	Dissipated Energy ratio - 200 µm/m					
Beam ID	Beam 3	Beam 13	Beam 14	Beam 15	Beam 18	Beam 21R
Number of cycles	355,055	224,119.23	630,228	360,465	276,236	1,024,247

Failure criterion	Dissipated Energy ratio - 140 µm/m			
Beam ID	Beam 6	Beam 22L	Beam 24R	Beam 30R
Number of cycles	-	1,561,886	1,486,372	-

Table 46 Typical fatigue test result using the dissipated energy ratio criteria

4.7 Stiffness/Air voids relationships

In this part the theoretical and the actual air voids of the beams are analysed, to see the variability between them. Also, the relationship between the position of the beam in the wheel compactor and the air voids are presented. In addition to that, we highlighted the relationship between the actual air voids and the viscoelastic stiffness (E0), and also the relationship between the actual air voids and the fatigue-related stiffness (extrapolated E00).

In this study we evaluated 33 beams, and the results were as follows:

Beam ID	Theoretical Air Voids [%]	Real Air Voids [%]
1	10.01	6.76
2	9.26	5.97
3	9.59	6.34
4	8.05	6.06
5	7.37	5.64
6	8.19	5.67
7	7.90	5.64
8	7.68	5.36
9	9.32	6.22
10	7.89	5.40
11	7.18	4.73
12	7.79	5.26
13	7.46	5.38
14	6.20	4.53
15	6.32	4.80
16	7.95	5.11
17	5.59	4.24
18	6.59	4.48
19L	7.71	5.29
20C	6.34	4.40
21R	6.85	5.21
22L	7.83	5.64
23C	5.99	4.77
24R	6.73	4.82
25L	10.1	4.7
26C	6.1	4.4
27R	2.9	4.1
28L	6.7	4.8
29C	6.2	4.0
30R.	6.0	4.1

31L	6.3	4.3
32C	5.4	4.1
33R	5.2	4.1
Mean	**7.17**	**5.04**
STD	**1.51**	**0.74**
C.V	**0.21**	**0.15**
Min	**2.91**	**4.01**
Max	**10.15**	**6.76**

Table 47 Air voids of the beams

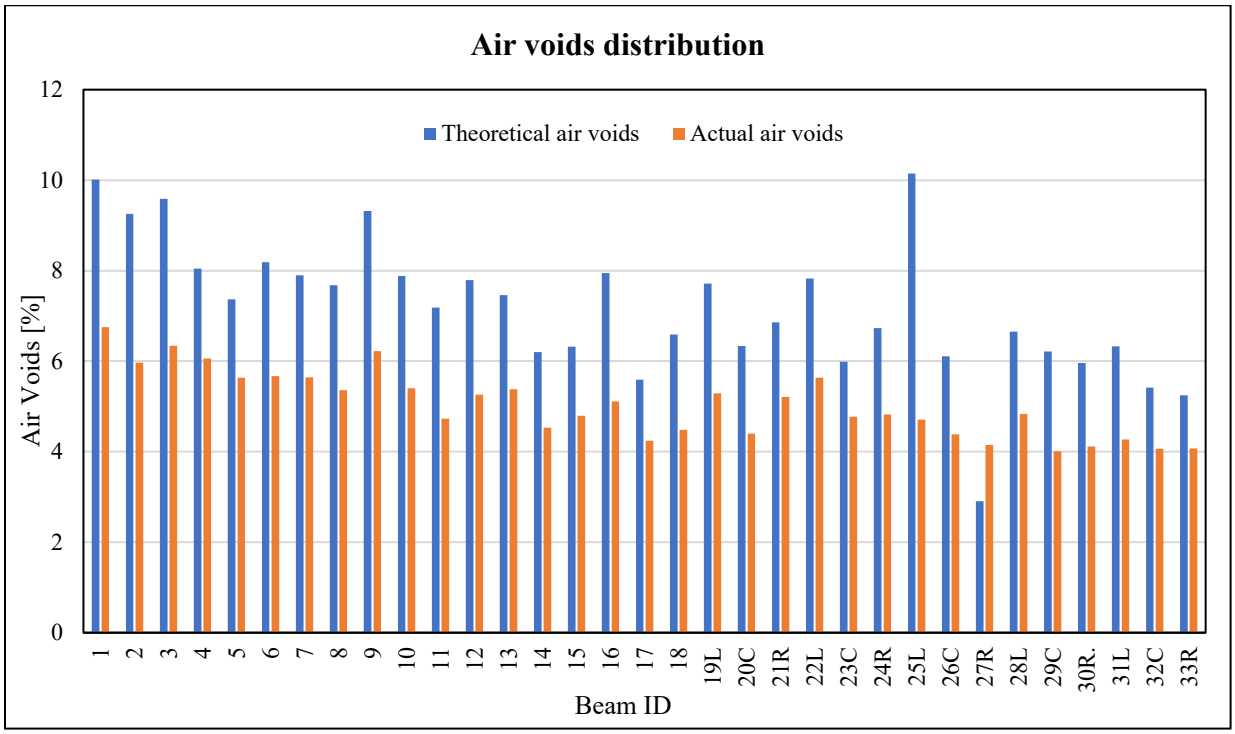

Figure 76 Air voids distribution

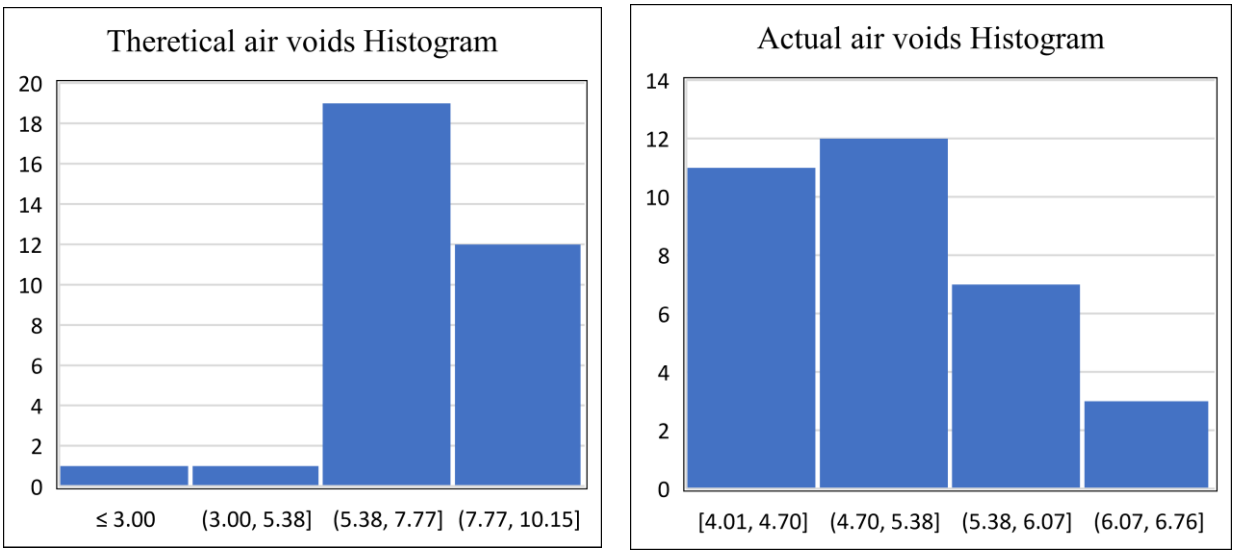

Figure 77 Air voids histograms

From the previous analysis we can see that:

- we have a reduction of approximately 2.13 % when comparing the theoretical and the actual air voids of the beams.
- While the theoretical air voids were comprised between 5.38 % to 10 %, the corresponding actual air voids were contained in the average 4 % to 6 %

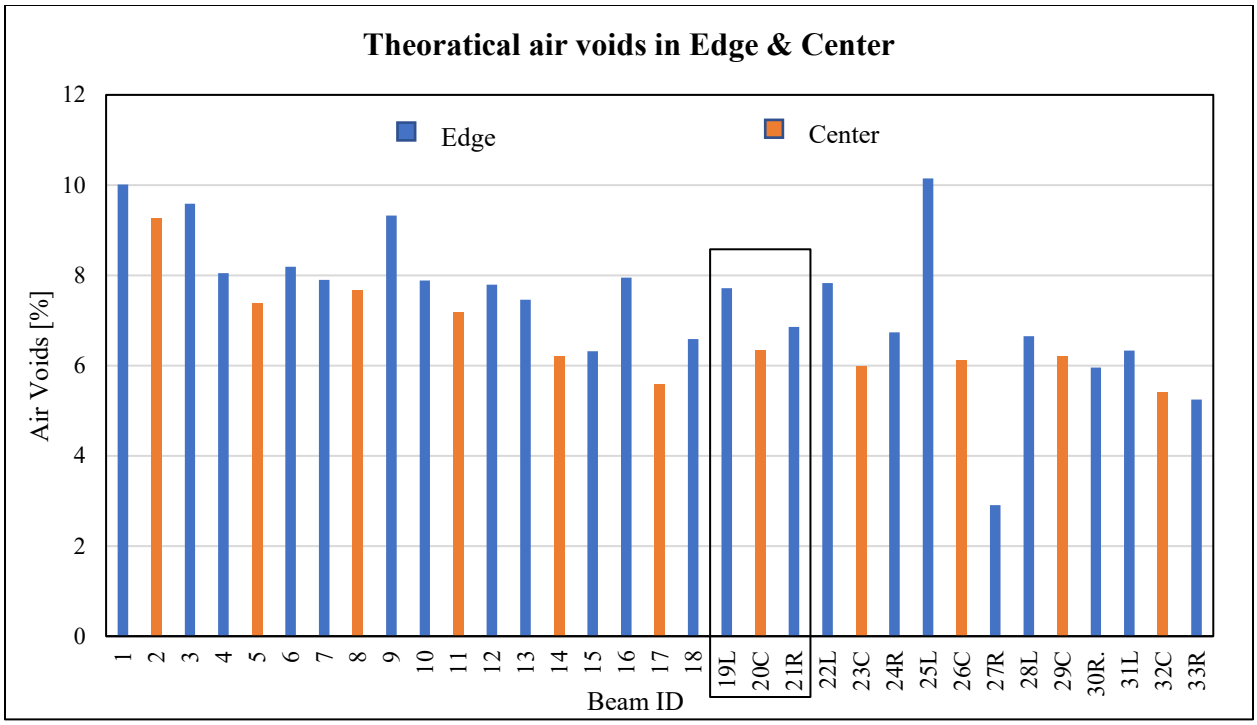

Figure 78 Effect of beam position on the theoretical air voids

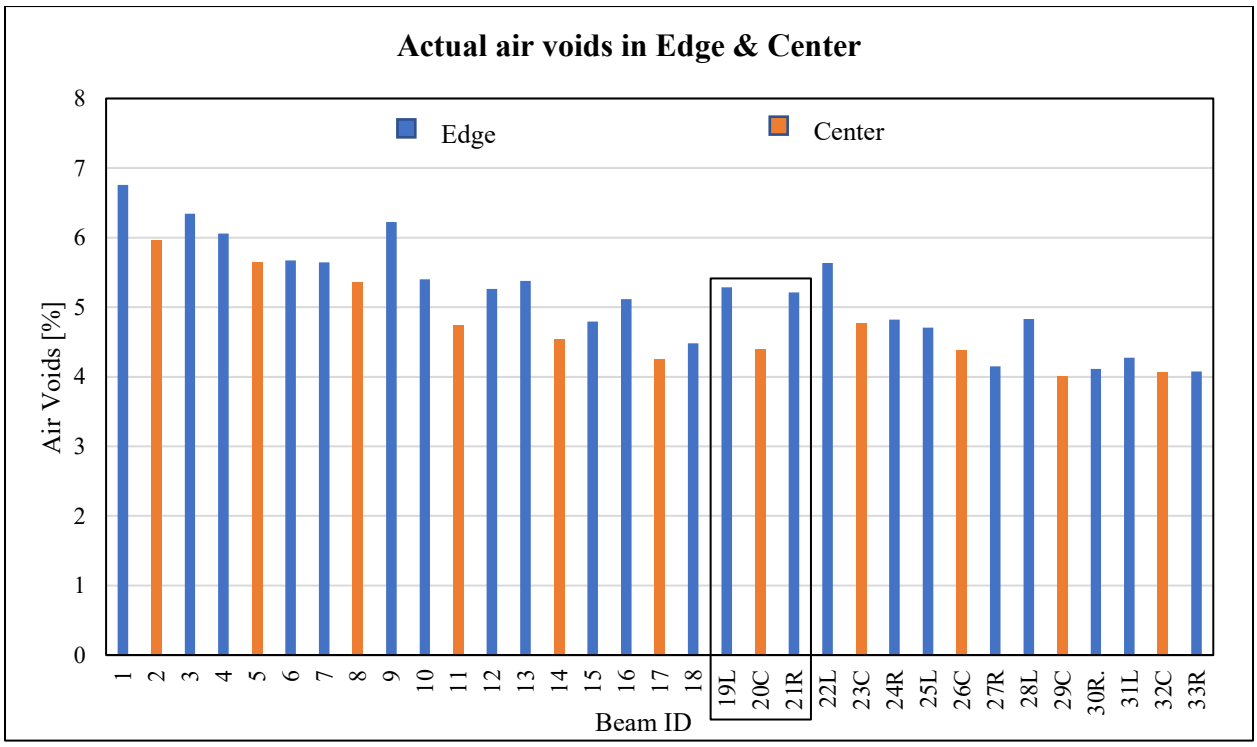

Figure 79 Effect of beam position on the actual air voids

The initial stiffness (E0) is tabulated as follows:

300 µm/m	
Beam ID	Initial stiffness E0 (MPa)
4	4309
7	4726
8	4526
9	3776
10	4584
12	5201
Avg.	4520
STD	470
C.V	9.60

200 µm/m	
Beam ID	Initial stiffness E0 (MPa)
3	4252
13	5095
14	5868
15	5626
18	5006
21R	5277
Avg.	5187
STD	562
C.V	9.23

140 µm/m	
Beam ID	Initial stiffness E0 (MPa)
6	4422
22L	4664
24R	5172
30R	5052
28L	5334
Avg.	4928
STD	375
C.V	13.11

Table 48 Beams initial stiffness

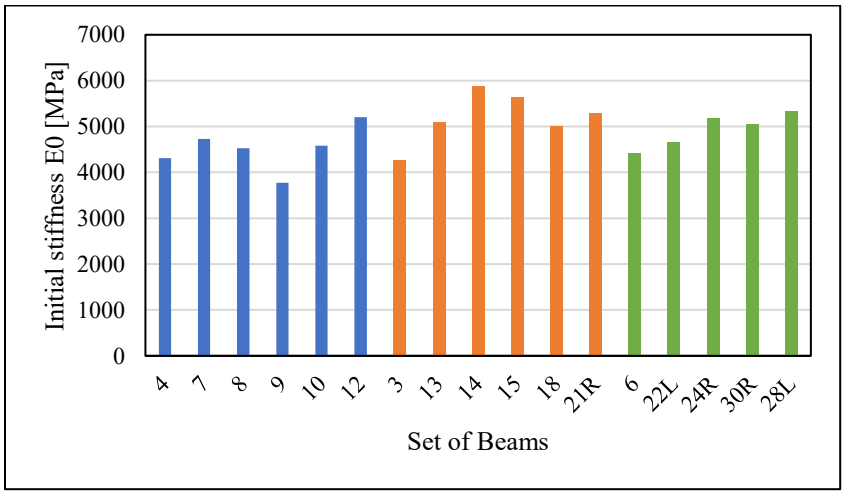

Figure 80 Beams initial stiffness

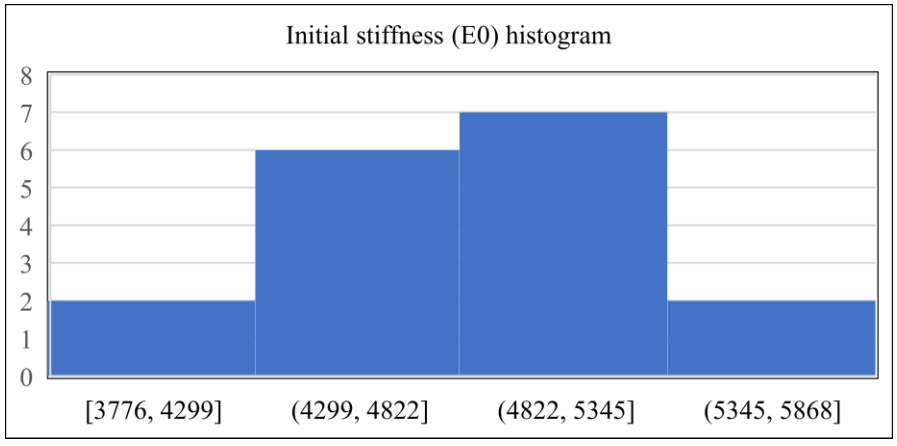

Figure 81 Initial stiffness histogram

As we can see, there is a good consistency between the results in terms of the standard deviation, since the majority of the results are comprised approximately between 4300 MPa to 5300 MPa.

The values for the initial stiffness (E0) and the corresponding air voids are tabulated as follows:

Strain level	Beam ID	Initial stiffness E0 (MPa)	Air voids [%]
300 µm/m	4	4309	6.06
	7	4726	5.64
	8	4526	5.36
	9	3776	6.22
	10	4584	5.40
	12	5201	5.26
200 µm/m	3	4252	6.34
	13	5095	5.38
	14	5868	4.53
	15	5626	4.80
	18	5006	4.48
	21R	5277	5.21
140 µm/m	6	4422	5.67
	22L	4664	5.64
	24R	5172	4.1
	30R	5052	4.1
	28L	5334	4.8

Table 49 Initial stiffness (E0) and the corresponding air voids

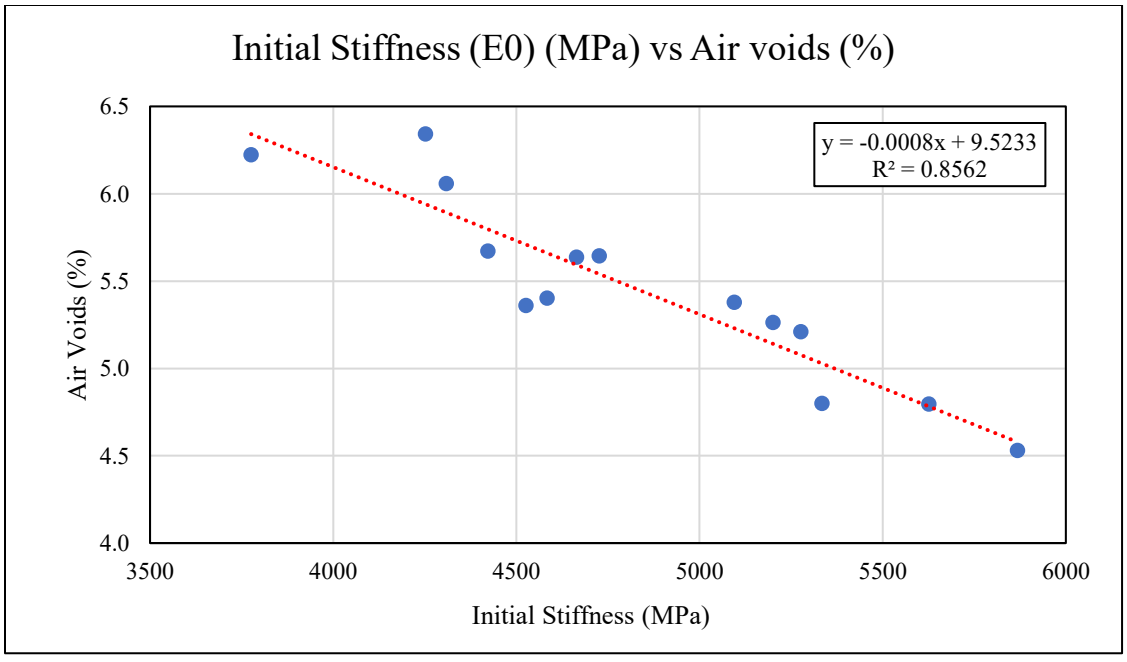

Figure 82 Initial stiffness / Air voids relationship

We can see that the air voids are decreasing as we increase the viscoelastic-related stiffness (E0).

The extrapolated stiffness (E00) is tabulated as follows:

300 µm/m	
Beam ID	Extrapolated stiffness E00 (MPa)
4	3311
7	2853
8	3361
9	3030
10	3261
12	3772
Avg.	3265
STD	314
C.V	10

200 µm/m	
Beam ID	Extrapolated stiffness E00 (MPa)
3	3351
13	3731
14	3858
15	4116
18	3487
21R	2456
Avg.	3500
STD	578
C.V	6

140 µm/m	
Beam ID	Extrapolated stiffness E00 (MPa)
6	1578
22L	2260
24R	1661
30R	1719
28L	1941
Avg.	1832
STD	275
C.V	7

Table 50 Beams extrapolated stiffness

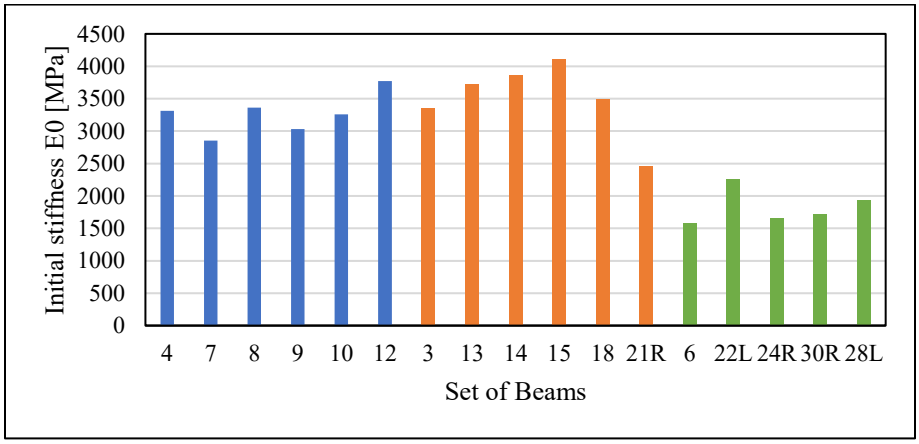

Figure 83 Beams extrapolated stiffness

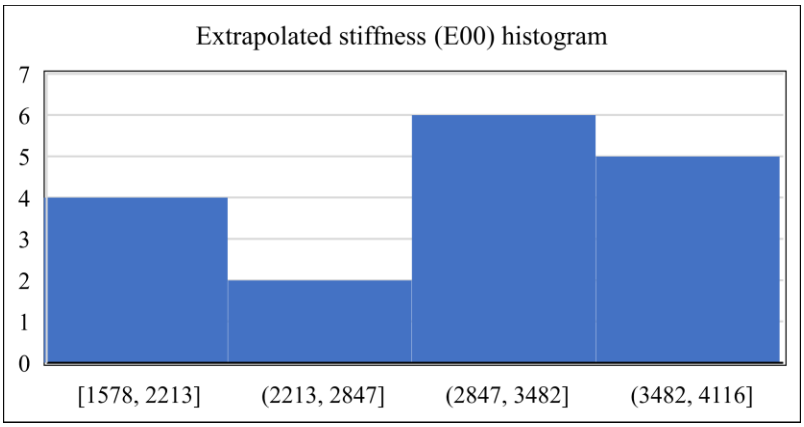

Figure 84 Extrapolated stiffness (E00) histogram

As we can see, the values of the extrapolated stiffness (E00) showed some heterogeneity if compared with the initial stiffness (E0).

The values for the extrapolated stiffness (E00) and the corresponding air voids are tabulated as follows:

Strain level	Beam ID	Extrapolated stiffness E00 (MPa)	Air voids [%]
300 µm/m	4	3311	6.06
	7	2853	5.64
	8	3361	5.36
	9	3030	6.22
	10	3261	5.40
	12	3772	5.26
200 µm/m	3	3351	6.34
	13	3731	5.38
	14	3858	4.53
	15	4116	4.80
	18	3487	4.48
	21R	2456	5.21
140 µm/m	6	1578	5.67
	22L	2260	5.64
	24R	1661	4.15
	30R	1719	4.11
	28L	1941	4.8

Table 51 Extrapolated stiffness (E00) and the corresponding air voids

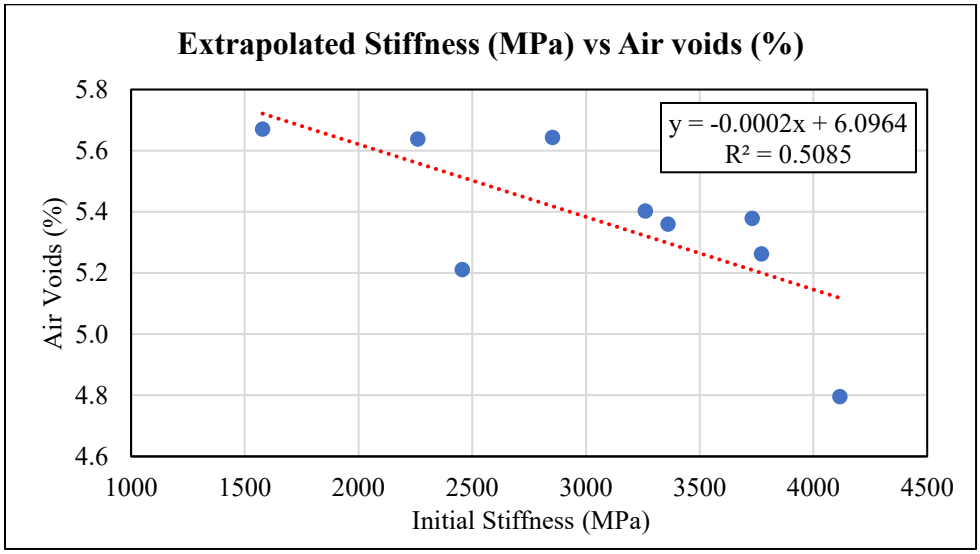

Figure 85 Extrapolated stiffness / Air voids relationship

We can see that the air voids are decreasing as we increase the damage-related stiffness (E00), however the data are more scattered compared to the case of the viscoelastic stiffness (E0).

4.8 Reliability analysis

As we saw in the previous analysis, the acquired data showed some variability. As a consequence, a statistical analysis has to be made in order to deal with this heterogeneity and to obtain a reliable values that can be used later as a represented values for the design.

The chosen statistical parameters to describe the data are the: average, standard deviation, minimum and maximum values, and the coefficient of variation. For a better graphical visualization of the data, some bar charts, histograms, boxes, and Whisker plots are provided.

This statistical analysis has been made in the previous part for the air voids and the beams stiffness. In addition to that, we are going to perform statistical analysis for the number of cycles to failure for each failure criteria, so we can estimate a represented values to be used later to construct the fatigue curves.

The number of cycles for each failure criteria under each strain level are represented in the following table:

300 µm/m	Beam 4	Beam 7	Beam 8	Beam 10	Beam 12
50% Reduction in E0	38,849	39,965	24,267	22,089	29,969
50% Reduction in E00	55,486	114,818	51,485	37,012	46,417
Peak in phase angle	44,842	40,037	73,861	19,125	61,203
Energy ratio	51,039	108,258	69,867	40,983	45,885
DER	53,097	116,875	70,581	39,357	48,240

200 µm/m	Beam 3	Beam 13	Beam 14	Beam 15	Beam 18	Beam 21R
50% Reduction in E0	293,539	163,850	338,846	249,911	161,354	163,433
50% Reduction in E00	350,309	226,758	645,657	361,225	284,010	1,267,030
Peak in phase angle	243,312	180,118	399,965	235,475	117,266	138,828
Energy ratio	296,506	197,022	558,927	317,867	279,684	1,207,666
DER	355,056	224,119	630,229	360,465	276,236	1,024,247

140 µs	6	22L	24R	30R	28L
50% Reduction in E0	1,049,189	263,031	1,059,341	833,898	1,122,019.00
50% Reduction in E00	1,853,855	1,689,577	1,801,174	1,689,577	1,889,693.00
Peak in phase angle	790,285	230,859	238,659	230,859	1,288,223.00
Energy ratio	-	1,657,457	1,727,836	1,920,142	1,780,062.50
DER	-	1,561,887	1,486,373	-	-

Table 52 Number of cycles to failure

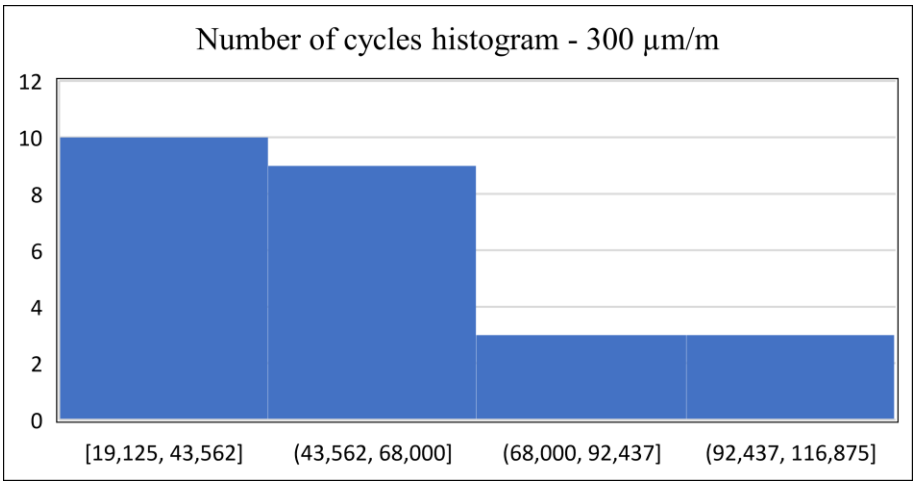

Figure 86 Number of cycles histogram - 300 µm/m

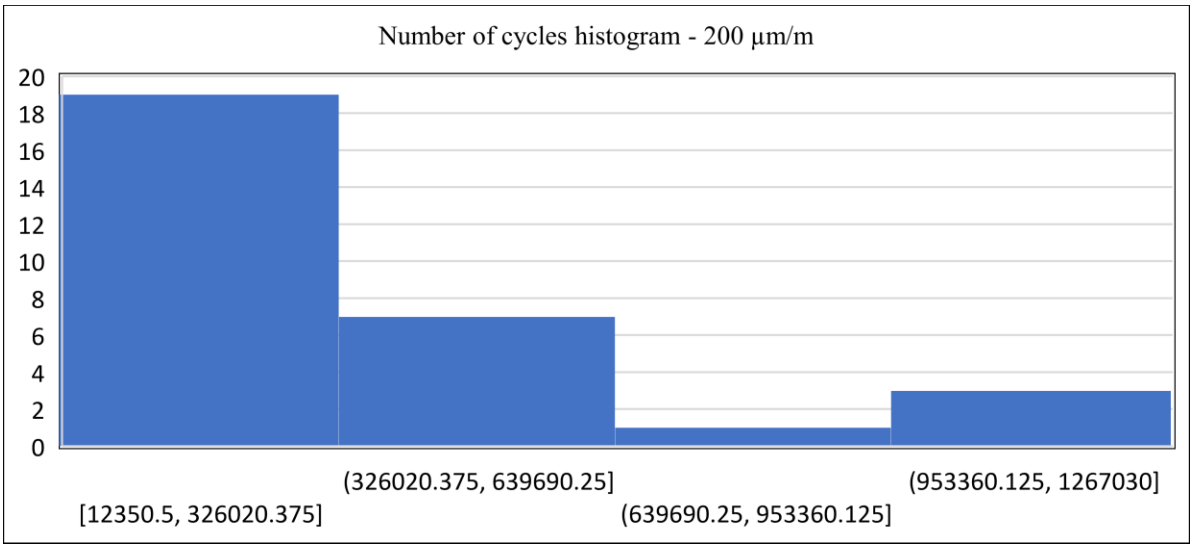

Figure 87 Number of cycles histogram - 200 µm/m

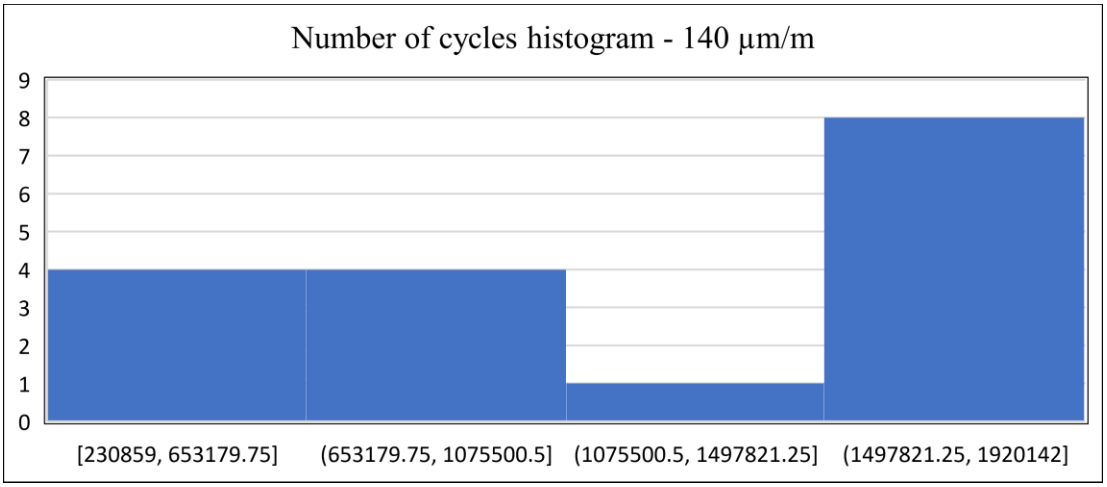

Table 53 Number of cycles histogram - 140 µm/m

300 µs	Beam 4	Beam 7	Beam 8	Beam 10	Beam 12	AVG	STD	C.V [%]
50% E0	38,849	39,965	24,267	22,089	29,969	31,028	8,182	26.37
50% E00	55,486	114,818	51,485	37,012	46,417	47,600	7,974	16.75
PPA	44,842	40,037	73,861	19,125	61,203	48,694	11,097	22.79
ER	51,039	108,258	69,867	40,983	45,885	51,943	12,634	24.32
DER	53,097	116,875	70,581	39,357	48,240	52,819	13,137	24.87
AVGERAGE	46,416.67							
E0	4309	4726	4526	4584	5201			
E00	3311	2853	3361	3261	3772			
Air voids	6.06	5.64	5.36	5.40	5.26			

200 µs	Beam 3	Beam 13	Beam 14	Beam 15	Beam 18	Beam 21R	AVG	STD	C.V [%]
50% E0	293,539	163,850	338,846	249,911	161,354	163,433	206,417	61,588	29.84
50% E00	350,309	226,758	645,657	361,225	284,010	1,267,030	305,575	62,650	20.50
PPA	243,312	180,118	399,965	235,475	117,266	138,828	199,433	49,229	24.68
ER	296,506	197,022	558,927	317,867	279,684	1,207,666	363,246	131,386	36.17
DER	355,056	224,119	630,229	360,465	276,236	1,024,247	405,496	154,688	38.15
AVGERAGE	296,033.63								
E0	4252	5095	5868	5626	5006	5277			
E00	3351	3731	3858	4116	3487	2456			
Air voids	6.34	5.38	5.38	4.80	4.48	5.21			

140 µs	6	22L	24R	30R	28L	AVG	STD	C.V [%]
50% E0	1,049,189	263,031	1,059,341	833,898	1,122,019.00	980,809	127,330	12.98
50% E00	1,853,855	1,689,577	1,801,174	1,689,577	1,889,693.00	1,758,546	82,491	4.69
PPA	790,285	230,859	238,659	230,859	1,288,223.00	233,459	4,503	1.93
ER	-	1,657,457	1,727,836	1,920,142	1,780,062.50	1,768,478	135,977	7.69
DER	-	1,561,887	1,486,373	-	-	1,524,130	53,397	3.50
AVGERAGE	1,253,084.24							
E0	4422	4664	5172	5052.00	5334.00			
E00	1578	2260	1661	1719	1941			
Air voids	5.67	5.64	4.1	4.1	4.8			

Table 54 Number of cycles statistical parameters

- The values of the initial stiffness (E0), the extrapolated stiffness (E00), and the air voids (%) are used to provide more statistical rationality, since the pure statistical analysis sometimes fails to exclude or include some values.
- The above table contains the refined data after carrying out the statistical analysis.
- Values in red are considered as outliers.
- (-) means the number of cycles is more than $2x10^6$), which outside the standard rage (10,000 to $2x10^6$), so the values were excluded.

Values in red are considered outliers (outside the 1st and 3rd quartiles), and they were defined by the Whisker plots as follows:

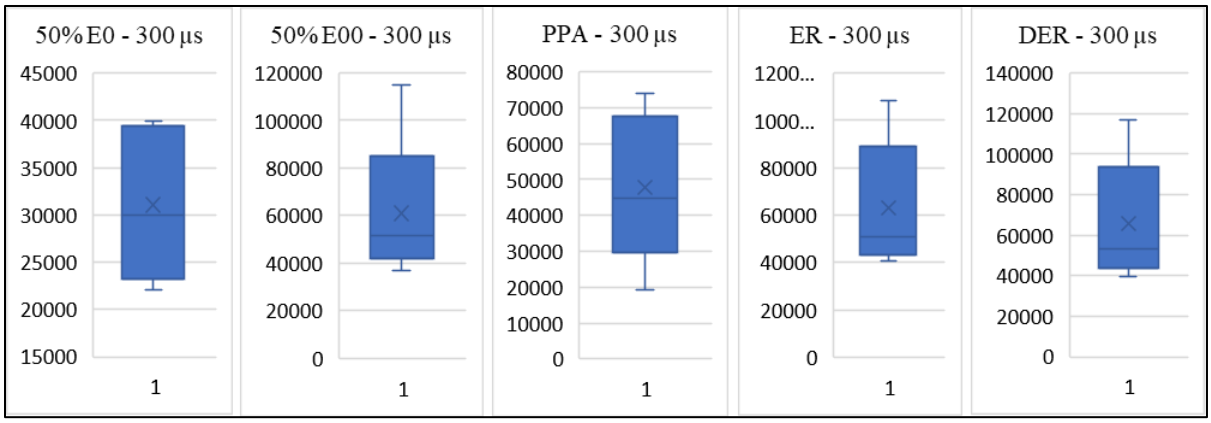

Figure 88 Whisker plots for cycles to failure - 300 µm/m

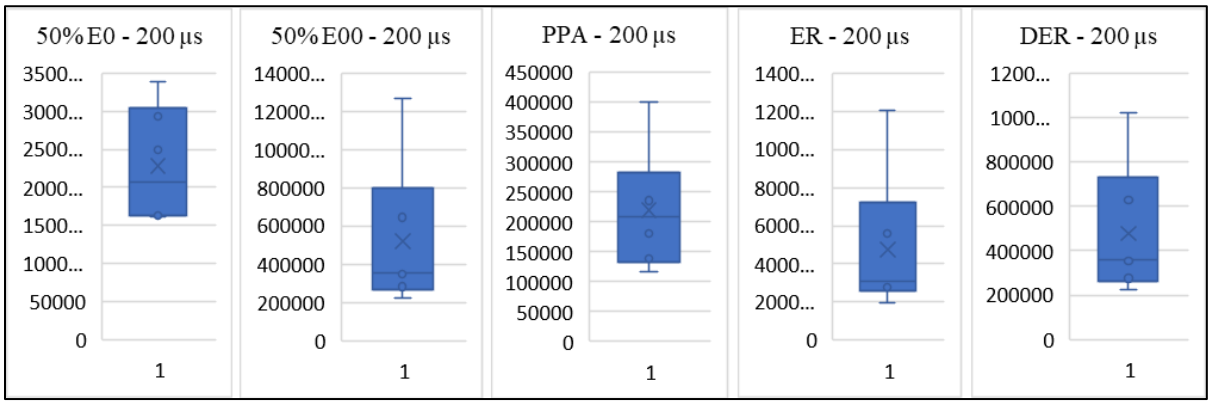

Figure 89Whisker plots for cycles to failure - 200 µm/m

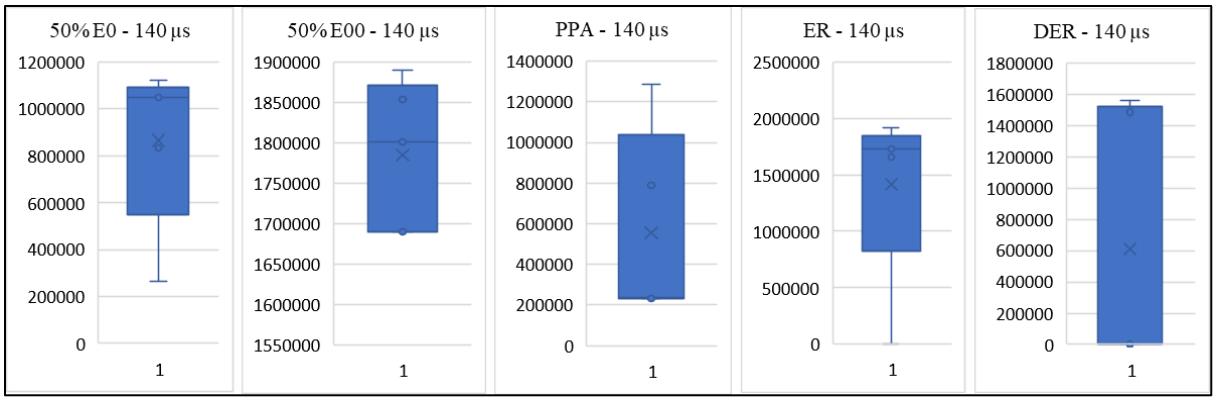

Figure 90 Whisker plots for cycles to failure - 140 µm/m

4.9 Comparison of failure criteria

from the previous results we can see some similarities and dissimilarities among our data. In the following points we can highlight the most important aspects:

- The "50 % reduction in the initial stiffness (E0)" and "Peak in the phase angle" failure criteria always yield the minimum average number of cycles, regardless of the strain level.

- The "50 % reduction in the extrapolated stiffness (E00)", "Energy ratio", and "Dissipated energy ratio" failure criteria gave the maximum average number of cycles, and also yield approximately the same results in terms on the average cycles to failure.

- The only drawback of the "50 % reduction in the extrapolated stiffness (E00)" failure criterion is the definition of the regression interval because it is different from one test to another, however this could be easily evaluated by fixing a high value for the coefficient of determination (R^2), for example more than 0.95 (less than 5 % error), while making sure we're always extrapolating inside Phase II.

- In comparison with the grand average at each strain level (averaging the cycles for the six replicates for the five failure criteria), we can twig that the "50 % reduction in the extrapolated stiffness (E00)", "Energy ratio", and "Dissipated energy ratio" have the closest values to the grand average.

- The only drawback of the "Dissipated Energy ratio "criterion is that the definition of the failure point is somehow subjective, since the intervals used to construct the intersection lines varies from each test to another, however the error in defining those intervals is small and does not significantly affect the results. The error can be controlled simply by fixing a high value for the coefficient of determination (R^2), for example more than 0.95 (less than 5 % error).

- The definition of the transitional period was very clear in the "Energy ratio" criterion because we always obtain a peak value, which indicates the transition between the crack initiation and crack propagation.

- In the "Peak in the phase angle" criteria, the transitional period was also clear in the higher strain amplitudes (300 μm/m, 200 μm/m), however at the low strain amplitude (140 μm/m) was didn't obtain rational results, since the peak were taking place at lower number of cycles compared with other failure criteria.

- If the outliers are to be included, it is difficult to obtain a comparable result.

4.10 Fatigue curves

In the following section the five fatigue curves are presented corresponding to the different failure criteria:

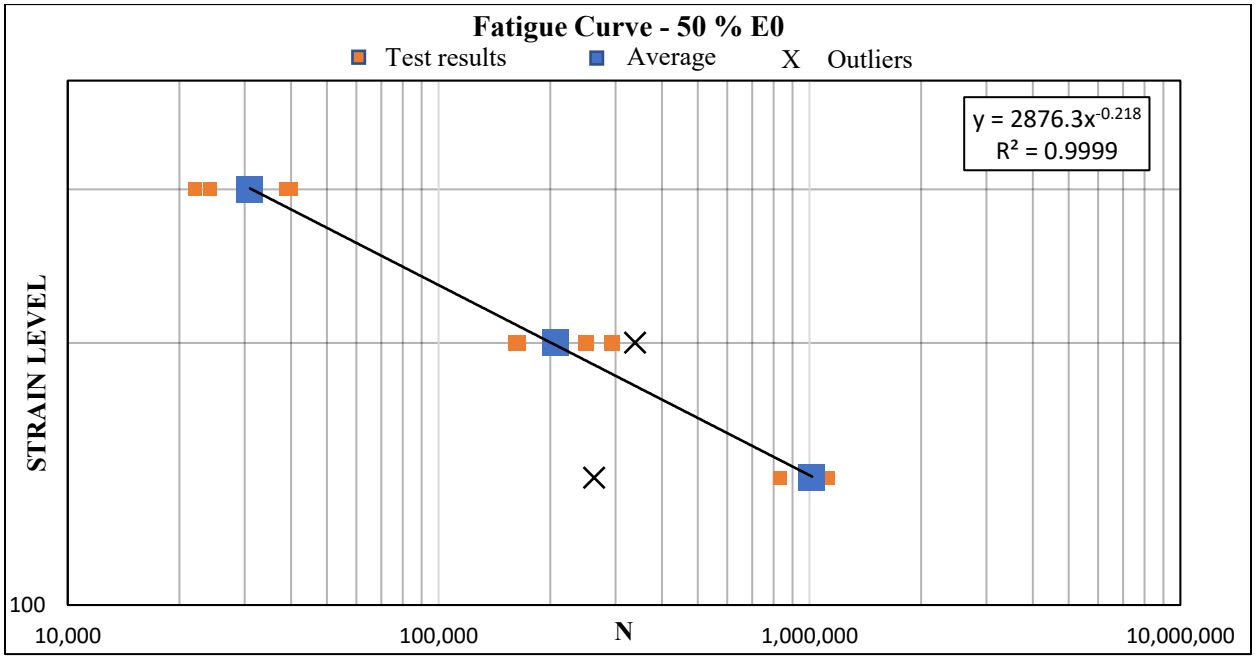

Figure 91 Fatigue Curve - 50 % E0

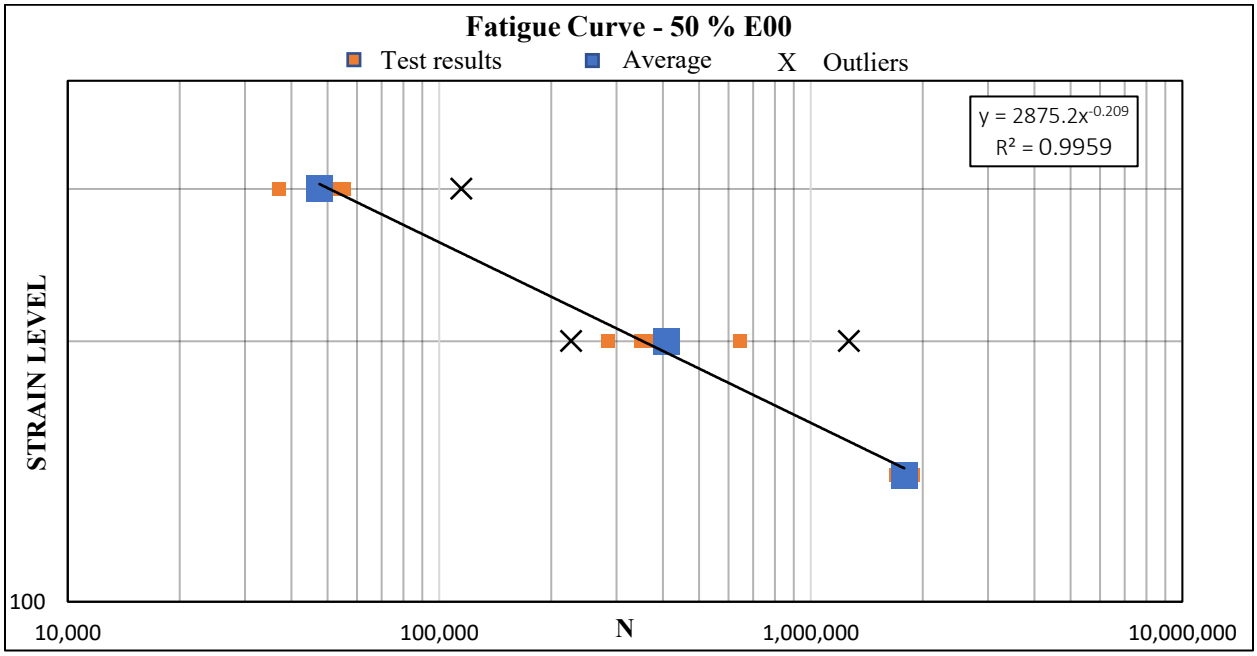

Figure 92 Fatigue Curve - 50 % E00

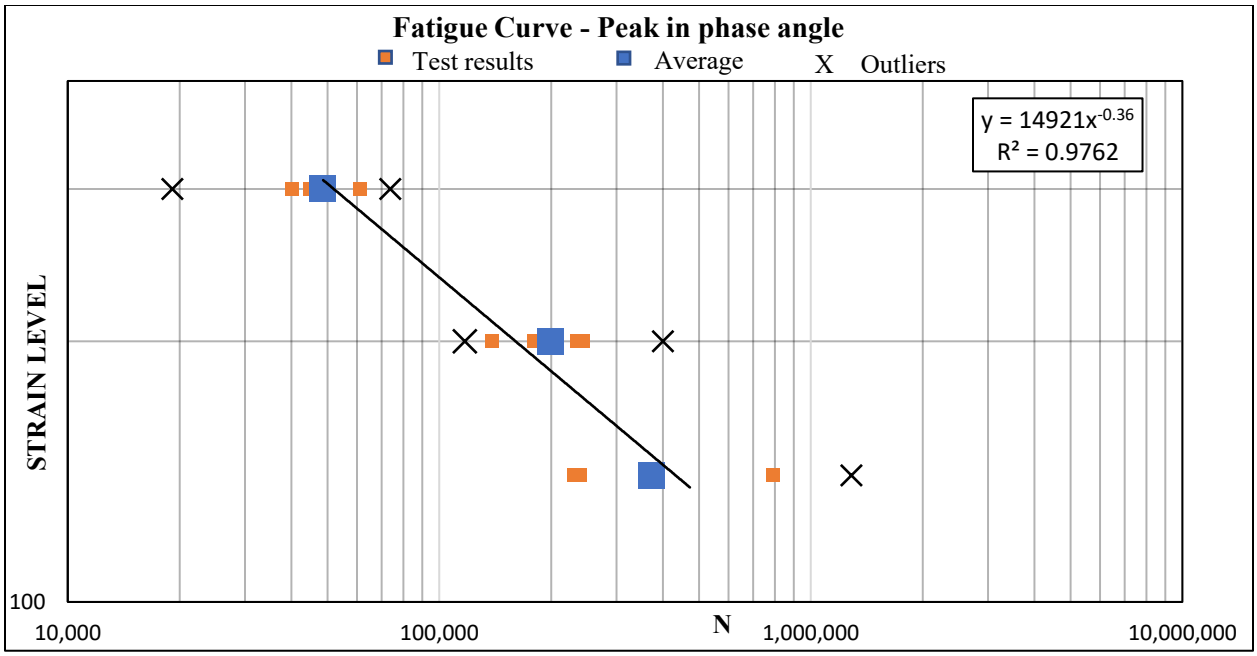

Figure 93 Fatigue Curve - Peak in phase angle

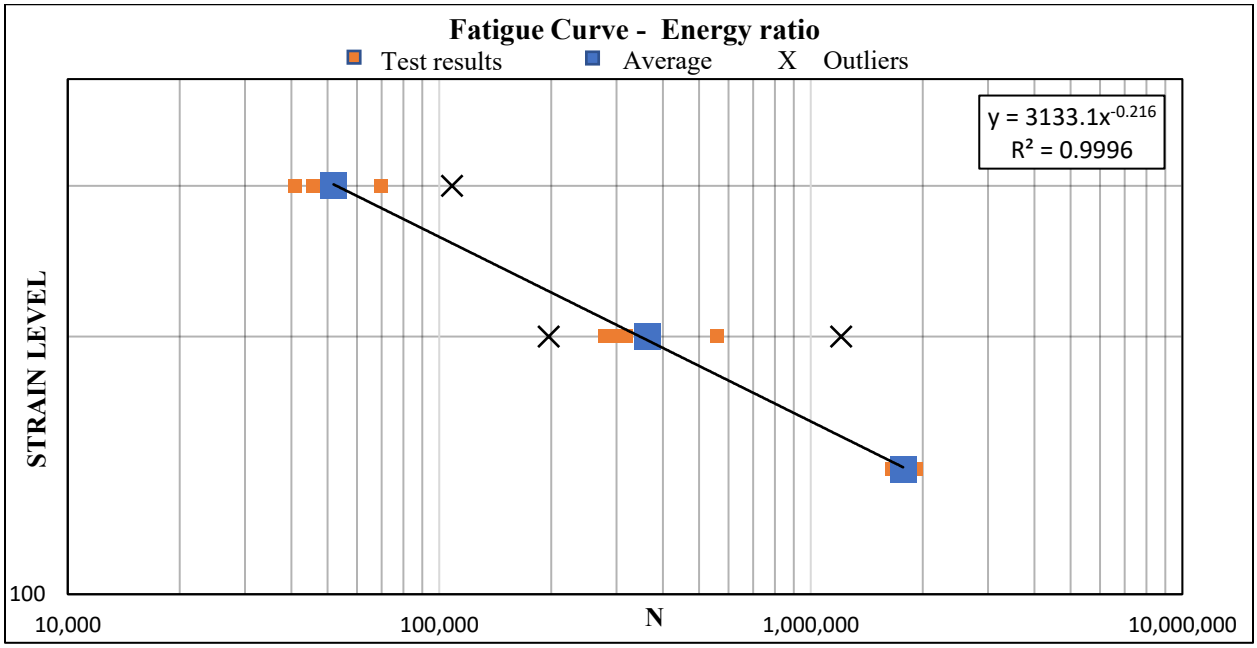

Figure 94 Fatigue Curve - Energy ratio

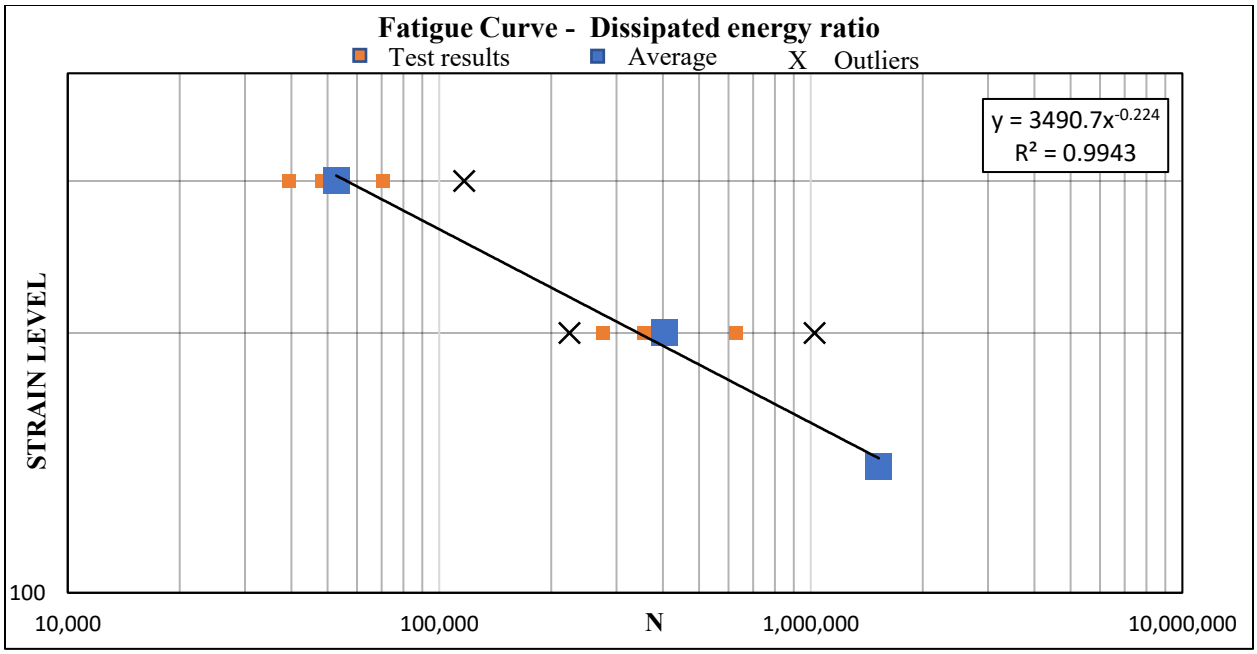

Figure 95 Fatigue Curve - Dissipated energy ratio

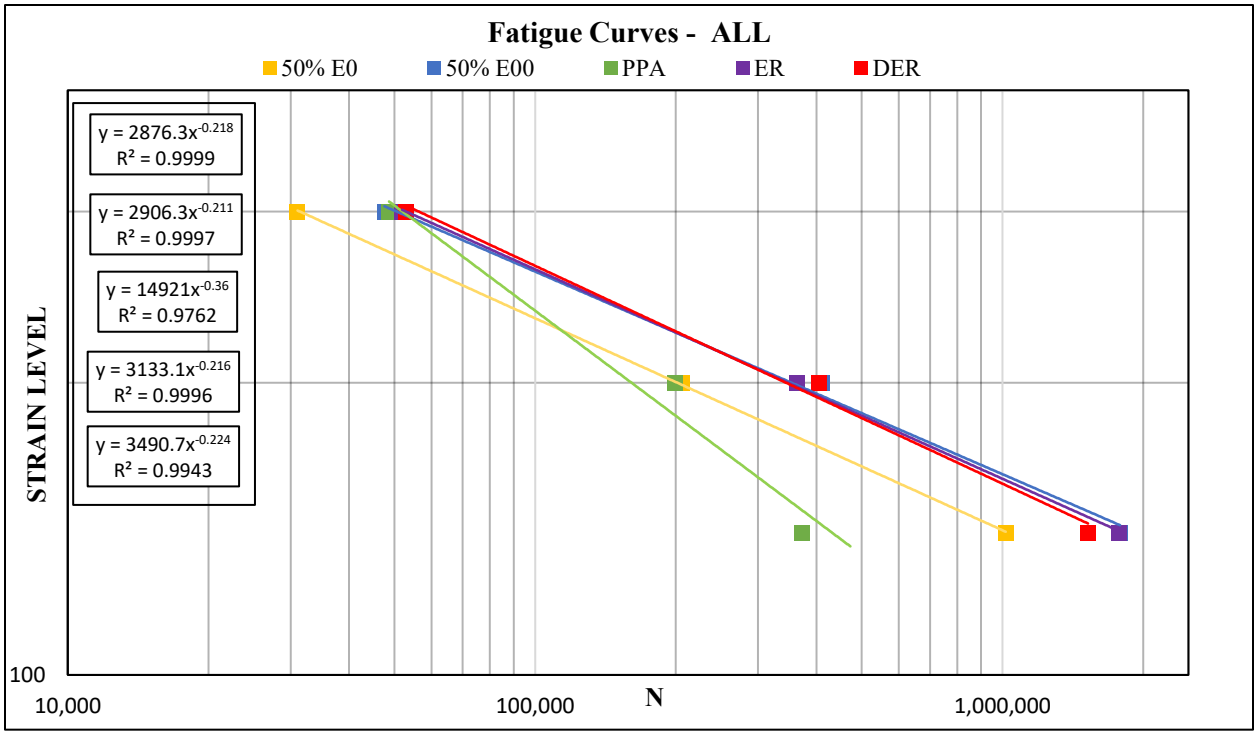

Figure 96 Fatigue curves

50% E0	
Strain Level µm/m	**N, Cycles**
300	31,028
200	206,417
140	1,016,111
ε_6	**141**
50% E00	
Strain Level µm/m	**N, Cycles**
300	47,600
200	305,575
140	1,784,775
ε_6	**161**
PPA	
Strain Level µm/m	**N, Cycles**
300	48,694
200	199,433
140	233,459
ε_6	**103**
ER	
Strain Level µm/m	**N, Cycles**
300	51,943
200	363,246
140	1,771,374
ε_6	**159**
DER	
Strain Level µm/m	**N, Cycles**
300	52,819
200	405,496
140	1,524,130
ε_6	**157**

Figure 97 Strain level at 1 million cycles

- In terms of the fatigue curves, we can clearly see that there is a very good consistency between the "50 % reduction in the extrapolated stiffness (E00)", "Energy ratio", and "Dissipated energy ratio" failure criteria, and they approximately yield the same $\varepsilon_6$values with an average of 159 µm/m.

- The "50 % reduction in the initial stiffness (E0)" and "Peak in the phase angle" failure criteria always yield the minimum $\varepsilon_6$values.

4.11 Sensitivity pavement design

In this section the previous results will be used to estimate the allowable number of load repetition that prevents fatigue cracking. The analysis is performed using KENLAYER software with the following pavement configuration:

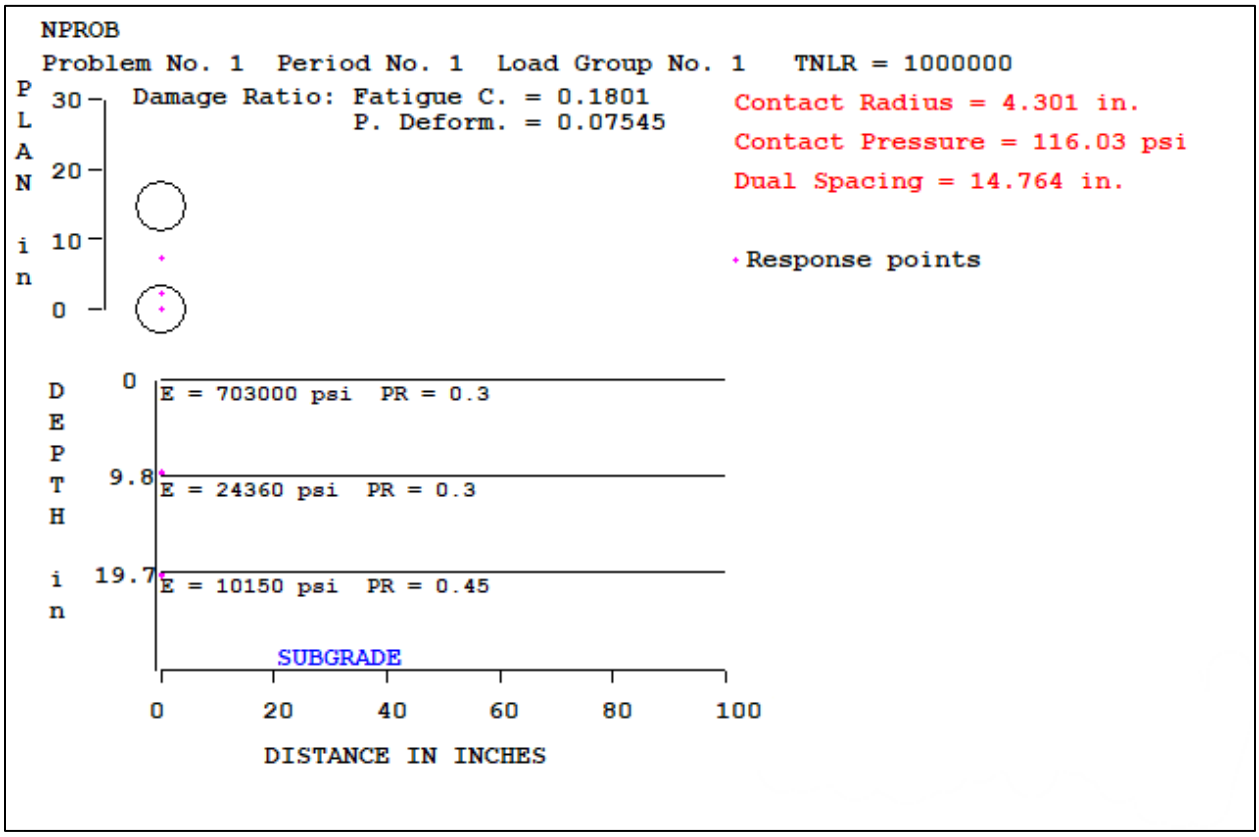

Figure 98 Pavement configuration

KENPAVE Inputs

For analysis all layers are assumed to be linearly elastic with a constant elastic modulus for each layer. Damage analysis and stress strain analysis are conducted separately. Other input parameters are listed below:

General Inputs:

- The number of periods in a year is 1.
- 1 million load repetition each period.
- The number of load groups is 1.
- The number of layers is 3 (HMA, Granular mix, Subgrade).
- The number of Z coordinates is calculated depending upon the number of interfaces and the intermediate points for analysis.
- All layer interfaces are assumed to be bonded.

- SI units are used for calculations
- The contact radius of circular loaded area is 10.925 cm (4.3 In) for single axle with dual wheels and contact pressure as 800 kPa (116 psi).
- The analysis was performed for the radial distances = 0, 5.4625 cm (2.15 In), 18.75 cm (7.38 In).

Material Property Inputs:

The modulus on the subgrade is taken as 70 MPa (10152 psi), with a thickness of 25 cm (9.84 In), and Poisson's Ratio of 0.35

The Granular mix has a thickness of 25 cm, Poisson's Ratio of 0.3 and a modulus calculated using the following equation:

$$E_{MG} = 0{,}2 \cdot (h_{MG})^{0{,}45} \cdot E_{supp}$$

Where:

E_{MG} Stiffness modulus of the granular foundation (MPa).
h_{MG} Thickness of the granular foundation (mm).
E_{supp} Stiffness modulus of the subgrade. (MPa).

The HMA has a thickness of 25 cm, a Poisson's Ratio of 0.3 and a modulus taken as the average of all tested beams equals to 4847.25 MPa (703034 psi)

Damage Analysis Inputs:

For the fatigue verification of bituminous mixture, the control parameter adopted to quantify the stress state induced by the load is the maximum tensile strain at the bottom of the asphalt layer. The corresponding transfer function is presented in equation:

$$N_f = \frac{1}{F_{aff}} \cdot F_{lab} \cdot F_a \cdot f_1 \cdot \left(\frac{1}{\varepsilon_t}\right)^{f_2} \cdot \left(\frac{1}{E}\right)^{f_3}$$

Where:

N_f Number of repetitions of the load that determines the achievement of boundary conditions of fatigue damage to the layer.
F_{aff} Reliability factor.
F_{lab} Translation factor that relates the performance in the laboratory to those in situ, assumed equal to 10
F_a Translation factor considering the self-healing capacity of the binding phase.
f_2, f_2, f_3 Regression parameters.
ε_t Unit tensile deformation at the bottom of the asphalt layer, expressed in m/m.
E Elastic modulus of bituminous conglomerate, expressed in MPa.

The transfer functions used in verification calculations may be based on the results of experimental investigations or may derive from models in the literature. For projects of significant importance, the regression parameters f_2, f_2, f_3, are obtained or experimentally verified by carrying out a complete study of the fatigue behavior of bituminous mixture, considering the level of strain imposed and the influence of temperature.

In the event that the characterization of the fatigue behavior does not include the execution of tests at different temperatures, it is possible to conduct the experimentation at a single reference temperature. It is advisable to adopt a fatigue test performance temperature in a range between 10 °C and 20 °C. In this case it will be possible to derive the regression parameters f_2, f_2 and fix the value of f_3 equal to 1.8.

In the case of preliminary or minor projects, it is also possible to derive the parameters f_1 and f_2 from the literature. For mixtures containing bituminous binders of the traditional type, it is recommended to set the parameter f_2 equal to 5 and determine the parameter f_1 according to the following equation:

$f_1 = (6918 \cdot 10^{-6}(0{,}856 \cdot V_b + 1{,}08))^5$

V_b Volumetric percentage of the binding phase, expressed as %

For our mixture that has $V_b = 12.87$ %, the estimated value of f_1 = 4.118E-6

Two damage analysis have been carried out by changing the regression parameters f_1, f_2, while keeping the third parameter f_3 fixed at 1.8.

The first analysis was performed by solving the value of f_1 that minimizes the summation of the squared differences between the number of cycles to failure obtained in the laboratory and the number of cycles obtained using the fatigue model. ($\sum(Nf_{lab} - Nf_{model})^2$)

The second analysis is performed by solving the values of f_1, f_2 that minimize the summation of the squared differences between the number of cycles to failure obtained in the laboratory and the number of cycles obtained using the fatigue model. ($\sum(Nf_{lab} - Nf_{model})^2$)

For both cases the initial values of f_1, f_2 are 4.118E-6 and 5 respectively.

In the KENLAYER software the fatigue parameters are notated as FT1, FT2 and FT3 respectively.

- The value of (FT3) is kept fixed at 1.8
- The value of (FT1), a (FT2), were changed according to the analysis type.

The results of the sensitivity pavement design are summarized in the following table:

50% E0						
Changing f1 only						
f1	FT1	f2 = FT2	f3 = FT3	Nf, allowable	Damage ratio	Design period [Years]
0.001430	0.002859	5.0	1.8	3.6830E+06	0.272	3.68
Changing f1,f2						
0.002133	0.004266	4.955	1.800	3.6580E+06	0.273	3.66
50% E00						
Changing f1 only						
f1	FT1	f2 = FT2	f3 = FT3	Nf, allowable	Damage ratio	Design period [Years]
0.00317	0.00633	5	1.8	8.15E+06	1.23E-01	8.15
Changing f1,f2						
2011.49089	4022.98178	3.491	1.8	6.15E+06	1.63E-01	6.15
Energy Ratio						
Changing f1 only						
f1	FT1	f2 = FT2	f3 = FT3	Nf, allowable	Damage ratio	Design period [Years]
0.00337	0.00674	5	1.8	8.68E+06	1.15E-01	8.68
Changing f1,f2						
96.87981	193.75961	3.840	1.8	6.95E+06	1.44E-01	6.95
Dissipated Energy Ratio						
Changing f1 only						
f1	FT1	f2 = FT2	f3 = FT3	Nf, allowable	Damage ratio	Design period [Years]
0.00295	0.00591	5	1.8	7.61E+06	1.31E-01	7.61
Changing f1,f2						
2854.74761	5709.49522	3.441	1.8	5.55E+06	1.80E-01	5.55
SHELL						
FT1		f2 = FT2	f3 = FT3	Nf, allowable	Damage ratio	Design period [Years]
0.0685		5.671	2.363	1.33E+07	5.14E-02	13.25
Asphalt Institute						
FT1		f2 = FT2	f3 = FT3	Nf, allowable	Damage ratio	Design period [Years]
0.0796		3.291	0.854	6.78E+06	1.48E-01	6.78

Table 55 KENLAYER output

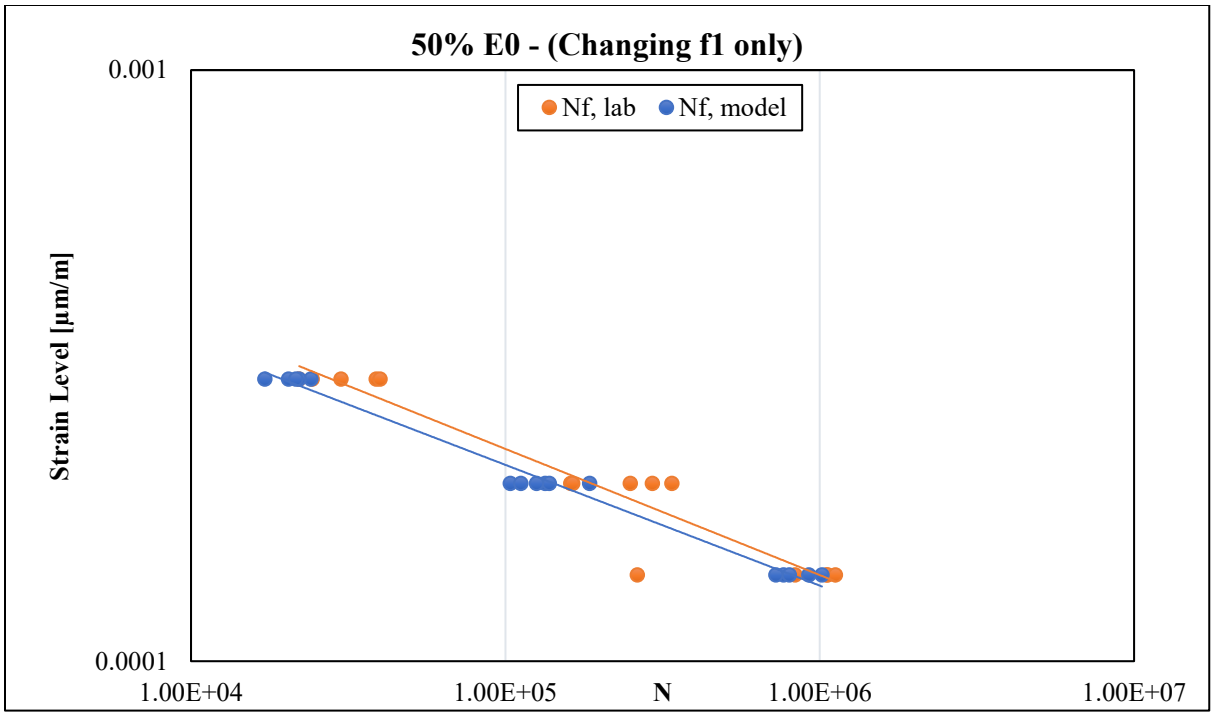

Figure 99 Transfer function - 50% E0 – changing f1 only

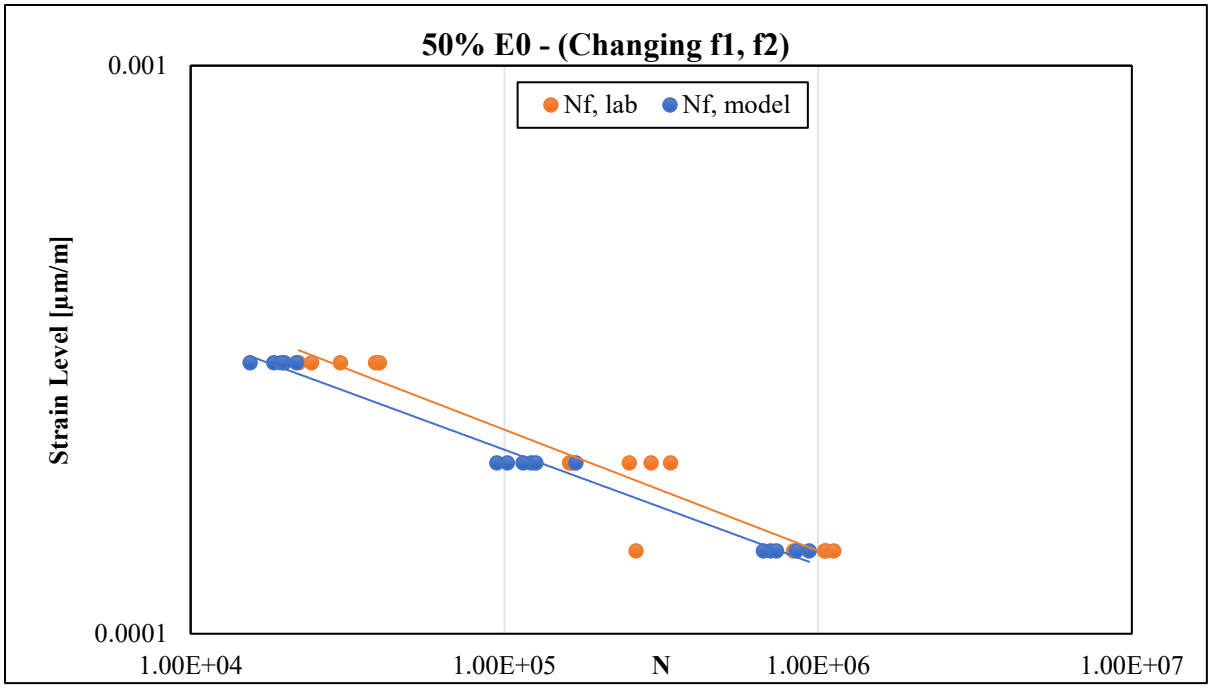

Figure 100 Transfer function - 50% E0 – changing f1, f2

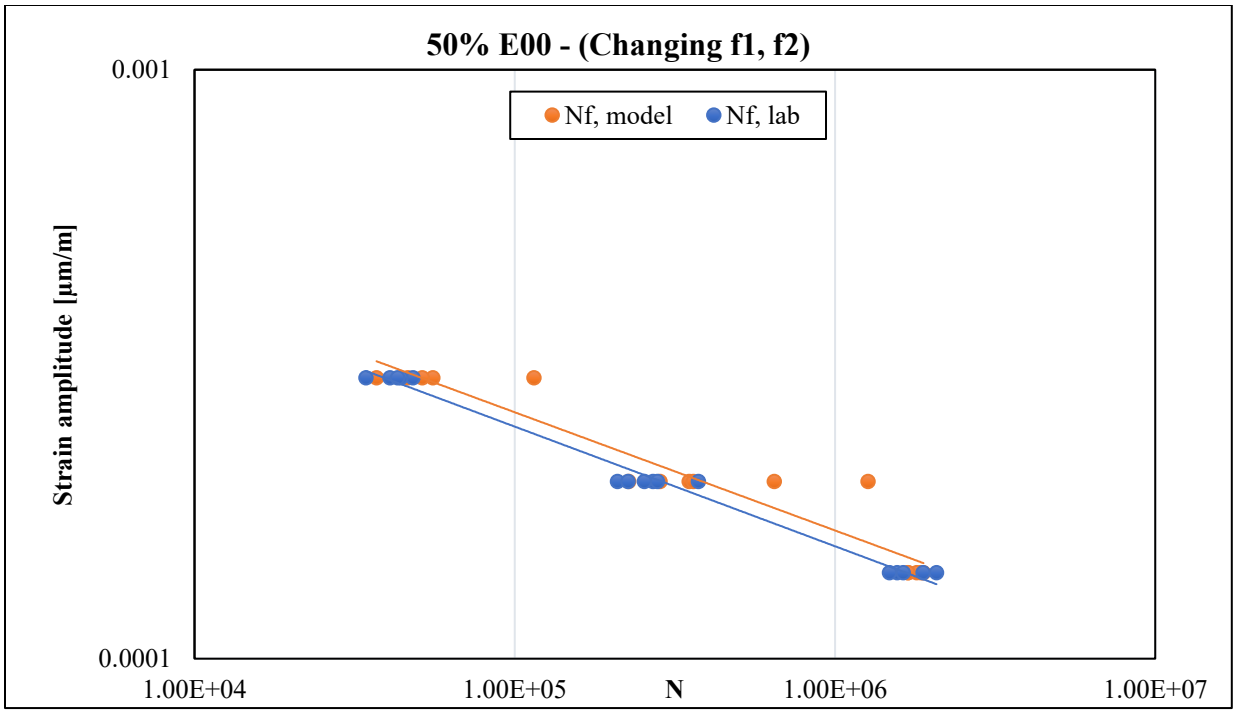

Figure 101 Transfer function - 50% E0 – changing f1 only

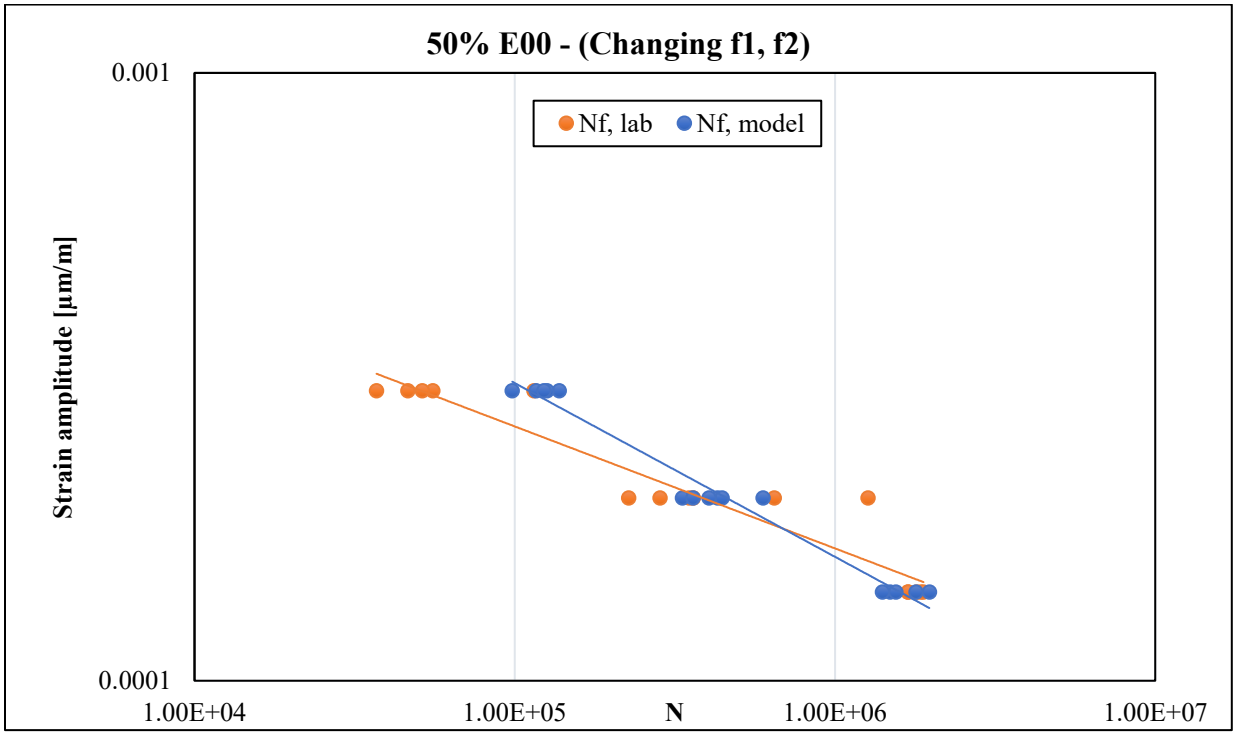

Figure 102 Transfer function - 50% E00 – changing f1, f2

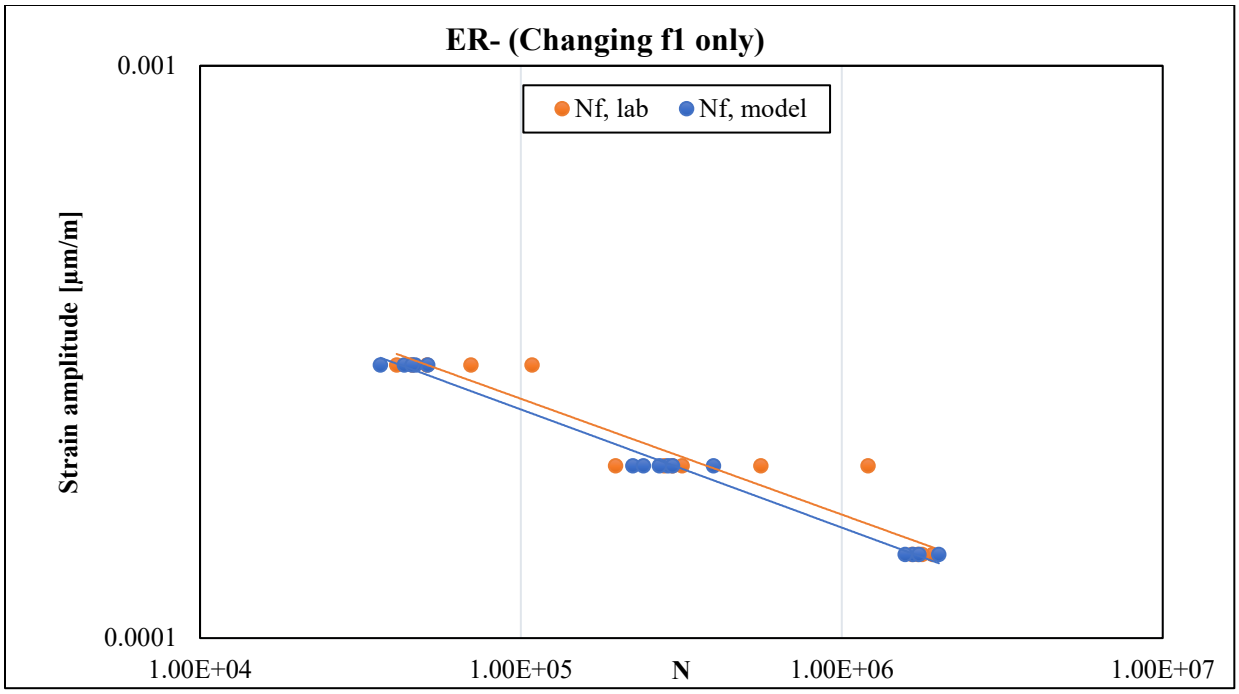

Figure 103 Transfer function - Energy Ratio - changing f1 only

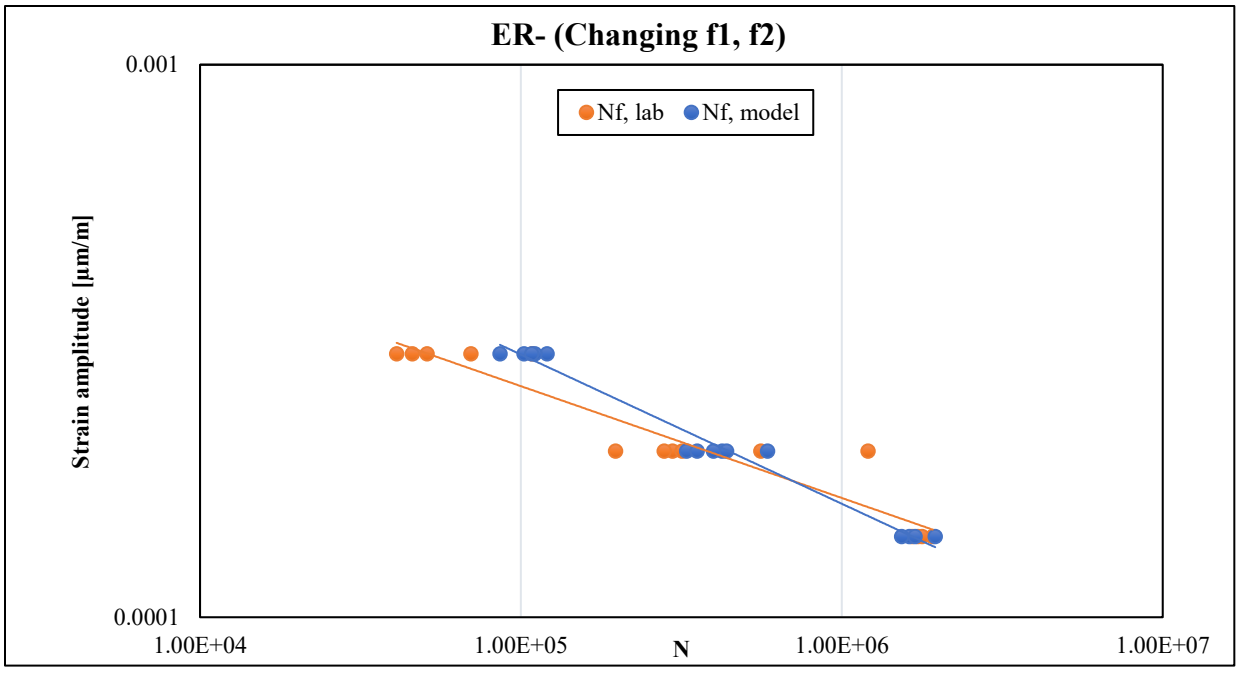

Figure 104 Transfer function - Energy Ratio - changing f1, f2

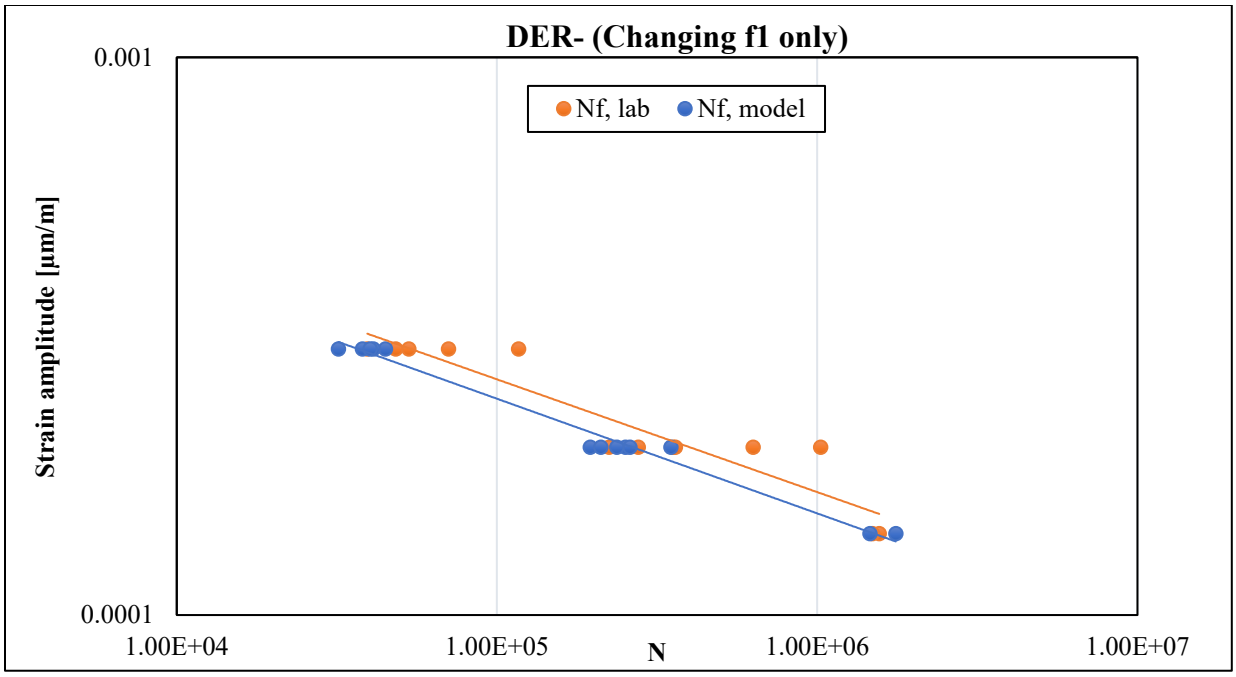

Figure 105 Transfer function - Dissipated Energy Ratio - changing f1 only

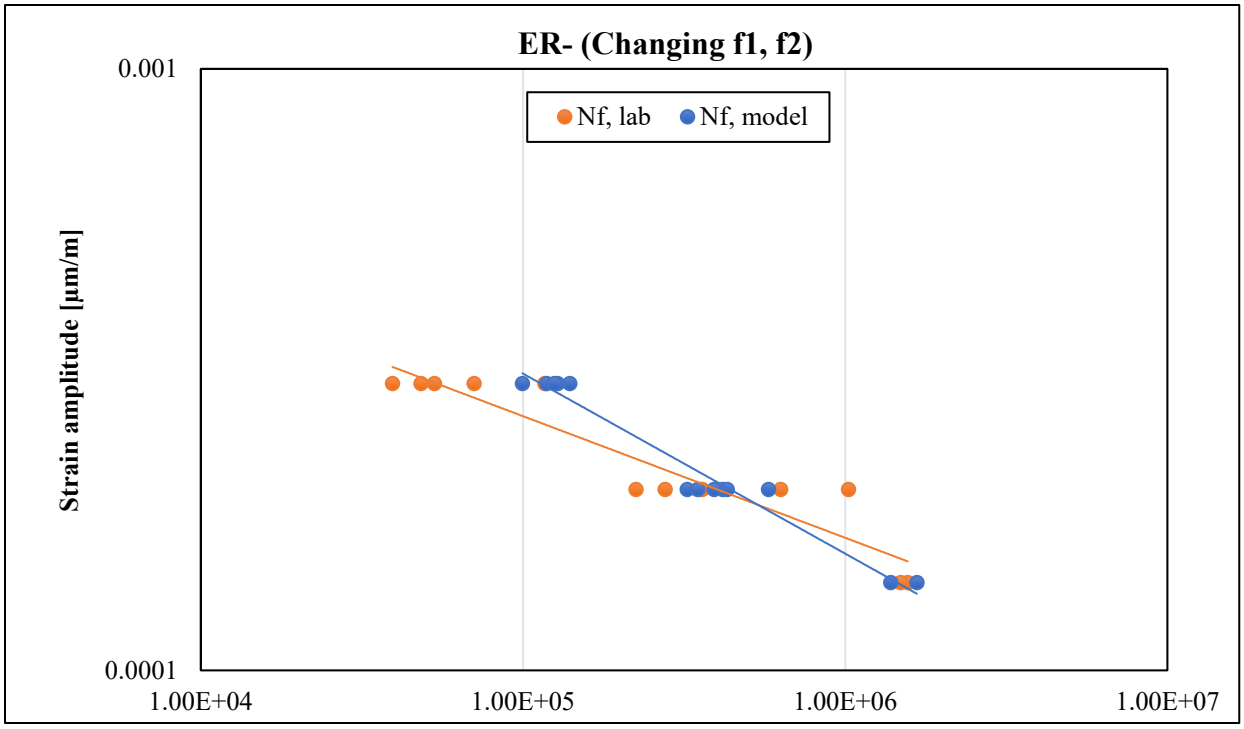

Figure 106 Transfer function - Dissipated Energy Ratio - changing f1, f2

From the previous analysis we can see that:

- There is a good consistency between the developed model, when compared with an external model like the Asphalt Institute model, where we obtained the same order of magnitude of allowable load repetitions.

- Considering the allowable number of load repetitions, we can see that when we are only changing the f1 parameter we got a relatively higher number of cycles, except for the conventical failure criterion where we obtained exactly the same results wither changing f1 only or f1, and f2 together.

- Regarding the other failure criteria: "50 % reduction in the extrapolated stiffness (E00)", " Energy ratio", and "Dissipated energy ratio" we obtained approximately 25% reduction of load repetition when moving from changing f1 only, to changing both f1, f2. Which mean a lower design period in the second case.

- When changing f1 only we got the same order of magnitude for the final diverged value of f1. (0.001430, 0.00317, 0.00337, 0.00295) for the: “50 % reduction in the initial stiffness (E0)”, "50 % reduction in the extrapolated stiffness (E00)", " Energy ratio", and "Dissipated energy ratio" respectively.

- When changing f1, f2 together we can twig that the values of f2 were diverging around the same order of magnitude (4.955, 3.491, 3.840, 3.441), while the values of f1 showed a significant heterogeneity (0.002133, 2011.49089, 96.87981, 2854.74761).

- This heterogeneity was very clear when drawing the fatigue curve of the model and the lab values. Nevertheless, this heterogeneity was not affecting the pavement design.

Chapter 5: Conclusion and recommendations

This last chapter includes a conclusion of the previous analysis stage. Some recommendations will be provided, along with the future opportunity areas for further research.

5.1 Conclusions

- The characterization of the fatigue resistance of bituminous mixtures was carried out in accordance with the [BS EN 12697-24-2018] using the four point bending test. A minimum of six beams have been tested adopting a minimum of three strain level, at 20 º C, with a reference frequency of 10 Hz, in strain-controlled testing configuration.

- Based on strain sweep procedure, the implemented strain amplitudes are 300 µm/m, 200 µm/m, and 140 µm/m.

- Five different failure criteria have been analysed, and they are: "50 % reduction in the initial stiffness (E0)", "50 % reduction in the extrapolated stiffness (E00)", "Peak in the phase angle", "Energy ratio", and "Dissipated energy ration".

- The "50 % reduction in the initial stiffness (E0)" and "Peak in the phase angle" failure criteria always yield the minimum average number of cycles, regardless of the strain level.

- The "50 % reduction in the extrapolated stiffness (E00)", "Energy ratio", and "Dissipated energy ratio" failure criteria gave the maximum average number of cycles.

- The "50 % reduction in the extrapolated stiffness (E00)", "Energy ratio", and "Dissipated energy ratio" failure criteria yielded approximately the same cycles to failure.

- The interpretation of "50 % reduction in the extrapolated stiffness (E00)", and "Dissipated energy ratio" failure criterion is prone to some subjectivity. In the first criteria this subjectivity is due to the definition of the regression interval in the intermediate phase, because it is different from one test to another. For the second failure criteria the subjectivity is due to the definition of the two intersection lines. Nevertheless, this subjectivity could be easily limited by fixing a high value for the coefficient of determination (R^2), for example more than 0.95 (less than 5 % error), while making sure we're always extrapolating inside Phase II for the first criteria.

- In comparison with the grand average at each strain level (averaging the cycles for the six replicates for the five failure criteria), we can twig that the "50 % reduction in the extrapolated stiffness (E00)", "Energy ratio", and "Dissipated energy ratio" have the closest values to the grand average.

- Among the previously mentioned criteria the "Energy ratio", and "Dissipated energy ratio" criteria gave the most reliable results, because the transitional period between crack initiation and crack propagation can be clearly seen, and hence the failure point could be easily achieved.

- In terms of the fatigue curves, we can conclude that there is a very good consistency between the "50 % reduction in the extrapolated stiffness (E00)", "Energy ratio", and "Dissipated energy ratio" failure criteria, and the approximately yield the same $\varepsilon_6$values with an average of 159 µm/m, and the last two are almost identical.

- The "50 % reduction in the initial stiffness (E0)" and "Peak in the phase angle" failure criteria always yield the minimum $\varepsilon_6$values.

- Regarding the relationship between the beam position in the roller compactor and the corresponding air voids; it was found that the beams in the center have the lowest air voids, while it wasn't clear whether the left or right edge beams have the highest air voids since they were exchanging roles.

- It was found that the visco-elastic-related stiffness (E0) is increasing as we reduce the air voids, while for the fatigue-related stiffness (E0) we obtained the same trend, but the values were more scattered.

- A sensitivity pavement design was carried out on a pre-defined pavement configuration to see how the pavement design if affected by changing the regression parameters f_1, f_2 that minimizes the summation of the squared differences between the number of cycles to failure obtained in the laboratory and the number of cycles obtained using the fatigue model. ($\sum(Nf_{lab} - Nf_{model})^2$) while keeping the 3rd parameter f_3 fixed at 1.8. The initial values of f_1, f_2 were 4.118E-6, and 5 respectively. It was found that changing these parameters doesn't really affect the pavement design when using the conventional failure criteria.

- When using the "50 % reduction in the extrapolated stiffness E00", " Energy ratio", and "Dissipated energy ratio" we obtained approximately 25% reduction of load repetition when moving from changing f1 only, to changing both f1, f2. Which mean a lower design period in the second case.

5.2 Recommendations and future work:

- Since this thesis is dedicated to characterize the fatigue resistance of bituminous mixtures using only the four-point bending test, it is recommended to carry out the same analysis using another tests like the Asphalt Mixture Performance Tester (AMPT).

- The experimental campaign could be extended to include the effect of temperature by testing beam replicates at higher and lower temperatures.

- Further research is recommended to validate the results achieved in this thesis.

References

[1] ASTM Committee D-4 on Road and Paving Materials., *Fatigue of compacted bituminous aggregate mixtures; a symposium presented at the seventy-fourth annual meeting, American Society for Testing and Materials, Atlantic City, N.J., 27 June-2 July 1971.* American Society for Testing and Materials, 1972.

[2] J. M. Read, "FATIGUE CRACKING OF BITUMINOUS PAVING MIXTURES," 1996.

[3] T. V. Scholz, "Durability of Bituminous Paving Mixtures," 1995.

[4] "Information Series 128 HMA Pavement Mix Type Selection Guide HMA Pavement Mix Type Selection Guide HMA Pavement Mix Type Selection Guide," 2001. [Online]. Available: www.hotmix.org

[5] D. Bergold, "VOLUMETRIC PROPERTIES OF ASPHALT MIXTURES WAQTC TM 13."

[6] *BSI Standards Publication Bituminous Mixtures-Test methods Part 26: Stiffness*. 2018.

[7] P. S. Pell, "Fatigue of Bituminous Materials in Flexible Pavements," *Journal of the Institute of Highways Engineers*, 1971.

[8] *BSI Standards Publication Bituminous Mixtures-Test methods Part 24: Resistance to fatigue*. 2018.

[9] N. Tapsoba, Cédric Sauzéat, and H. di Benedetto, "Analysis of Fatigue Test for Bituminous Mixtures," 2013, doi: 10.1061/(ASCE)MT.1943.

[10] *BSI Standards Publication Bituminous Mixtures-Test methods Part 31: Specimen preparation by gyratory compactor*. 2019.

[11] BSI Group and European Committee for Standardization., *Bituminous mixtures - Test method. Part 33: Specimen prepared by roller compactor.*

[12] *Bituminous mixtures - Test methods - Part 27: Sampling*. 2017.

[13] "Standard Test Method for Determining Fatigue Failure of Asphalt-Aggregate Mixtures with the Four-Point Beam Fatigue Device 1", doi: 10.1520/D8237-21.

[14] Aashto, "Standard Method of Test for Determining the Damage Characteristic Curve and Failure Criterion Using the Asphalt Mixture Performance Tester (AMPT) Cyclic Fatigue Test," 2020.

[15] Aashto, "Standard Method of Test for Rutting and Fatigue Resistance of Asphalt Mixtures Using Incremental Repeated Load Permanent Deformation (iRLPD)," 2020.

[16] L. Wang, *Mechanics of asphalt: microstructure and micromechanics*. McGraw-Hill Professional, 2011.

[17] J. B., P. J. C., P. M., B. R., L. P., and L. A. M. (1998). Sousa, "Effect of aggregate gradation on fatigue life of asphalt concrete mixes," 1998.

[18] A. A., D. J. A., and M. C. L. (1996) Tayebali, "Development and evaluation of surrogate fatigue models for SHRP A-300A abridged mix design procedure," 1996.

[19] J. (2007). Uzan, "Evaluation of fatigue cracking," 2007.

[20] M. and S. J. A. Castro, "Estimation of asphalt concrete fatigue curves – A damage theory approach," 2008.

[21] D., P.-C. G., de L. R. C., P. J. M., and C. A. Bodin, "Continuum damage approach to asphalt concrete fatigue modelling," 2004.

[22] W. van Dijk, "Practical fatigue characterization of bituminous mixes," 1975.

[23] K. A. and S. H. T. Ghuzlan, "Fatigue damage analysis in asphalt concrete mixtures using the dissipated energy approach," 2006.

[24] K. S., N. K., and B. H. U. Bonnetti, "Measuring and defining fatigue behaviour of asphalt binders.," 2002.

[25] G. M. Rowe and M. G. Bouldin, "IMPROVED TECHNIQUES TO EVALUATE THE FATIGUE RESISTANCE OF ASPHALTIC MIXTURES," 2000. [Online]. Available: https://www.researchgate.net/publication/304115473

[26] J. Zhang, M. Sabouri, M. N. Guddati, and Y. R. Kim, "Development of a failure criterion for asphalt mixtures under fatigue loading," *Road Materials and Pavement Design*, vol. 14, pp. 1–15, 2013, doi: 10.1080/14680629.2013.812843.
[27] S., et al., Mangiafico, "Quantification of biasing effects during fatigue tests on asphalt mixes: non-linearity, self-heating and thixotropy," 2015.
[28] H. di Benedetto, C. De, L. Roche, H. Baaj, A. Pronk, and R. Lundstr6m, "Fatigue of bituminous mixtures," 2004.
[29] R. Reese, "Properties of Aged Asphalt Binder Related to Asphalt Concrete Fatigue Life," *Asphalt Paving Technology, AAPT, Vol. 66, pp: 604-632.*, 1997.
[30] Z. JUN, "Development of Failure Criteria for Asphalt Concrete Mixtures under Fatigue Loading".
[31] P. C., K. P. A. J. C. and P. A. C., Hopman, "A Renewed Interpretation Method for Fatigue Measurement, Verification of Miner's Rule," *4th Eurobitume Symposium, Volume 1, Madrid*, 1989.
[32] G. M., Rowe, "Performance of Asphalt Mixtures in the Trapezoidal Fatigue Test," *Association of Asphalt Paving Technologist*, 1993.
[33] A. Subhy, D. lo Presti, and G. Airey, "New simplified approach for obtaining a reliable plateau value in fatigue analysis of bituminous materials," *Engineering Failure Analysis*, vol. 79, pp. 263–273, Sep. 2017, doi: 10.1016/j.engfailanal.2017.05.021.
[34] S. H. C. K.A. Ghuzlan, "Energy-derived, damage-based failure criterion for fatigue testing," 2000.
[35] Yang H. Huang, *Pavement Analysis and Design*.
[36] R. E.., M. I. D. and S. M. H. SMITH, "Highway Pavement Distress Identification Manual for Highway Condition and Quality of Highway Construction Survey," 1979.
[37] British Standards Institution, *Bituminous mixtures. Test methods. Part 39, Binder content by ignition.*
[38] *BSI Standards Publication Determination of particle distibution- Sieving method*. 2012.
[39] *BSI Standards Publication Bituminous Mixtures-Test methods - Determination of the maximum density of Asphalt*. 2019.
[40] *BSI Standards Publication Tests for mechanical and physical properties of aggregates Part 6: Determination of particle density and water absorption*. 2013.
[41] *BSI Standards Publication Bituminous Mixtures-Test methods -Specimen preparation by gyratory compactor*. 2019.
[42] "Standard Test Method for Determining Fatigue Failure of Asphalt-Aggregate Mixtures with the Four-Point Beam Fatigue Device 1", doi: 10.1520/D8237-21.
[43] A. C. Pronk, M. Gajewski, and W. Bańkowski, "Application of a material fatigue damage model in 4PB tests," *International Journal of Pavement Engineering*, vol. 19, no. 9, pp. 805–814, Sep. 2018, doi: 10.1080/10298436.2016.1210441.

Appendix

Slabs and beams measurements

1st Slab	
Thickness (cm)	5.13
wt. In Air (g)	10378.5
wt. In Water (g)	6031.5
SSD (g)	10486.9
Temperature (°C)	16.3

Mould size			Volume	TMD	Mass	$\rho_{geo, real}$	V% geo
w [cm]	L [cm]	H [cm]	[cm^3]	[g/cm^3]	[g]	[g/cm^3]	(-)
18.0	50.0	5.13	4615.9	2.501	10378.5	2.248	10.1

M air	M water	M ssd	T	ρ_w	ρ_{SSD}	TMD	V% real
[g]	[g]	[g]	[°C]	[kg/m^3]	[kg/m^3]	[kg/m^3]	[%]
10378.5	6031.5	10486.9	16.3	999.0	2327	2501	6.96

Table 56 1st Slab

1st set of Beams								
ID	B	H	L	V	M	ρ geo	TMD	V% geo
[-]	[mm]	[mm]	[mm]	[m^3]	[g]	[kg/m^3]	[kg/m^3]	[%]
1	51.1	51.6	410.0	0.001082	2434.3	2250.6	2501.0	10.0
2	51.0	50.9	410.0	0.001064	2414.9	2269.5	2501.0	9.3
3	51.0	52.0	410.0	0.001087	2458.0	2261.1	2501.0	9.6

ID	M air	M water	M ssd	T	ρ_w	ρ_{SSD}	TMD	V% real
[-]	[g]	[g]	[g]	[°C]	[kg/m^3]	[kg/m^3]	[kg/m^3]	[%]
1	2434.3	1398.2	2441.0	16.1	999.0	2332	2501	6.8
2	2414.9	1394.1	2419.9	16.1	999.0	2352	2501	6.0
3	2458.0	1415.4	2463.7	16.1	999.0	2342	2501	6.3

Table 57 1st set of Beams

2nd Slab	
Thickness (mm)	5.09
wt. In Air (g)	10353.2
wt. In Water (g)	6035
SSD (g)	10452.3
Temperature (°C)	14.9

Mould size			Volume	TMD	Mass	$\rho_{geo, real}$	V% geo
w [cm]	L [cm]	H [cm]	[cm^3]	[g/cm^3]	[g]	[g/cm^3]	(-)
18.0	50.0	5.09	4576.7	2.501	10353.2	2.262	9.6

M air	M water	M ssd	T	ρ_w	ρ_{SSD}	TMD	V% real
[g]	[g]	[g]	[°C]	[kg/m^3]	[kg/m^3]	[kg/m^3]	[%]
10353.2	6035.0	10452.3	14.9	999.2	2342	2501	6.36

Table 58 2nd Slab

2nd set of Beams								
ID	B	H	L	V	M	ρ geo	TMD	V% geo
[-]	[mm]	[mm]	[mm]	[m^3]	[g]	[kg/m^3]	[kg/m^3]	[%]
4	51.2	50.6	408.0	0.001058	2432.0	2299.7	2501.0	8.0
5	50.5	49.6	408.0	0.001023	2369.9	2316.7	2501.0	7.4
6	51.2	50.1	408.0	0.001046	2401.9	2296.2	2501.0	8.2

ID	M air	M water	M ssd	T	ρ_w	ρ_{SSD}	TMD	V% real
[-]	[g]	[g]	[g]	[°C]	[kg/m^3]	[kg/m^3]	[kg/m^3]	[%]
4	2432.0	1401.9	2436.1	15.4	999.1	2349	2501	6.1
5	2369.9	1370.7	2374.0	15.4	999.1	2360	2501	5.6
6	2401.9	1391.6	2408.8	15.4	999.1	2359	2501	5.7

Table 59 1st set of Beams

3rd Slab	
Thickness (cm)	5.09
wt. In Air (g)	10388.6
wt. In Water (g)	6084.7
SSD (g)	10507.3
Temperature (° C)	16.1

Mould size			Volume	TMD	Mass	ρ geo, real	V% geo
w [cm]	L [cm]	H [cm]	[cm^3]	[g/cm^3]	[g]	[g/cm^3]	(-)
18.0	50.0	5.09	4580.8	2.501	10388.6	2.268	9.3

M air	M water	M ssd	T	ρ_w	ρ_{SSD}	TMD	V% real
[g]	[g]	[g]	[°C]	[kg/m^3]	[kg/m^3]	[kg/m^3]	[%]
10388.6	6084.7	10507.3	16.1	999.0	2347	2501	6.17

Table 60 3rd Slab

3rd set of BEAMS								
ID	B	H	L	V	M	ρ geo	TMD	V% geo
[-]	[mm]	[mm]	[mm]	[m^3]	[g]	[kg/m^3]	[kg/m^3]	[%]
7	51.6	50.9	408.0	0.001073	2470.7	2303.4	2501.0	7.9
8	51.6	50.6	409.0	0.001068	2465.1	2309.0	2501.0	7.7
9	50.9	50.7	408.0	0.001053	2388.4	2267.9	2501.0	9.3

ID	M air	M water	M ssd	T	ρ_w	ρ_{SSD}	TMD	V% real
[-]	[g]	[g]	[g]	[°C]	[kg/m^3]	[kg/m^3]	[kg/m^3]	[%]
7	2470.7	1429.0	2475.0	15.6	999.1	2360	2501	5.6
8	2465.1	1428.0	2468.5	15.6	999.1	2367	2501	5.4
9	2388.4	1381.4	2398.8	15.6	999.1	2345	2501	6.2

Table 61 3rd set of Beams

4th Slab	
Thickness (cm)	5.04
wt. In Air (g)	10373.6
wt. In Water (g)	6051.5
SSD (g)	10446
Temperature (°C)	16

Mould size			Volume	TMD	Mass	$\rho_{geo, real}$	V% geo
w [cm]	L [cm]	H [cm]	[cm^3]	[g/cm^3]	[g]	[g/cm^3]	(-)
18.0	50.0	5.04	4532.9	2.501	10373.6	2.289	8.5

M air	M water	M ssd	T	ρ_w	ρ_{SSD}	TMD	V% real
[g]	[g]	[g]	[°C]	[kg/m^3]	[kg/m^3]	[kg/m^3]	[%]
10373.6	6051.5	10446.0	16.0	999.0	2358	2501	5.71

Table 62 4th Slab

4th set of Beams								
ID	B	H	L	V	M	ρ geo	TMD	V% geo
[-]	[mm]	[mm]	[mm]	[m^3]	[g]	[kg/m^3]	[kg/m^3]	[%]
10	50.9	50.1	409.0	0.001044	2404.0	2303.8	2501.0	7.9
11	50.9	49.4	409.0	0.001026	2382.6	2321.4	2501.0	7.2
12	50.8	50.1	408.0	0.001039	2396.4	2306.1	2501.0	7.8

ID	M air	M water	M ssd	T	ρ_w	ρ_{SSD}	TMD	V% real
[-]	[g]	[g]	[g]	[°C]	[kg/m^3]	[kg/m^3]	[kg/m^3]	[%]
10	2404.0	1393.2	2408.3	16.0	999.0	2366	2501	5.4
11	2382.6	1386.0	2385.0	16.0	999.0	2383	2501	4.7
12	2396.4	1388.9	2399.3	16.0	999.0	2369	2501	5.3

Table 63 4th set of Beams

5th Slab	
Thickness (cm)	5.02
wt. In Air (g)	10387.8
wt. In Water (g)	6076.6
SSD (g)	10464
Temperature (° C)	16.3

Mould size			Volume	TMD	Mass	$\rho_{geo, real}$	V% geo
w [cm]	L [cm]	H [cm]	[cm^3]	[g/cm^3]	[g]	[g/cm^3]	(-)
18.0	50.0	5.02	4518.5	2.501	10387.8	2.299	8.1

M air [g]	M water [g]	M ssd [g]	T [°C]	ρ_w [kg/m^3]	ρ_{SSD} [kg/m^3]	TMD [kg/m^3]	V% real [%]
10387.8	6076.6	10464.0	16.3	999.0	2365	2501	5.43

Table 64 5th Slab

5th set of Beams								
ID	B	H	L	V	M	ρ geo	TMD	V% geo
[-]	[mm]	[mm]	[mm]	[m^3]	[g]	[kg/m^3]	[kg/m^3]	[%]
13	51.3	49.7	409.0	0.001044	2415.2	2314.4	2501.0	7.5
14	51.5	48.8	409.0	0.001027	2410.3	2346.0	2501.0	6.2
15	51.6	49.8	408.0	0.001049	2458.2	2342.9	2501.0	6.3

ID	M air	M water	M ssd	T	ρ_w	ρ_{SSD}	TMD	V% real
[-]	[g]	[g]	[g]	[°C]	[kg/m^3]	[kg/m^3]	[kg/m^3]	[%]
13	2415.2	1403.8	2423.0	18.1	998.6	2366	2501	5.4
14	2410.3	1405.2	2413.3	18.1	998.6	2388	2501	4.5
15	2458.2	1429.8	2460.8	18.1	998.6	2381	2501	4.8

Table 65 5th set of Beams

6th Slab	
Thickness (cm)	4.96
wt. In Air (g)	10327.9
wt. In Water (g)	6036.8
SSD (g)	10381.8
Temperature (°C)	18.1

Mould size			Volume	TMD	Mass	$\rho_{geo, real}$	V% geo
w [cm]	L [cm]	H [cm]	[cm^3]	[g/cm^3]	[g]	[g/cm^3]	(-)
18.0	50.0	4.96	4464.5	2.501	10327.9	2.313	7.5

M air	M water	M ssd	T	ρ_w	ρ_{SSD}	TMD	V% real
[g]	[g]	[g]	[°C]	[kg/m^3]	[kg/m^3]	[kg/m^3]	[%]
10327.9	6036.8	10381.8	18.1	998.6	2374	2501	5.09

Table 66 6th Slab

6th set of Beams								
ID	B	H	L	V	M	ρ geo	TMD	V% geo
[-]	[mm]	[mm]	[mm]	[m^3]	[g]	[kg/m^3]	[kg/m^3]	[%]
16	50.6	49.1	409.0	0.001017	2341.2	2302.2	2501.0	7.9
17	50.5	48.8	409.0	0.001007	2378.7	2361.1	2501.0	5.6
18	51.1	49.7	408.0	0.001035	2417.8	2336.3	2501.0	6.6

ID	M air	M water	M ssd	T	ρ_w	ρ_{SSD}	TMD	V% real
[-]	[g]	[g]	[g]	[°C]	[kg/m^3]	[kg/m^3]	[kg/m^3]	[%]
16	2341.2	1360.9	2346.2	17.7	998.7	2373	2501	5.1
17	2378.7	1389.3	2381.1	18.7	998.5	2395	2501	4.2
18	2417.8	1409.6	2420.2	18.7	998.5	2389	2501	4.5

Table 67 6th set of Beams

7th Slab	
Thickness (cm)	4.94
wt. In Air (g)	10181.8
wt. In Water (g)	5937.5
SSD (g)	10248.3
Temperature (° C)	19.3

Mould size			Volume	TMD	Mass	$\rho_{geo, real}$	V% geo
w [cm]	L [cm]	H [cm]	[cm^3]	[g/cm^3]	[g]	[g/cm^3]	(-)
18.0	50.0	4.94	4441.7	2.501	10181.8	2.292	8.3

M air	M water	M ssd	T	ρ_w	ρ_{SSD}	TMD	V% real
[g]	[g]	[g]	[°C]	[kg/m^3]	[kg/m^3]	[kg/m^3]	[%]
10181.8	5937.5	10248.3	19.3	998.4	2358	2501	5.71

Table 68 7th Slab

7th set of Beams								
ID	B	H	L	V	M	ρ geo	TMD	V% geo
[-]	[mm]	[mm]	[mm]	[m^3]	[g]	[kg/m^3]	[kg/m^3]	[%]
19L	51.1	48.4	408.0	0.001010	2330.2	2308.1	2501.0	7.7
20C	50.2	49.3	408.5	0.001012	2370.0	2342.5	2501.0	6.3
21R	50.8	48.7	408.0	0.001009	2350.8	2329.6	2501.0	6.9

ID	M air	M water	M ssd	T	ρ_w	ρ_{SSD}	TMD	V% real
[-]	[g]	[g]	[g]	[°C]	[kg/m^3]	[kg/m^3]	[kg/m^3]	[%]
19L	2330.2	1353.1	2335.3	19.0	998.5	2369	2501	5.3
20C	2370.0	1382.6	2372.3	19.0	998.5	2391	2501	4.4
21R	2350.8	1364.9	2355.0	19.0	998.5	2371	2501	5.2

Table 69 7th set of Beams

8th Slab	
Thickness (cm)	5.00
wt. In Air (g)	10355.2
wt. In Water (g)	6048.5
SSD (g)	10432.6
Temperature (°C)	18.1

Mould size			Volume	TMD	Mass	$\rho_{geo, real}$	V% geo
w [cm]	L [cm]	H [cm]	[cm^3]	[g/cm^3]	[g]	[g/cm^3]	(-)
18.0	50.0	5.00	4497.8	2.501	10355.2	2.302	7.9

M air	M water	M ssd	T	ρ_w	ρ_{SSD}	TMD	V% real
[g]	[g]	[g]	[°C]	[kg/m^3]	[kg/m^3]	[kg/m^3]	[%]
10355.2	6048.5	10432.6	18.1	998.6	2359	2501	5.69

Table 70 8th Slab

8th set of Beams								
ID	B	H	L	V	M	ρ geo	TMD	V% geo
[-]	[mm]	[mm]	[mm]	[m^3]	[g]	[kg/m^3]	[kg/m^3]	[%]
22L	51.2	49.6	409.0	0.001039	2394.4	2305.3	2501.0	7.8
23C	51.3	49.1	409.0	0.001029	2419.9	2351.2	2501.0	6.0
24R	50.5	49.8	409.0	0.001029	2399.9	2332.6	2501.0	6.7

ID	M air	M water	M ssd	T	ρ_w	ρ_{SSD}	TMD	V% real
[-]	[g]	[g]	[g]	[°C]	[kg/m^3]	[kg/m^3]	[kg/m^3]	[%]
22L	2394.4	1386.5	2399.9	17.0	998.8	2360	2501	5.6
23C	2419.9	1408.8	2423.7	17.0	998.8	2382	2501	4.8
24R	2399.9	1396.3	2403.3	17.0	998.8	2380	2501	4.8

Table 71 8th set of Beams

9th Slab	
Thickness (cm)	4.93
wt. In Air (g)	10354.6
wt. In Water (g)	6060.4
SSD (g)	10409.9
Temperature (° C)	20.5

Mould size			Volume	TMD	Mass	$\rho_{geo, real}$	V% geo
w [cm]	L [cm]	H [cm]	[cm^3]	[g/cm^3]	[g]	[g/cm^3]	(-)
18.0	50.0	4.93	4433.2	2.501	10354.6	2.336	6.6

M air	M water	M ssd	T	ρ_w	ρ_{SSD}	TMD	V% real
[g]	[g]	[g]	[°C]	[kg/m^3]	[kg/m^3]	[kg/m^3]	[%]
10354.6	6060.4	10409.9	20.5	998.2	2376	2501	4.99

Table 72 9th Slab

9th set of Beams								
ID	B	H	L	V	M	ρ geo	TMD	V% geo
[-]	[mm]	[mm]	[mm]	[m^3]	[g]	[kg/m^3]	[kg/m^3]	[%]
25L	51.8	49.4	409.5	0.001047	2353.5	2247.2	2501.0	10.1
26C	51.8	48.9	409.5	0.001039	2438.8	2348.2	2501.0	6.1
27R	50.9	48.7	409.5	0.001014	2463.1	2428.3	2501.0	2.9

ID	M air	M water	M ssd	T	ρ_w	ρ_{SSD}	TMD	V% real
[-]	[g]	[g]	[g]	[°C]	[kg/m^3]	[kg/m^3]	[kg/m^3]	[%]
25L	2353.5	1372.2	2358.1	19.5	998.4	2383	2501	4.7
26C	2438.8	1423.1	2441.3	19.5	998.4	2391	2501	4.4
27R	2463.1	1440.0	2465.8	19.5	998.4	2397	2501	4.1

Table 73 9th set of Beams

10th Slab	
Thickness (cm)	4.99
wt. In Air (g)	10387.8
wt. In Water (g)	6074.5
SSD (g)	10437.8
Temperature (° C)	19.3

Mould size			Volume	TMD	Mass	$\rho_{geo, real}$	V% geo
w [cm]	L [cm]	H [cm]	[cm^3]	[g/cm^3]	[g]	[g/cm^3]	(-)
18.0	50.0	4.99	4492.6	2.501	10387.8	2.312	7.5

M air	M water	M ssd	T	ρ_w	ρ_{SSD}	TMD	V% real
[g]	[g]	[g]	[°C]	[kg/m^3]	[kg/m^3]	[kg/m^3]	[%]
10387.8	6074.5	10437.8	19.3	998.4	2377	2501	4.96

Table 74 10th Slab

10th set of Beams								
ID	B	H	L	V	M	ρ geo	TMD	V% geo
[-]	[mm]	[mm]	[mm]	[m^3]	[g]	[kg/m^3]	[kg/m^3]	[%]
28L	50.6	48.6	409.0	0.001005	2346.3	2334.6	2501.0	6.7
29C	51.1	48.7	409.5	0.001019	2389.2	2345.6	2501.0	6.2
30R	51.0	49.9	409.5	0.001042	2451.7	2352.0	2501.0	6.0

ID	M air	M water	M ssd	T	ρ_w	ρ_{SSD}	TMD	V% real
[-]	[g]	[g]	[g]	[°C]	[kg/m^3]	[kg/m^3]	[kg/m^3]	[%]
28L	2346.3	1366.3	2350.6	18.9	998.5	2380	2501	4.8
29C	2389.2	1397.2	2390.9	18.9	998.5	2401	2501	4.0
30R	2451.7	1433.3	2454.1	18.9	998.5	2398	2501	4.1

Table 75 10th set of Beams

11th Slab	
Thickness (cm)	4.95
wt. In Air (g)	10377.2
wt. In Water (g)	6068.8
SSD (g)	10415.3
Temperature (° C)	19.1

Mould size			Volume	TMD	Mass	$\rho_{geo, real}$	V% geo
w [cm]	L [cm]	H [cm]	[cm^3]	[g/cm^3]	[g]	[g/cm^3]	(-)
18.0	50.0	4.95	4455.5	2.501	10377.2	2.329	6.9

M air	M water	M ssd	T	ρ_w	ρ_{SSD}	TMD	V% real
[g]	[g]	[g]	[°C]	[kg/m^3]	[kg/m^3]	[kg/m^3]	[%]
10377.2	6068.8	10415.3	19.1	998.5	2384	2501	4.69

Table 76 11th Slab

10th set of Beams								
ID	B	H	L	V	M	ρ geo	TMD	V% geo
[-]	[mm]	[mm]	[mm]	[m^3]	[g]	[kg/m^3]	[kg/m^3]	[%]
31L	51.4	48.5	409.0	0.001019	2388.0	2342.7	2501.0	6.3
32C	51.1	48.6	409.0	0.001016	2404.5	2365.5	2501.0	5.4
33R	49.9	49.3	409.0	0.001006	2383.8	2369.8	2501.0	5.2

ID	M air	M water	M ssd	T	ρ_w	ρ_{SSD}	TMD	V% real
[-]	[g]	[g]	[g]	[°C]	[kg/m^3]	[kg/m^3]	[kg/m^3]	[%]
31L	2388.0	1395.6	2391.3	20.1	998.3	2394	2501	4.3
32C	2404.5	1406.3	2406.7	20.1	998.3	2399	2501	4.1
33R	2383.8	1395.1	2387.0	20.1	998.3	2399	2501	4.1

Table 77 11th set of Beams